Thermal evolution of the continental crust of Calabria during the Hercynian orogeny: constraints from metamorphic phase equilibria and isotopic dating

Dissertation
zur Erlangung des Doktorgrades
der Mathematisch-Naturwissenschaftlichen Fakultät
der Christian-Albrechts-Universität
zu Kiel

vorgelegt von
Thorsten Graeßner

Kiel
1999

VORWORT

Im Rahmen eines wissenschaftlichen Projektes über die aufgeschlossenen Krustenprofile in Kalabrien/S-Italien, welches von der Deutschen Forschungsgemeinschaft gefördert wurde (Titel Sche 265/9-1), wurde mir die Möglichkeit gegeben, in den vergangenen dreieinhalb Jahren am Institut für Geowissenschaften der Universität Kiel zu promovieren. Während mehrerer Geländeaufenthalte in Kalabrien, insbesondere im Aspromonte und in der Sila, habe ich nicht nur die für diese Studie nötigen Gesteinsproben gewonnen, sondern auch Land und Leute kennengelernt. Diese Eindrücke und die mir entgegengebrachte Gastfreundschaft werde ich nicht vergessen und haben meinen positiven Gesamteindruck von Kalabrien bestimmt.

Für die stete Diskussionsbereitschaft während der Durchführung dieser Arbeit, die insbesondere die beiden Petrologie-Kapitel betreffen, möchte ich mich bei meinem Betreuer Prof. Dr. Volker Schenk bedanken. Sein immerwährendes Interesse und seine Motivationshilfen waren entscheidend für die gewonnenen wissenschaftlichen Erkenntnisse. Seine Begeisterungsfähigkeit in Vorlesungen und auch auf Exkursionen weckte mein Interesse auf den Gebieten der Petrologie und der Geochronologie und überzeugte mich, in diesem Bereich zu promovieren.

Zur Durchführung radiometrischer Altersbestimmungen im Rahmen dieser Arbeit verbrachte ich mehrere Aufenthalte, in den Jahren 1996 bis 1999, am Zentrallaboratorium für Geochronologie der Universtät Münster. Für die Betreuung während dieser Aufenthalte möchte ich mich bei Prof. Dr. Klaus Mezger und Dr. Michael Bröcker bedanken, die mich in die Praxis der Isotopendatierung einführten und immer ansprechbar für fortführende fruchtbare Diskussionen waren. Ohne die zusätzliche Hilfe von Heidi Baier und Sigmund Rochnowski im Labor und an den Massenspektrometern wäre diese Arbeit nicht entstanden.

Diese Arbeit besteht aus drei Kapiteln, denen eine allgemeine Einführung und Zusammenfassung vorangestellt ist. Diese Kapitel sind so konzipiert, daß sie zwar getrennt voneinander als Artikel publiziert werden können (das erste Kapitel ist bereits im *Journal of Metamorphic Geology* 1999 erschienen), aber auch eine zusammenhängende Monographie darstellen.

Für die gute Zusammenarbeit in der Arbeitsgruppe in Kiel bedanke ich mich besonders bei Dr. Peter Appel, der mich beim Einarbeiten in neue Computerprogramme immer unterstützt hat, und bei meinem Zimmerkollegen Timm John, der auch in der Schlußphase dieser Arbeit sich nicht von meinem Stress hat abbringen lassen, für gute Laune und viel Tee zu sorgen.

Ein besonderer Dank gilt an dieser Stelle auch Bärbel Burmeister, die bis zuletzt Bilder für mich entwickelt hat. Ebenso bedanke ich mich bei Frau Barbara Mader und Dr. Dietrich Ackermand für die Unterstützung an der Mikrosonde in Kiel und bei Andreas Fehler, für die Herstellung vieler Gesteins-Dünnschiffe.

Ein Dank geht auch an Dr. Andreas Kronz vom Institut für Geochemie der Universität Göttingen, der mir bei der Herstellung der im dritten Kapitel benutzten CL- und BSE-Aufnahmen an der dortigen Mikrosonde geholfen hat.

Ringrazio anche i miei amici italiani a Taverna, in particolar modo la famiglia Rodano che durante il mio soggiorno nella primavera 1996 mi ha dato in affitto un piccolo appartamento e mi ha invitato spesso a cena.

Ich danke meinen Eltern, deren finanzielle Unterstützung meine Geländeaufenthalte in Kalabrien erst möglich machten.

Zum Schluß möchte ich mich insbesondere bei Renate bedanken, ohne die wahrscheinlich mein Leben bis jetzt anders verlaufen wäre.

INTRODUCTION AND SUMMARY

Tectonically exposed cross-sections through the continental crust offer the possibility to study the effects of thermal and tectonic events during orogenic cycles on the lithologies of different crustal levels. To compare the thermal conditions and evolutions of the different levels of the crust, all subsections, from the upper to the lower crust, have to be exposed and their metamorphisms should be related to the same orogenic event, i.e. should be of the same age in all crustal levels. This thesis is aimed to reconstruct the metamorphic, magmatic and tectonic events in the Calabrian crust. For this purpose, intensive phase petrological and textural studies on metamorphic rocks of different levels of that crust have been conducted. Isotopic dating of metamorphic and magmatic minerals supplement the petrological studies and allow to decipher the time relationship between metamorphism and granite magmatism in the crust.

Up to now, the most continuous crustal section has been documented in the Serre of southern Calabria, where geological mapping and petrological work revealed a 5-7 km thick profile through the granulite facies lower crust with peak *P-T* conditions of 690-800 °C at 5.5-7.5 kbar (Schenk, 1984, 1990). These rocks are overlain by large mesaluminous to calcalkaline granodiorites and tonalites and minor peraluminous granites which intruded mainly into the middle crust and lead to intrusive contacts with the over- and underlying rocks. Peraluminous granites intruded also into the greenschist to amphibolite facies gneisses of the upper crust of the Aspromonte area further in the south. Previous geochronological studies on granulite facies metamorphism and granitoid intrusions into mid-to lower crustal levels indicate a synchroneity of metamorphic and magmatic events at 300 ± 10 Ma (Schenk, 1980, 1990). However, these studies did not address the chronological and thermal relationships between the lower crustal metamorphism, peraluminous magmatism and the metamorphism of Palaeozoic sediments representing the uppermost level of that crust. This is a subject of this thesis.

A second scope of this study is the metamorphic and magmatic history of the deeper parts of the 'Sila nappe' of northern Calabria. The lithostratigraphic sequence of the Sila nappe resembles the one of southern Calabria, but has been interpreted differently: As a whole it represents an Alpine nappe resting on high-pressure ophiolitic rocks. Its deeper part, the granulite facies 'Mt. Gariglione Complex', has been subdivided by some authors into a Hercynian nappe stack (Zanettin Lorenzoni, 1980; Lorenzoni & Zanettin Lorenzoni, 1983), in contrast to Dubois (1970, 1976) who attributes all Hercynian granulite facies rocks to only one Alpine unit. The present study focus on the petrology of the granulite facies gneisses to check whether the Mt. Gariglione Complex consists of a nappe pile or represents only one Hercynian unit. Furthermore, the *P-T* paths of these rocks are deduced to get information on the geodynamic causes of metamorphism. Isotopic dating of the granulite facies rocks and of peraluminous granites which intruded at mid-crustal levels of the Sila nappe reveals a constrain on the relationship between peak metamorphism and granitoid magmatism as well as on post-metamorphic cooling of the Mt. Gariglione Complex.

The thesis is subdivided into three chapters. The **first chapter** adresses the metamorphic petrology of Palaeozoic metasediments of the Aspromonte massif which represent the uppermost part of the crust in southern Calabria. During a late-Hercynian low-pressure/high-temperature metamorphism a sequence of metamorphic zones at chlorite, biotite, garnet, staurolite-andalusite and sillimante-muscovite grade was developed. Three foliations were formed during deformation of the metasediments due to regional metamorphism. The peak metamorphic assemblages grew mainly syntectonically but mineral growth outlastet the deformation. Similar textural relationships are reported from the granulite facies lower crust of the same crustal section in the Serre. Pressures estimated for the base of the upper crustal metasediments are *c.* 2.5 kbar and temperatures range from <350 °C in the chlorite zone, increasing to 500 °C in the lower garnet zone, and reaching 620 °C in the sillimanite-muscovite zone. These *P-T* conditions indicate a geothermal gradient for peak metamorphism of about 60 °Ckm^{-1} for the amphibolite facies upper crust, which is much higher than that for the granulite facies lower crustal rocks of 30-35 °Ckm^{-1} of the same crustal section. The small temperature difference between the base of the upper crust (620 °C at *c.* 2.5 kbar) and the top of the lower crust (690 °C at 5.5 kbar) can be explained by intrusions of granitoids into mid- to upper crustal levels synchronuous with metamorphism during the late-Hercynian orogeny.

The **second chapter** deals with the granulite facies 'Mt Gariglione Complex', the granulite facies lower part of the Sila nappe in northern Calabria. This large unit (*c.* 900 km^2) consists mainly of metapelitic migmatites, with subordinate metabasites and metacarbonates, which were metamorphosed during the late-Hercynian orogeny. A metamorphic gradient through this high-grade complex can be deduced from mineral chemistry and phase relations of metapelites and is indicated by a systematic change in compositions of ferromagnesian minerals in divariant assemblages. As in southern Calabria, this supports a model of an exposed profile through a segment of the former lower continental crust. Due to partial re-equilibration of matrix phases the continuous change in peak metamorphic conditions is best defined by mineral equilibria of dehydration melting reactions and only partly supported by conventional geothermobarometry and by applying the multi-equilibrium method (TWEEQU; Berman, 1991). The highest *P-T* conditions of prograde metamorphism reveal *c.* 4 kbar and 740 °C at the top and *c.* 6 kbar and 770 °C at the base of the section leading to an unusual high geothermal gradient of 35-50°C/km^{-1}. Therefore the lower crustal rocks of the Mt. Gariglione Complex represent a shallower section through the former continental crust (14-21 km) than the one in the Serre of southern Calabria (19-26 km). The prograde *P-T* path is characterized by moderate loading and proceeded in the stability field of sillimanite. The post-Hercynian form of the retrograde path shows a stage of isothermal uplift from granulite facies conditions into mid-crustal levels (10-15 km), followed by nearly isobaric cooling to greenschist facies conditions. Therefore the *P-T* path of the lower crustal section in the Sila of northern Calabria resembles that of the Serre in southern Calabria.

The **third chapter** concentrates on the geochronological dating of the late-Hercynian orogenic event which controlled the thermal evolution of all levels of the continental crust in northern and southern Calabria. U-Pb dating of monazite from upper crustal paragneisses of southern Calabria yields ages for amphibolite facies metamorphism of 295-293 Ma, which is identical to monazite ages of granulites in the lower crust and similar to the intrusion ages of calcalkaline and mesaluminous granitoids at mid-crustal levels (300 ± 10 Ma; Schenk, 1990). Monazite and xenotime of peraluminous granites (Cittanova and Punta d'Atò granites) of the middle to upper crust of the same crustal section provide intrusion ages of 303-302 Ma which seem to be slightly older than the upper crustal metamorphism. Zircon of a metabasic intrusion into the lower crust yields a lower concordia intercept age of 290 Ma, which can be interpreted as the time of metamorphism or if inherited lead is the reason for discordance of the magmatic zircons, as the minimum age of the magmatic intrusion.

Dating of monazite from granulite facies migmatites in the Sila nappe and of peraluminous granites of the middle crust of the exposed crustal segment in northern Calabria reveals also a synchroneity of peak metamorphism and intrusion at 304-302 Ma. As indicated by metamorphic textures, the lower crustal rocks were uplifted into mid-crustal levels at the end of the granulite facies metamorphism. This was followed by nearly isobaric slow cooling (3 °CMa^{-1}) which seems to be undisturbed by any tectonic event as indicated by a regular sequence of biotite and muscovite Rb-Sr and K-Ar ages between 210 and 123 Ma. The thermal history is therefore similar to that of the lower crust of southern Calabria (Schenk, 1990).

Finally, it can be concluded that the thermal structure of the Calabrian crust during the late-Hercynian orogeny - as it is reflected by peak metamorphic assemblages and textures and by U-Pb geochronology - was mainly controlled by advective heat input through magmatic intrusions into all crustal levels at the time of metamorphism. Therefore, for both of the exposed crustal profiles an ancient geotectonic setting as a continantal arc above a subduction zone is favoured.

CHAPTER ONE

Low-pressure metamorphism of Palaeozoic pelites in the Aspromonte, southern Calabria: constraints for the thermal evolution in the Calabrian crustal cross-section during the Hercynian orogeny

(published in *Journal of Metamorphic Geology*, **17**, 157-172, 1999)

1.1 ABSTRACT

During Hercynian low-pressure/high-temperature metamorphism of Palaeozoic metasediments of the southern Aspromonte (Calabria), a sequence of metamorphic zones at chlorite, biotite, garnet, staurolite-andalusite and sillimanite-muscovite grade was developed. These metasediments represent the upper part of an exposed tilted cross-section through the Hercynian continental crust. *P-T* information on their metamorphism supplements that already known for the granulite facies lower crust of the section and allows the reconstruction of the thermal conditions in the Calabrian crust during the late Hercynian orogenic event.

Three foliations formed during deformation of the metasediments. The peak metamorphic assemblages grew mainly syntectonically (S2) during regional metamorphism, but mineral growth outlasted the deformation. This is in accordance with the textural relationships found in the lower part of the same crustal section exposed in the northern Serre. Pressure conditions recorded for the base of the upper crustal metasediments are *c*. 2.5 kbar and estimated temperatures range from < 350 °C in the chlorite zone increasing to 500 °C in the lower garnet zone, and reaching 620 °C in the sillimanite-muscovite zone. Geothermal gradients for the peak of metamorphism indicate a much higher value for the upper crust (*c*. 60 °C km^{-1}) than for the granulite facies lower crust (30-35 °C km^{-1}). The small temperature difference between the base of the upper crust (620 °C at *c*. 2.5 kbar) and the top of the lower crust (690 °C at 5.5 kbar) can be explained by intrusions of granitoids into the middle crust, which, in this crustal section, took place synchronously with the regional metamorphism *c*. 310 to 295 Ma ago.

It is concluded that the thermal structure of the Calabrian crust during the Hercynian orogeny - as it is reflected by peak metamorphic assemblages - is mainly controlled by advective heat input through magmatic intrusions into all levels of the crust.

Mineral abbreviations are from Kretz (1983).

1.2 INTRODUCTION

Exposed cross sections through the continental crust, comprising granulite facies lower crustal rocks, a wide range of granitoids in the middle crust and amphibolite to greenschist facies upper crustal rocks, offer the possibility to study and compare the thermal conditions during an orogenic event in different levels of the crust. A prerequisite for this approach is that metamorphic assemblages found in that crust are related to the same orogenic process, i.e. are of the same age in the compared sub-sections. The tilted crustal profile of southern Calabria, which has been metamorphosed during the Hercynian orogeny, is one of the few examples suitable for such a study. The lower crustal part, in the Serre (80 km to the north of the study area; Fig. 1.1), forms a continuous 7 to 8 km thick profile (5.5 to 7.5 kbar; Schenk, 1984, 1990) comprising granulite facies metabasites in its deeper part which are overlain by a volumetrically larger unit of metapelites. The uppermost crustal section (the 'Stilo unit', Figs 1.1 & 1.2) is only locally preserved and exhibits a prograde sequence from sub-greenschist to amphibolite facies grade. Fortunately, metapelites, which are especially suitable for mapping of isograds and evaluation of metamorphic conditions, dominate in the upper and the lower crustal sections. Dating of monazite and zircon has revealed similar ages of *c*. 310 to 295 Ma for the metamorphism in the upper and the lower crust and for the granitoid magmatism (Schenk, 1980, 1990). The latter affected mainly the middle crust but intrusions of the same age occur in the upper and lower crust as well (Fig. 1.1).

This paper concentrates on the petrology of the Hercynian metamorphism of upper crustal Palaeozoic sediments of the Aspromonte massif, southern Calabria. In this area, a metamorphic zonation from the chlorite zone up to the sillimanite-muscovite zone developed at low pressures. This high-temperature/low-pressure metamorphism contrasts to medium-pressure type of metamorphism in the lower crust (Schenk, 1990), which can be explained by intrusions into the middle crust synchronous with regional metamorphism.

1.3 GEOLOGICAL SETTING OF SOUTHERN CALABRIA

The Calabrian massif is situated in the southern part of the Appenine mountain system and consists of pre-Alpine crust which was involved in the Alpine orogeny. The Alpine mountain system became dismembered due to later movements of microplates in the western Mediterranean (e.g. Alvarez, 1976). Some authors (Amodio-Morelli *et al*., 1976; Scandone, 1979; Bonardi *et al.*, 1982) regard the Calabrian massif as a piece of Adriatic crust that was thrust firstly (Alpidic stage) onto ophiolitic units in the west and later (Apenninic stage), together with its underlying base, backwards onto the Apenninic carbonate platform in the east. In contrast, Dietrich (1988) regards the Calabrian massif as derived from the European continent, thrust only towards the east, overriding the ophiolitic units and resting now with its ophiolitic base upon the Adriatic platform units.

The tectonically higher units of the massif consist in their deeper parts of granulite facies lower crustal gneisses, which are overlain by Hercynian granitoids (Fig. 1.1). The latter intruded into the overlying amphibolite facies upper crustal gneisses and Palaeozoic rocks. This sequence thus consists of rocks from very different crustal levels and may have stored - if they were part of the same Hercynian crustal segment - valuable information about the former thermal conditions at different levels of that Hercynian crust. The most continuous section has been documented in southern Calabria, where geological mapping and petrological work revealed a continuous profile through the granulite facies lower crust (Schenk, 1984). At the top of this section, at the contact with the overlying late Hercynian granitoids, blastomylonitic recrystallization of the granulitic metapelites took place at high temperatures. These textures, together with synchronous metamorphism and magmatism, as well as the occurrence of similar biotite cooling ages in both units, are evidence that a transition from Hercynian granulite facies lower crust into granitoid middle crust is exposed (Schenk, 1990) that was not much modified by Alpine tectonics.

The section exposed in the Aspromonte area, forming the southern part of the Calabrian massif (Fig. 1.1), consists mainly of amphibolite facies paragneisses and pre-Hercynian (*c.* 520 Ma; Schenk & Todt, 1989) orthogneisses. These upper crustal rocks were intruded by late Hercynian granites of the same cycle as those intruding at the top of the lower crust, thus supporting the interpretation that the lower and upper crustal rocks were part of the same crustal section at least since late Hercynian time (cf. discussion in Schenk, 1990). However, according to most authors (e.g. Bonardi *et al.*, 1979; Bonardi *et al.*, 1992; Crisci *et al.*, 1982; Platt & Compagnoni, 1990), the Tertiary history of the upper crustal part in the Aspromonte involved the formation of at least three Alpine thrust sheets. Low grade phyllites of the 'Mandanici unit' occur only in two windows and are overlain by gneisses of the 'Aspromonte unit' occupying most of the Aspromonte area (Fig. 1.1; Bonardi *et al.*, 1980; Bonardi *et al.*, 1984a). The third nappe rests on top of the Aspromonte unit and consists of phyllites of the so called 'Stilo unit', grading downwards into greenschist to amphibolite facies schists. Similar phyllites occur locally along the eastern (Sila, Serre) and southern (Aspromonte) borders of the massif (Fig. 1.1). In some places, Cambrian to Carboniferous sedimentation ages have been documented palaeontologically (Bouillin *et al.*, 1984).

In contrast to the above named authors, who interpret the Palaeozoic phyllites of the southern Aspromonte, the metamorphism of which is the subject of this paper, as an Alpine nappe ('Stilo unit'; Bonardi *et al.*, 1979; Crisci *et al.*, 1982; Bonardi *et al.*, 1984b), Acquafredda *et al.* (1994) regard them as a parautochthonous cover of an older basement (the Aspromonte unit). As will be discussed later on the basis of Hercynian metamorphic isograds, at least the position of the assumed Alpine nappe boundary cannot be correct.

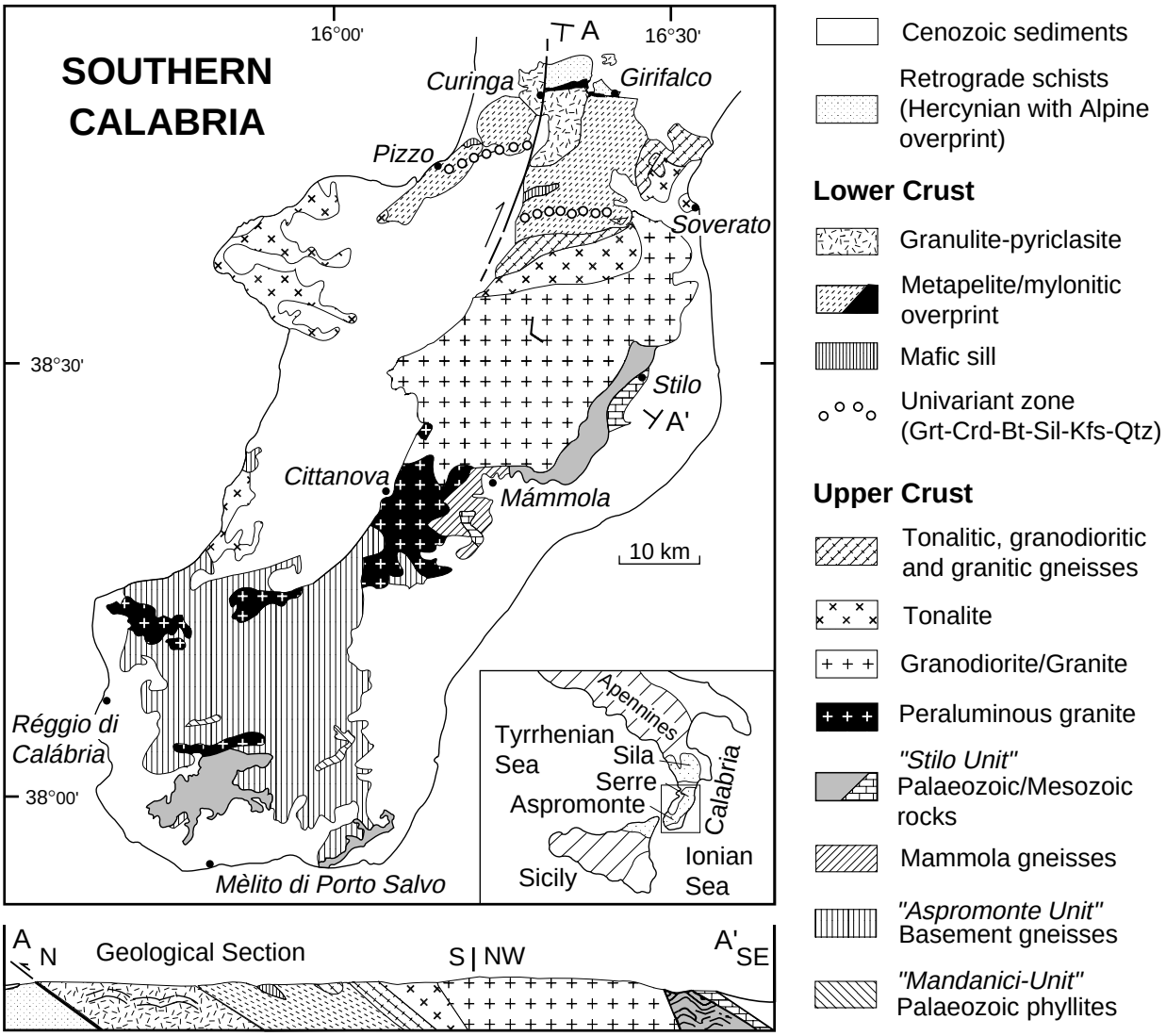

Fig. 1.1 Simplified geological map of southern Calabria and a cross section through the Serre. Modified from Schenk (1980, 1990) (lower crust) and Bonardi *et al.* (1992) (upper crust).

1.4 DISTRIBUTION OF METAMORPHIC ZONES

Palaeozoic metasediments occur in two separate areas of the southern Aspromonte. Only the larger (*c*. 100 km^2), western area, around the village of Bagaladi, will be considered here (Figs 1.1 & 1.2). In the south, the phyllites are overlain by the Stilo-Capo d'Orlando flysch of Miocene age. In the north, according to Crisci *et al.* (1982) and Bonardi *et al.* (1984b), a 1 to 1.5 km broad band of basement gneisses of the underlying Aspromonte unit separates the supposed Alpine nappe of the Stilo unit schists from a late Hercynian peraluminous granite. The latter forms a 12 km long, east-west elongated body parallel to the assumed boundary between the 'Stilo' and the 'Aspromonte' nappes (Figs 1.1 & 1.2). The Palaeozoic sequence, resting on the southern slope of the Aspromonte, and the main regional foliation (S2) dip approximately 30°

towards the south. Late-stage folds (D3) of the regional schistosity, the crenulation cleavage (S3) and mineral lineations (e.g. andalusite and ilmenite porphyroblasts) associated with the regional foliation, all strike approximately east-west.

Metapelitic rocks constitute the major part of the Palaeozoic sediments ('Stilo unit') in this area, but they contain some minor intercalations of semipelitic rocks (greywackes and carbonate-rich schists). On the basis of field observations and petrographic analysis of 170 thin sections, five metamorphic zones have been recognized, namely the chlorite, biotite, garnet, staurolite-andalusite and sillimanite-muscovite zones. Assemblages and sample locations are given in Fig. 1.2. The zones trend east-west and increase in grade towards the north, i.e. where the structurally deeper-lying parts of the sequence are exposed.

The isograd mapping given in Fig. 1.2 is in general agreement with that of Crisci *et al*. (1982), who recognized two kinematic phases, each followed by a static overprint. However, the isograds of Crisci *et al*. (1982) show some noticeable differences to those in Fig. 1.2. In Fig. 1.2 the biotite-in and garnet-in isograds are shifted 1 to 2 km towards the south and - more importantly - we have established an additional sillimanite-in isograd, which trends parallel to, and north of, the assumed Alpine nappe boundary between Stilo and Aspromonte units. The sillimanite isograd is characterized by incipient fibrolitic sillimanite formation at the expense of biotite, similar to that described in other areas (e.g. Barrovian zones, Harte & Johnson, 1969). Its position and orientation fit perfectly into a pattern of continuously increasing metamorphic temperatures from the staurolite-andalusite into the sillimanite-muscovite zone. Muscovite +quartz remains stable up to the contact with the east-west elongated peraluminous granite north of Bagaladi, which intruded the sequence in the late Hercynian.

In the central and northwestern part of the study area, along the well exposed river sections between F. S. Pietro and F. Tuccio (Fig. 1.2), there is no sharp lithological boundary between the assumed Stilo and Aspromonte units but only a slight change from pelitic to increasingly more psammitic compositions towards the north. This is reflected in the disappearence of staurolite and garnet from most rocks (Fig. 1.2). The deformation history (cf. later section) is the same on both sides of the assumed nappe boundary and there is no break in the metamorphic grade. This contrasts to the pattern in the eastern part of the area. Here, garnet zone schists of the Stilo unit rest on retrogressed sillimanite bearing gneisses (Fig. 1.2), and there is a pronounced lithological change from schist to gneiss at the boundary between both units, even in the northeast (sillimanite grade) where no clear break in the metamorphic grade seems to exist. Based on these observations, we agree with former authors that there is a cover (Stilo unit) -basement (Aspromonte unit) relationship, but we conclude that the boundary between both units is cut by the granite (Fig. 1.2). This is similar to the situation at the eastern side of the Serre where the Serre granodiorite intrudes the amphibolite facies 'Mammola gneiss' and the metasediments of the Stilo unit as well (Colonna *et al.*, 1973), which came in tectonic contact prior to the granodiorite

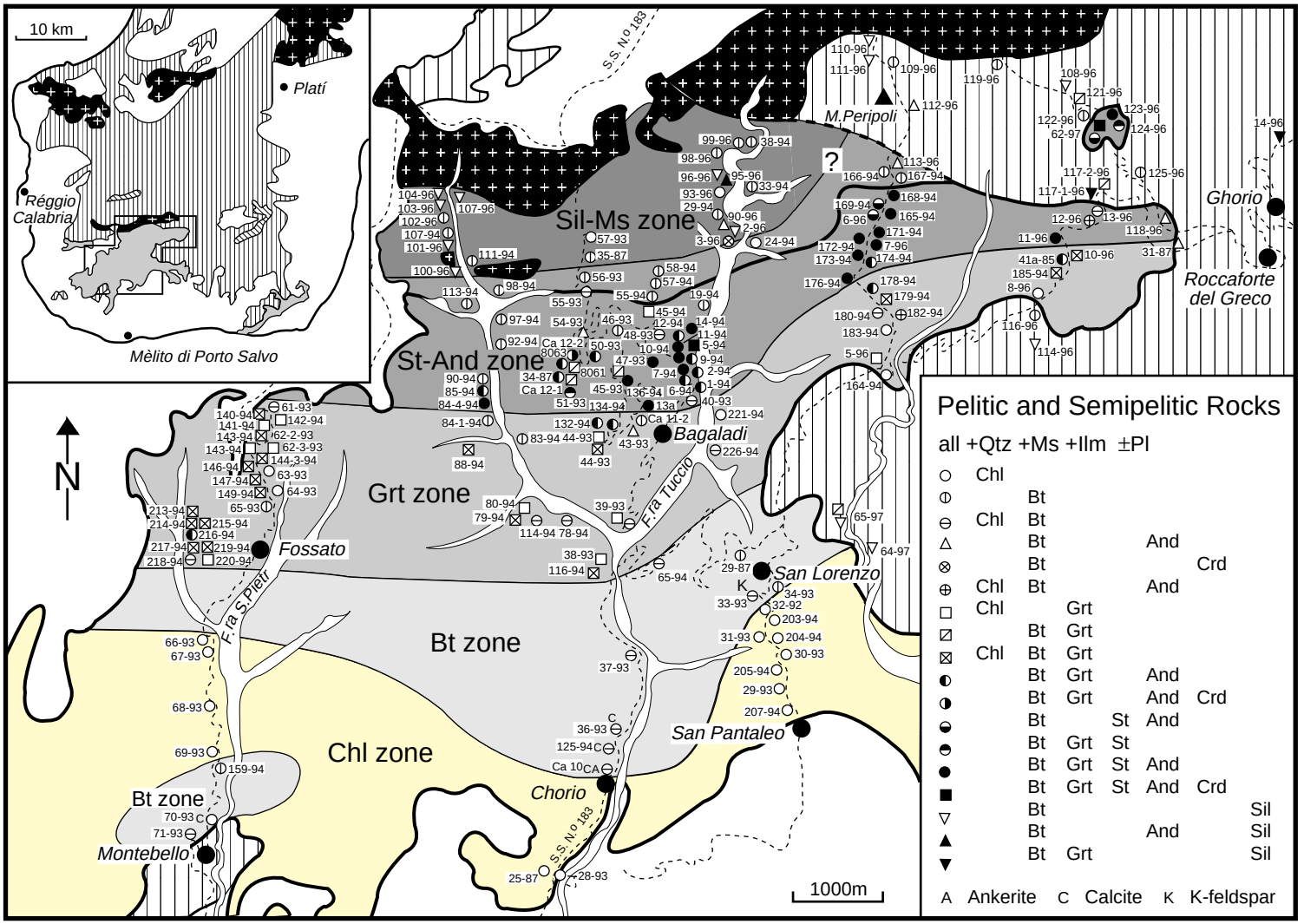

Fig. 1.2 Regional distribution of mineral assemblages of pelitic and semipelitic Palaeozoic rocks of the southern Aspromonte massif ('Stilo Unit'). Heavy line: area of Palaeozoic rocks of the Stilo Unit tectonically overlying the Aspromonte Unit after Crisci et al. (1982); heavy dashed line south of M. Peripoli: approximate position of the boundary between Stilo and Aspromonte Unit according to this study. Thick dotted line represents the nappe boundary between Stilo and Aspromonte units according to Crisci et al. (1982). Simplified geological map in inset after Bonardi et al. (1992). For ornament types see Fig. 1.1.

intrusion. In the Aspromonte area, the boundary between both units has been overprinted by sillimanite grade metamorphism, which makes its identification difficult. In the lower grade zones of the Stilo unit (in the southeast of the area) the boundary is more obvious. Isotopic dating is needed to resolve the cover-basement relationship in this area. However, from the relationship at the granite contact it is obvious that Stilo and Aspromonte units were already in contact at the time of Hercynian granite intrusion.

1.5 METAMORPHIC TEXTURES

The pelites are fine-grained phyllites and micaschists; those of the garnet and staurolite-andalusite zones show macroscopically recognizable porphyroblasts of garnet, biotite and ilmenite at the mm-scale and andalusite up to the cm-scale. Even the metagreywackes and carbonate-rich schists have the appearance of fine-grained (< 0.4 mm) phyllites with detrital feldspar and calcite porphyroblasts up to 2 mm and 0.6 mm across, respectively. The most abundant mineral assemblages in the metapelites are (in addition to muscovite, quartz and plagioclase): Chl (chlorite zone); Chl-Bt (biotite zone); Chl-Bt-Grt (garnet zone); Bt-Grt-St-And (staurolite-andalusite zone); Bt-Sil (sillimanite-muscovite zone; Fig. 1.2). However, some metapelitic rocks of the upper garnet and the staurolite-andalusite zones display the higher grade assemblage Bt-Grt-And. Andalusite is ubiquitous in assemblages with staurolite (except for only two samples) and occurs in samples from the upper garnet to the lower sillimanite-muscovite zone. Ilmenite, as the main accessory phase, is present in all samples. Meta-greywackes contain the same parageneses throughout all zones (Bt±Chl±Kfs in addition to Ms+Qtz±Pl). Meta-carbonate rocks occur only in the biotite zone with the abundant assemblage Chl-Bt-Cal-Ms-Qtz-Pl. Relics of ankerite-inclusions in calcite as a second carbonate phase have been found in one biotite zone sample. In this case biotite is intergrown with chlorite and seems to nucleate at the margin of muscovite.

The slaty cleavage S1 is best seen in samples from the chlorite zone where it is indicated by chlorite and white mica crystallized parallel to the sedimentary layering (Fig. 1.3a). S2 is parallel to axial planes of isoclinal folds in intercalated quartz-feldspar-rich and phyllosilicate-rich sedimentary layers. At fold hinges, S2 cuts perpendicular through the S1 fabric (Fig. 1.3a,b). This new foliation represents the main regional foliation and can be recognized throughout all metamorphic zones. The peak-metamorphic assemblages of each zone grew syntectonically during the formation of this foliation. Phyllosilicates and ilmenite laths lie parallel to S2, other minerals such as plagioclase, andalusite (Fig. 1.3c), staurolite, and most of the garnet show spiral-shape inclusion fabrics, which have traditionally been interpreted as developed during syntectonic (S2) growth of rotating porphyroblasts (Fig. 1.3d).

In all metamorphic zones two textural generations of biotite and muscovite can be distinguished: small elongated crystals lying with their {001} cleavage parallel to the S2 foliation (Bt 1, Ms 1) and large porphyroblasts oriented with their cleavage oblique to it (Bt 2 in Fig. 1.3e,

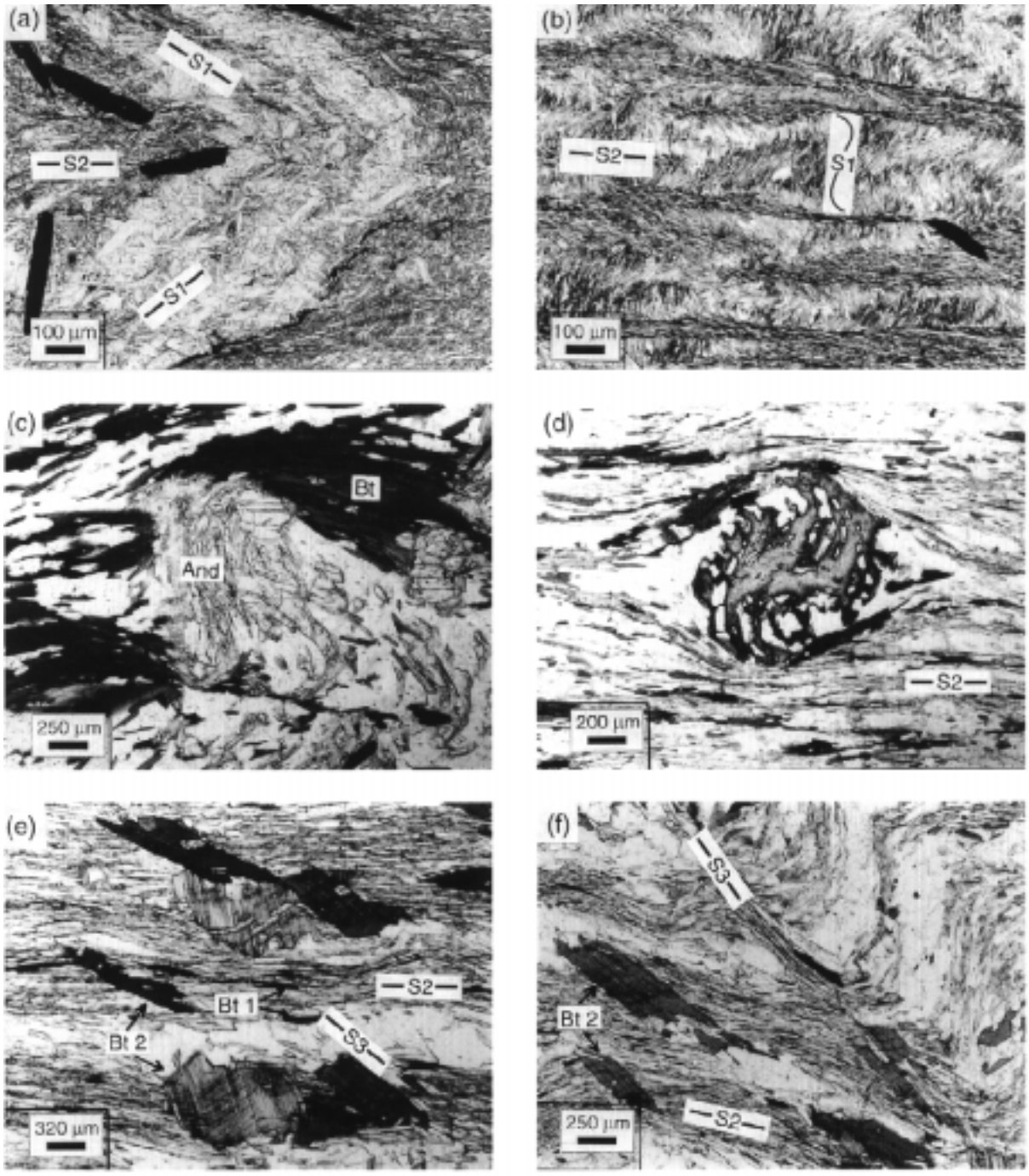

Fig. 1.3 (a) Chlorite zone: folded sedimentary layering defined by alternating quartz-poor and quartz-rich layers. S1, indicated by newly grown mica and chlorite, is parallel to the sedimentary layering. Chlorite and muscovite of S2 are parallel to the axial plane of the fold. (b) Garnet zone: development of the S2 foliation across S1 foliation. (c) Staurolite-andalusite zone: deformed S2 foliation with rotated andalusite porphyroblast. (d) Staurolite-andalusite zone: spiral-shaped garnet interpreted as grown syntectonically with the development of S2. Continuous quartz-spirals within garnet are linked with the outside strain shadows. (e) Two textural types of biotites: small elongated crystals (Bt 1) with their {001} cleavage parallel to the S2 foliation and large oblique Bt 2 porphyroblasts. The latter are rotated and show well defined kinkbands, and are parallel to a third foliation (S3). (f) Staurolite-andalusite zone: folding of the S2 foliation leading to the development of a S3 foliation parallel to the axial plane. Biotite porphyroblasts (Bt 2) lie with the{001} cleavage parallel to S3.

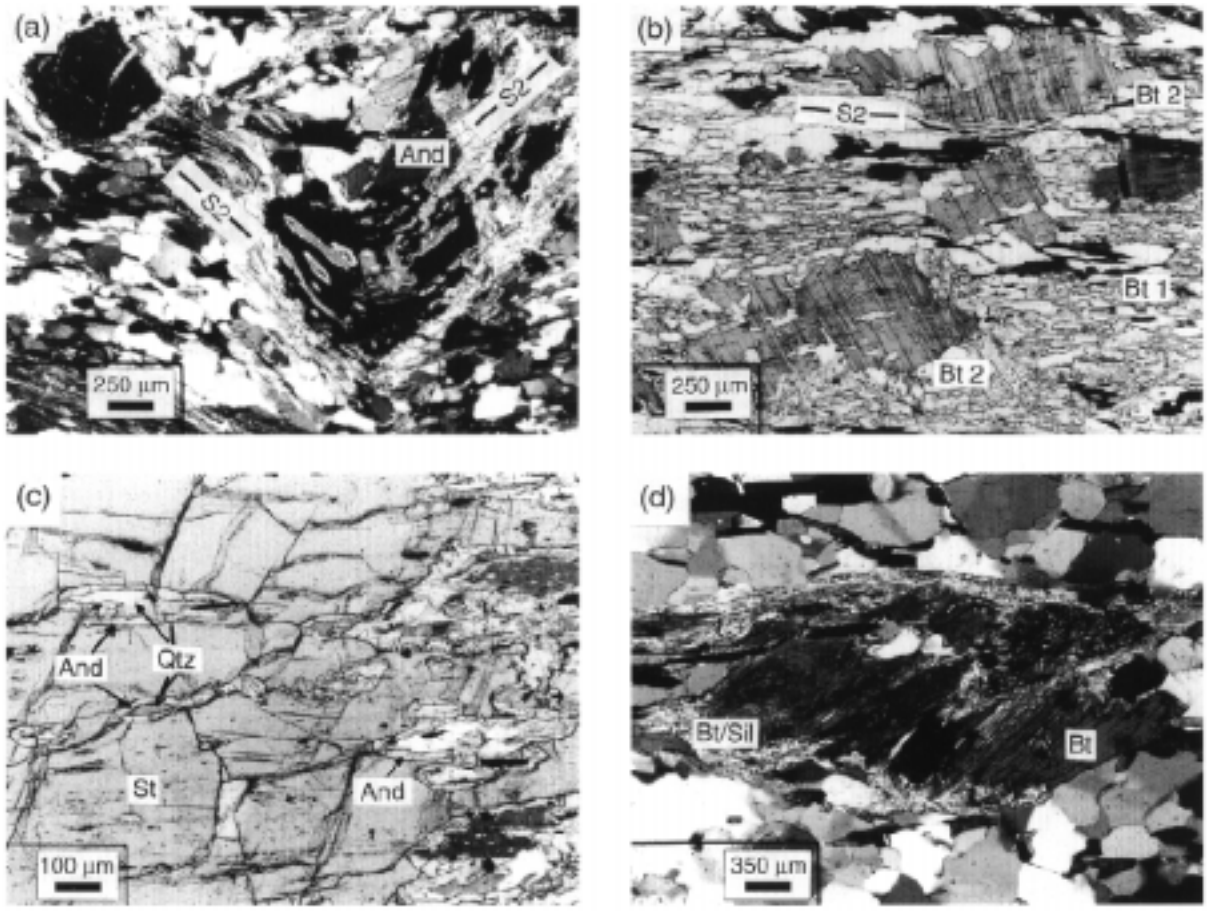

Fig. 1.4 (a) Staurolite-andalusite zone: undeformed andalusite porphyroblast has overgrown a fold of S2 and includes biotite and quartz. (b) Staurolite-andalusite zone: poikilitic andalusite porphyroblast has overgrown the S2 foliation and includes late stage S3-parallel biotite porphyroblasts (Bt 2).(c) Staurolite-andalusite zone: Staurolite porphyroblast surrounded by reaction rims of andalusite. (d) Sillimanite-muscovite zone: fibrolitic sillimanite grows at the expense of biotite.

Ms 2). In the chlorite and biotite zones, Bt 2 is randomly oriented and cuts across the S2 foliation due to postkinematic growth. In the higher metamorphic zones, however, the larger biotite porphyroblasts are rotated and include sigmoidal inclusion trails of S2. They are lying with their {001} cleavage parallel to a third foliation, S3 (Fig. 1.3e,f), which developed through folding (mm-scale) of the S2 foliation. This deformation is not only apparent in thin section but also in the field as open east-west trending folds (D3).

Mineral growth outlasted the deformation, as indicated by cordierite and andalusite porphyroblasts either growing statically over pre-existing folds of S2 (Fig. 1.4a) or enclosing S3-parallel biotite porphyroblasts (Bt 2 in Fig. 1.4b). Staurolite that is not in contact with andalusite often nucleates at the margin of garnet or in phyllosilicate-rich layers. In more aluminous assemblages staurolite is commonly surrounded by andalusite reaction rims, which may also be developed around quartz inclusions in large staurolite porphyroblasts (Fig. 1.4c). Sillimanite of the sillimanite-muscovite zone develops only in rocks with a psammitic Al-poorer bulk composition.

It occurs as fibrolite, forming welts and knots of tiny fibres overgrowing biotite and/or muscovite (Fig. 1.4d), even in andalusite-bearing assemblages. In a few samples fibrolite appears to grow within the S2 foliation beside late stage muscovite which overgrows the S2 fabric.

Retrograde reaction textures are observed mainly in the garnet and staurolite-andalusite zone. Very common are aggregates of muscovite+quartz±biotite±plagioclase grown at the expense of garnet (cf. e.g. Gibson, 1992). In some cases this replacement has resulted in atoll-like garnets. Ubiquitous is secondary chlorite formed after garnet and biotite.

1.6 MINERAL CHEMISTRY

To constrain the *P-T* conditions in the different metamorphic zones, nine samples were studied with the electron microprobe (Table 1.1), using a Camebax microprobe in the wavelength-dispersive mode with 15 kV acceleration potential and 15 nA beam current. Corrections were carried out with the PAP correction program (Pouchou & Pichoir, 1984).

The composition of *garnet* (Table 1.2) is essentially in the range of Alm_{51-81}, Grs_{5-14}, Prp_{1-8}, Sps_{3-45}. Most analysed grains from the garnet and staurolite-andalusite zones exhibit single stage growth zoning patterns (Fig. 1.5b), with distinctive 'bell-shaped' Mn profiles, typical of greenschist to amphibolite facies garnet. Most garnet is characterized by an increase of the almandine and pyrope components and decrease of spessartine and grossular components and of X_{Fe}-values from core to rim. An exception is the garnet of a sample from the lower garnet zone (116-94; Fig. 1.5a), which shows a slight increase in grossular component from core to rim and a conspicuous flat zoning profile with nearly constant X_{Fe}.

Garnet of the staurolite-andalusite zone (sample 47-93; Fig. 1.5c) is clouded with numerous submicroscopical tiny inclusions at the rims (fluids, opaques) and exhibits an abrupt change in prograde zoning within the clouded *c*. 100 mm thick rim. Similar garnet was described by Hames & Menard (1993), who explained this formation as due to metasomatic dissolution and reprecipitation of pre-existing garnet. Only garnet with these clouded rims shows an increase of

Table 1.1 Mineral assemblages of the analysed samples; sample locations are shown in Fig. 1.2; the metamorphic zone of each sample is also indicated; all samples with muscovite, quartz and ilmenite.

Sample	Chl	Bt	Grt	St	Crd	And	Plg	Kfs	Met. zone
28-93	x						x		Chl
33-93	x	x					x	x	Bt
36-93[1]	x	x							Bt
116-94[2]	x	x	x						Grt
217-94	x	x	x				x		Grt
44-93	x	x	x				x		Grt
41a-85		x	x			x	x		Grt
47-93		x	x	x		x	x		St-And
5-94		x	x	x	x	x	x		St-And

Mineral abbreviations after Kretz (1983).
1: 5 Vol % Calcite
2: all biotite alterated to chlorite

Table 1.2 Representative garnet and biotite analyses and structural formulae.

Sample	116-94	116-94	217-94	217-94	44-93	44-93	41a-85	41a-85	47-93	47-93	5-94	5-94
Mineral	Grt	Grt	Grt	Grt	Grt	Grt	Grt	Grt	Grt	Grt	Grt	Grt
Met. zone	Grt	Grt	Grt	Grt	Grt	Grt	Grt	Grt	St-And	St-And	St-And	St-And
	core	rim	core	rim	core	rim	core	rim	core	rim	core	rim
SiO_2	36.50	36.76	36.81	37.09	36.69	37.05	36.83	37.21	36.96	37.01	37.21	37.51
Al_2O_3	20.32	20.39	20.10	20.95	20.09	20.46	20.57	20.94	20.57	20.74	20.66	21.04
FeO	30.97	31.48	24.28	33.88	19.67	27.38	22.69	33.35	28.08	35.13	30.94	35.56
MgO	0.94	0.96	0.32	1.39	0.88	1.49	0.64	1.55	0.73	1.52	1.10	1.89
MnO	7.00	5.78	13.64	2.47	19.67	10.84	15.76	6.43	7.13	4.39	5.90	1.53
CaO	3.49	4.14	4.31	5.10	2.71	2.75	3.50	1.82	6.34	0.95	4.32	3.47
Total	99.22	99.51	99.46	100.88	99.71	99.97	99.99	101.30	99.81	99.74	100.13	101.00
Structural formulae on a basis of 24 oxygens												
Si	6.00	6.02	6.05	5.97	6.02	6.03	6.01	5.99	6.01	6.04	6.03	6.01
Al	3.94	3.93	3.89	3.97	3.89	3.92	3.96	3.97	3.94	3.99	3.95	3.97
Fe(2+)	4.26	4.31	3.34	4.56	2.70	3.73	3.10	4.49	3.82	4.79	4.19	4.77
Mg	0.23	0.23	0.08	0.33	0.22	0.36	0.16	0.37	0.18	0.37	0.27	0.45
Mn	0.98	0.80	1.90	0.34	2.74	1.49	2.18	0.88	0.98	0.61	0.81	0.21
Ca	0.62	0.73	0.76	0.88	0.48	0.48	0.61	0.31	1.10	0.17	0.75	0.60
Total	6.08	6.07	6.07	6.11	6.13	6.06	6.04	6.05	6.08	5.94	6.02	6.02
Alm	70.06	70.98	54.94	74.64	44.07	61.48	51.24	74.18	62.78	80.75	69.67	79.15
Grs	10.11	11.96	12.50	14.39	7.79	7.91	10.13	5.19	18.16	2.80	12.46	9.90
Prp	3.80	3.86	1.29	5.45	3.51	5.96	2.58	6.14	2.91	6.23	4.42	7.49
Sps	16.03	13.20	31.27	5.52	44.64	24.66	36.05	14.49	16.14	10.22	13.46	3.46
Fe/(Fe + Mg)	0.95	0.95	0.98	0.93	0.93	0.91	0.95	0.92	0.96	0.93	0.94	0.91

Sample	33-93	217-94	44-93	41a-85	47-93	5-94
Mineral	Bt	Bt	Bt	Bt	Bt	Bt
Met. zone	Bt	Grt	Grt	Grt	St-And	St-And
	matrix	cont. Grt	matrix	matrix	cont Grt	matrix
SiO_2	34.96	35.98	31.34	34.27	34.51	33.68
TiO_2	2.67	1.30	1.63	1.60	1.72	1.61
Al_2O_3	16.85	20.01	18.08	19.60	19.98	19.50
Cr_2O_3	0.00	0.00	0.00	0.00	0.00	0.10
FeO	22.99	21.27	24.72	22.44	23.27	23.00
MgO	6.64	7.70	9.77	7.16	6.59	7.27
MnO	0.28	0.19	0.31	0.14	0.10	0.09
Na_2O	0.04	0.06	0.08	0.13	0.08	0.18
K_2O	9.81	8.45	6.52	9.29	9.32	8.67
Total	94.24	94.96	92.46	94.63	95.57	94.10
Structural formulae on a basis of 22 oxygens						
Si	2.76	2.75	2.52	2.67	2.67	2.64
Al(IV)	1.24	1.26	1.48	1.33	1.33	1.36
Al(VI)	0.33	0.55	0.23	0.47	0.49	0.45
Ti	0.16	0.08	0.10	0.09	0.10	0.10
Cr	0.00	0.00	0.00	0.00	0.00	0.01
Fe(2+)	1.52	1.36	1.66	1.46	1.50	1.51
Mg	0.78	0.88	1.17	0.83	0.76	0.85
Mn	0.02	0.01	0.02	0.01	0.01	0.01
Total	2.80	2.87	3.19	2.87	2.86	2.91
Na	0.01	0.01	0.01	0.02	0.01	0.03
K	0.99	0.82	0.67	0.92	0.92	0.87
Total	0.99	0.83	0.68	0.94	0.93	0.90
Fe/(Fe + Mg)	0.66	0.61	0.59	0.64	0.66	0.64

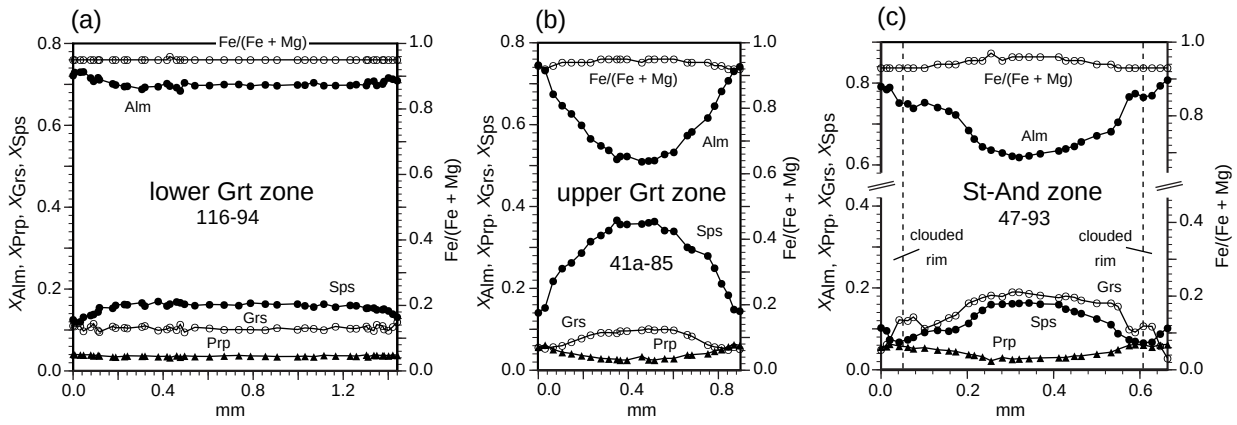

Fig. 1.5 Garnet zoning profiles from Palaeozoic metapelites, southern Aspromonte: (a) lower garnet zone, (b) upper garnet zone, (c) staurolite-andalusite zone. Each profile extends from rim to rim through the core of the garnets.

spessartine content towards the outer part of the rim, suggesting resorption during retrogression (Fig. 1.5c). The zone of spessartine enrichment may coincide (sample 5-94) with a slight increase of X_{Fe} due to retrograde Fe-Mg exchange with matrix minerals. The spessartine content of cores of all analysed garnet is relatively high and decreases from the garnet zone ($Sps_{16\text{-}44}$) to the staurolite-andalusite zone ($Sps_{11\text{-}16}$) which suggests the start of intracrystalline homogenization in the higher grade zones.

Staurolite compositions are very similar in all analysed samples (Table 1.3). MnO and ZnO contents are very low and vary only slightly (0.23-1.25 and 0.17-1.2 wt%, respectively). Staurolite is unzoned and shows lower X_{Fe}-values (0.87-0.88) than coexisting garnet.

Compositions of *biotite* from all metamorphic zones are given in Table 1.2. No compositional differences have been observed between the two textural types of biotites (Fig. 1.3). Some biotite, especially that of sample 44-93 (garnet zone), show low K_2O content, probably resulting from partial alteration to chlorite. Surprisingly, the X_{Fe}-values increase from the garnet towards the staurolite-andalusite zone, which is opposite to the shift one would expect with increasing metamorphic grade. No systematic increase in Ti- and Mg-content with increasing metamorphic grade is found (Fig. 1.6), in contradiction with findings in other areas (e.g. Robinson *et al.*, 1982).

All samples of pelitic composition contain primary *muscovite*. There is no compositional difference between those lying parallel or oblique to the S2 foliation. With increasing metamorphic grade the composition of muscovite becomes more homogeneous within and between samples and the phengite component decreases (Fig. 1.7a; Table 1.3). Exceptions are micas from the chlorite zone which are similar to those from the garnet zone and plot in a narrow compositional range despite their low metamorphic grade. Similar gradual reduction in the phengite component of muscovite with metamorphic grade has been described by several authors (e.g. Mather, 1970;

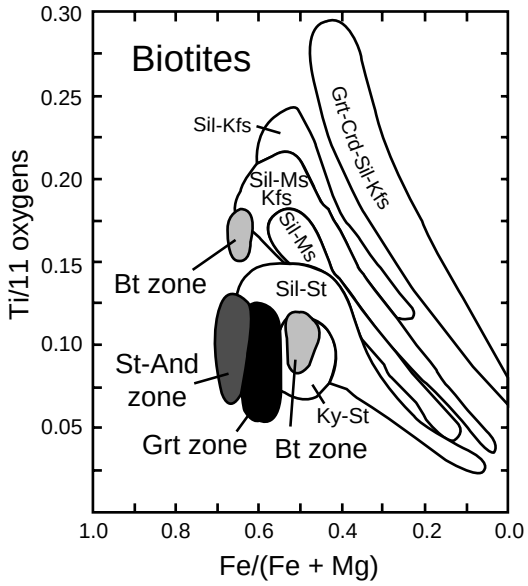

Fig. 1.6 Plot of Ti (per 11 oxygens) as a function of Fe/(Fe+Mg) for biotites from different metamorphic zones. Unshaded fields: compositional ranges of biotite from metamorphic zones in New England (Robinson *et al.*, 1982).

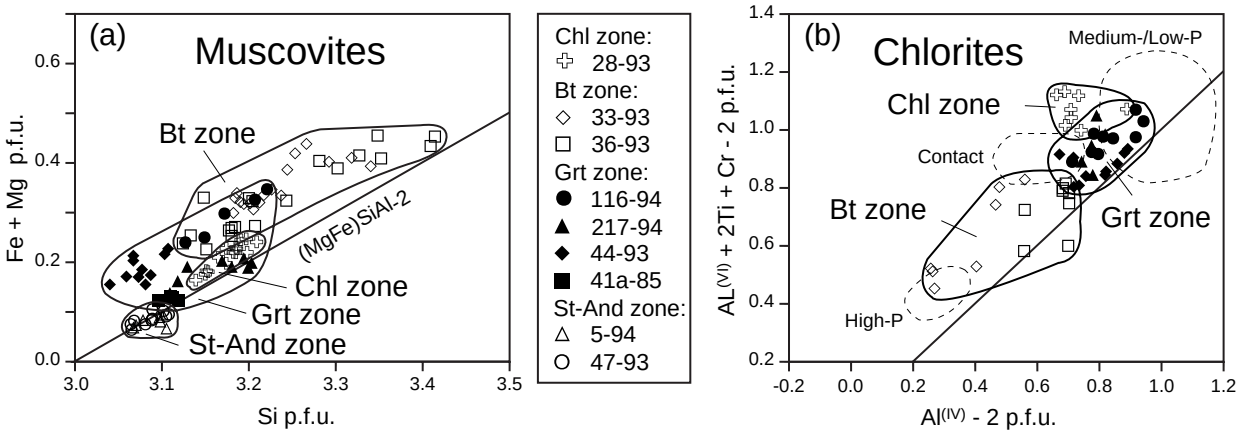

Fig. 1.7 (a) Chemical compositions of muscovites from different metamorphic zones. Si (per 11 oxygens) against Fe+Mg. The line of phengite substitution is indicated. (b) Chlorite compositions of the different metamorphic zones on a formula proportion diagram (Al(VI)+2Ti+Cr-2 versus Al(IV)-2). The end member clinochlore/chamosite plots at the origin. Compositional variation along the 1:1 tie line represents the Tschermak substitution. Indicated fields of different metamorphic regimes after Laird (1988).

Wang *et al.*, 1986; Dempster & Tanner, 1997) in different low- to medium-pressure metamorphic terranes. This is interpreted as due to continuing re-equilibration of detrital white micas and formation of muscovite by net-transfer reactions (e.g. reactions (2) and (3), see below; cf. discussion in Miyashiro & Shido, 1985).

Table 1.3 Representative muscovite, chlorite, staurolite and plagioclase analyses and structural formulae.

Sample	28-93	33-93	36-93	116-94	217-94	44-93	41a-85	47-93	5-94
Mineral	Ms	Ms	Ms	Ms	Ms	Ms	Ms	Ms	Ms
Met. zone	Chl	Bt	Bt	Grt	Grt	Grt	Grt	St-And	St-And
SiO_2	47.99	46.77	47.81	47.11	48.67	45.84	47.12	47.32	47.27
TiO_2	0.33	0.58	0.51	0.27	0.25	0.29	0.29	0.24	0.24
Al_2O_3	33.16	31.07	31.05	32.44	34.34	34.81	35.45	36.22	36.38
Cr_2O_3	0.03	0.02	0.10	0.04	0.00	0.00	0.00	0.00	0.00
FeO	2.06	3.17	2.63	3.47	1.44	2.36	1.27	1.00	0.90
MgO	1.17	1.39	1.82	1.03	1.15	0.54	0.62	0.00	0.41
MnO	0.03	0.04	0.97	0.02	0.00	0.00	0.00	0.48	0.00
Na_2O	0.69	0.17	0.37	0.73	0.52	1.62	1.23	1.36	1.37
K_2O	10.08	10.97	10.72	9.73	10.17	9.16	9.59	9.21	9.36
Total	95.54	94.18	95.98	94.84	96.54	94.65	95.57	95.83	95.93
Structural formulae on a basis of 22 oxygens									
Si	3.19	3.19	3.20	3.17	3.18	3.08	3.11	3.10	3.10
Al(IV)	0.82	0.81	0.80	0.83	0.82	0.92	0.89	0.90	0.90
Al(VI)	1.78	1.69	1.65	1.75	1.83	1.83	1.87	1.90	1.91
Ti	0.02	0.03	0.03	0.01	0.01	0.02	0.01	0.01	0.01
Cr	0.00	0.00	0.01	0.00	0.00	0.00	0.00	0.00	0.00
Fe(2+)	0.11	0.18	0.15	0.20	0.08	0.13	0.07	0.06	0.05
Mg	0.12	0.14	0.18	0.10	0.11	0.05	0.06	0.05	0.04
Mn	0.00	0.00	0.06	0.00	0.00	0.00	0.00	0.00	0.00
Total	2.03	2.04	2.07	2.06	2.03	2.03	2.01	2.02	2.01
Na	0.09	0.02	0.05	0.10	0.07	0.21	0.16	0.17	0.17
K	0.85	0.95	0.92	0.84	0.85	0.78	0.81	0.77	0.78
Total	0.94	0.98	0.96	0.93	0.91	1.00	0.97	0.94	0.96
Fe/(Fe + Mg)	0.50	0.56	0.45	0.65	0.41	0.71	0.53	0.54	0.55

Sample	28-93	33-93	36-93	116-94	217-94	44-93
Mineral	Chl	Chl	Chl	Chl	Chl	Chl
Met. zone	Chl	Bt	Bt	Grt	Grt	Grt
SiO_2	24.37	25.02	25.16	22.96	24.55	24.42
TiO_2	0.04	0.20	0.04	0.10	0.09	0.06
Al_2O_3	22.52	18.44	21.91	22.87	22.28	22.57
Cr_2O_3	0.00	0.02	0.00	0.00	0.04	0.00
FeO	29.92	31.68	24.84	32.22	29.07	27.47
MgO	10.75	10.36	15.13	9.01	12.28	13.18
MnO	0.10	0.27	0.14	0.26	0.37	0.55
CaO	0.00	0.04	0.39	0.00	0.00	0.00
Total	87.70	86.03	87.61	87.42	88.68	88.30
Structural formulae on a basis of 28 oxygens						
Si	5.26	5.60	5.30	5.06	5.22	5.18
Al(IV)	2.74	2.40	2.70	2.94	2.78	2.82
Al(VI)	2.99	2.46	2.74	3.00	2.81	2.83
Ti	0.01	0.03	0.01	0.02	0.01	0.01
Cr	0.00	0.00	0.00	0.00	0.01	0.00
Fe(2+)	5.40	5.93	4.37	5.94	5.17	4.88
Mg	3.46	3.46	4.75	2.96	3.90	4.17
Mn	0.02	0.05	0.03	0.05	0.07	0.10
Ca	0.00	0.01	0.09	0.00	0.00	0.00
Total	11.87	11.94	11.98	11.96	11.97	11.98
Fe/(Fe + Mg)	0.61	0.63	0.48	0.67	0.57	0.54

Sample	28-93	33-93	217-94	44-93	44-93	41a-85	41a-85	47-93
Mineral	Pl	Pl	Pl	Pl	Pl	Pl	Pl	Pl
Met. zone	Chl matrix	Bt matrix	Grt matrix	Grt rim	Grt core	Grt rim	Grt core	St-And matrix
SiO_2	69.71	68.17	62.64	67.12	68.64	67.00	66.73	65.79
Al_2O_3	19.68	19.31	23.26	20.84	19.88	20.56	21.48	22.16
Fe_2O_3	0.12	0.03	0.12	0.09	0.00	0.02	0.00	0.08
CaO	0.00	0.00	4.94	1.67	0.45	1.17	1.87	3.06
Na_2O	11.48	11.38	8.91	10.91	11.51	10.93	10.58	9.55
K_2O	0.05	0.07	0.06	0.07	0.07	0.04	0.09	0.07
Total	101.04	98.96	99.93	100.70	100.55	99.72	100.75	100.71
Structural formulae on a basis of 8 oxygens								
Si	3.01	3.00	2.78	2.93	2.98	2.94	2.91	2.87
Al(IV)	1.00	1.00	1.22	1.07	1.02	1.06	1.10	1.14
Total	4.01	4.01	3.99	4.00	4.00	4.01	4.01	4.01
Fe(3+)	0.00	0.00	0.00	0.00	0.00	0.00	0.00	0.00
Ca	0.00	0.00	0.24	0.08	0.02	0.06	0.09	0.14
Na	0.96	0.97	0.77	0.92	0.97	0.93	0.89	0.81
K	0.00	0.00	0.00	0.00	0.00	0.00	0.01	0.00
Total	0.97	0.98	1.01	1.01	1.00	0.99	0.99	0.96
An	0.00	0.00	23.41	7.77	2.11	5.57	8.83	14.97
Ab	99.69	99.59	76.29	91.83	97.49	94.22	90.66	84.61
Kfs	0.31	0.41	0.30	0.40	0.40	0.20	0.51	0.42

Sample	47-93	5-94
Mineral	St	St
Met. zone	St-And	St-And
SiO_2	27.49	26.87
TiO_2	0.33	0.41
Al_2O_3	54.23	54.8
FeO	12.64	12.52
MgO	0.97	1.06
MnO	0.23	1.25
ZnO	1.20	0.17
Total	97.09	97.08
Basis of Si + Al = 25.53		
Si	7.68	7.50
Ti	0.07	0.09
Al	17.85	18.03
Fe(2+)	2.95	2.92
Mg	0.40	0.44
Mn	0.05	0.04
Zn	0.25	0.26
Total	29.26	29.28
Fe/(Fe + Mg)	0.88	0.87

Sample	5-94
Mineral	Crd
Met. zone	St-And
SiO_2	48.32
TiO_2	0.04
Al_2O_3	30.86
FeO	11.27
MgO	6.18
MnO	0.19
CaO	0.03
Na_2O	0.77
Total	97.66
basis of 18 oxygens	
Si	5.09
Al	0.91
Al	2.92
Ti	0.00
Total	2.93
Fe(2+)	0.99
Mg	0.97
Mn	0.02
Total	1.98
Ca	0.00
Na	0.16
Total	0.16
Fe/(Fe+Mg)	0.51

Prograde *chlorite* is only present from the chlorite up to the garnet zone (Table 1.2). Retrograde chlorite, that formed as an alteration product of biotite and garnet has the same composition as the prograde variety. No correlation between metamorphic grade and Al-content can be observed (Fig. 1.7b).

Feldspar from the chlorite and biotite zones is nearly pure albite (Table 1.3). An exception is sample 33-93 from the biotite zone, with a greywacke composition, which contains albite (An_{01}) along with alkali feldspar (Kfs_{93}). In the garnet zone the anorthite component is slightly higher (up to An_{09}), but one sample (217-94) even contains oligoclase (An_{20-23}) which is unzoned. In retrograde crystallized oligoclase of the same sample the An-component rises up to An_{27-31}. Two

samples have zoned plagioclase: increasing anorthite content from core to rim (An_{02} to An_{07}), in sample 44-93, whereas the opposite zoning was observed in sample 41a/85 (core An_{09} to rim An_{06}). In the staurolite-andalusite zone, plagioclase was found in only one sample (47-93). The composition of plagioclase clusters around two ranges, An_{05-09} and An_{13-15}, indicating that equilibrium was not attained. Peak-metamorphic compositions are most likely represented by the higher An values whereas the former ones might be relics of plagioclase grown early in metamorphic history. Retrograde plagioclase replacing garnet has An_{10-12}.

Ilmenite occurs as primary matrix phase, as porphyroblast and as inclusion in garnet. MnO content ranges between 0.02 and 0.14 wt%.

One of the analysed samples (5-94) of the staurolite zone contains *cordierite* besides garnet, staurolite and andalusite. The cordierite is unzoned with Na_2O contents at about 0.8 wt% and X_{Fe} at 0.51, pointing to low metamorphic pressures.

1.7 PHASE RELATIONS AND REACTION HISTORY

The observed mineral assemblages, the analysis of reaction textures and the mineral compositions can be used to reconstruct the reaction history of the rocks. For depicting phase compatibilities in metapelites, which contain quartz and muscovite and had a vapour phase in excess, the AFM projection (Thompson, 1957) is widely used. Since MnO and CaO very often are essential constituents in garnet and are also common as minor components in other minerals of metapelitic assemblages, the simple projection of these assemblages in the AFM diagram violates the rules of the Thompson projection. In the literature there is no unanimous opinion on how to treat those 'extra components'. In most cases MnO is ignored, which shifts the compositions of coexisting phases to lower X_{Fe}. In this paper we deal with the influence of 'extra components' on the plotting position of the studied minerals in two ways: first MnO and FeO are combined into a single component in the AFM projection following e.g. Azor & Ballèvre (1997). Figure 1.8a-c shows the results of this procedure for muscovite+quartz-bearing assemblages from the chlorite to staurolite-muscovite zones. As can be inferred from composition of coexisting phases, the studied metapelites are all Al-poor and Fe-rich (only sample 36-93 of the biotite zone is relatively Mg-rich), and most of their bulk compositions plot below the garnet-chlorite tie line. No significant shift of the three phase fields can be recognized with increasing metamorphic grade.

A second approach of the graphical presentation utilizes the scheme of 'thermodynamic projection' described by Spear (1988). The method is used to correct the compositions of the minerals to the composition that they would have if there were no, in our case, MnO and CaO in the system. Figure 1.8d shows the results when the minerals are plotted in a composition triangle (FeO-MgO-MnO) projected to CaO=0 (calculation was performed with the Gibbs program by Spear & Menard, 1989; version 4.7, 1997). Garnet is particularly MnO-rich and its MnO-content therefore has an influence on the projected plotting position of coexisting minerals. This influence

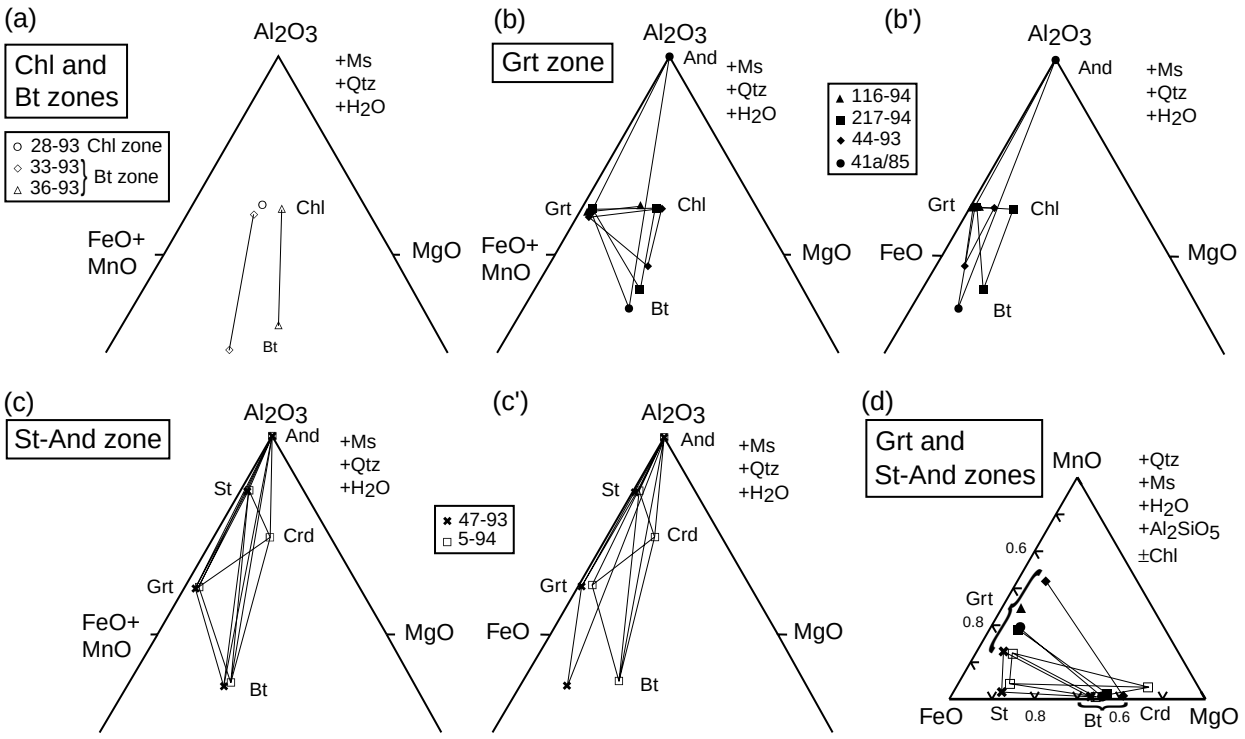

Fig. 1.8 (a) to (c) Al_2O_3-(FeO+MnO)-MgO projection from quartz, muscovite and H_2O of coexisting minerals in different metamorphic zones of the Palaeozoic metapelites of the southern Aspromonte. (b') and (c') AFM projections for mineral compositions computed at X_{CaO}~X_{MnO}~0 (after Spear, 1988). (d) Composition triangle (FeO-MgO-MnO) showing composition of coexisting minerals of the garnet and staurolite-andalusite zones projected to X_{Grs} =0.0001 in a nearly CaO free system.

is recognizable in the Al_2O_3-FeO-MgO triangles (Fig. 1.8b', c') for extrapolated CaO and MnO free compositions. It is obvious that the 'extra components' MnO and CaO shift the compositions of the coexisting phases to lower X_{Fe}, though biotite, chlorite and staurolite contain no appreciable content of these components. For sample 5-94 with only small amounts of grossular and spessartine in garnet (X_{Grs}= 0.10 and X_{Sps}= 0.03), the shift of the plotting positions is only minor.

Phase relations of low- to medium-grade metapelites and the influence of the extra component MnO on these phase relations in *P-T* space were a matter of debate in recent years (Spear & Cheney, 1989; Droop & Harte, 1995; Mahar *et al.*, 1997). The most important effect of Mn on the pelitic assemblages studied here is that the fractionation of Mn into garnet expands the *P-T* stability field of the assemblage Grt-Chl-Bt (eg. Spear & Cheney, 1989; Symmes & Ferry, 1992; Mahar *et al.*, 1997). Figure 1.8d shows the relatively high MnO content of garnet in the three-phase AFM assemblage Grt-Chl-Bt of the Stilo unit garnet zone. An additional example of the Mn influence on phase relations is given by the occurrence, in the pure KFMASH-system, of the higher-grade assemblage Grt-Bt-And together with the assemblage Grt-Bt-Chl in the garnet zone or together with Grt-St-Bt-And in the staurolite-andalusite zone (Figs 1.2 & 1.8b,b'). As is obvious from the FeO-MgO-MnO projection of sample 41a/85 in Fig. 1.8d, the apparently higher

grade assemblage Grt-Bt-And is stabilized to lower grades by the incorporation of MnO into garnet. This applies also to the four-phase AFM assemblage Grt-St-Bt-And, which is not only characteristic of the andalusite-staurolite zone of the Stilo unit (Fig. 1.8c,c'), but also very common in several other low-*P* metamorphic terranes (e.g. Pyrenees and South Australia; Gibson, 1992; Dymoke & Sandiford, 1992). However, as can be seen from Fig. 1.8d, staurolite is found only in samples with low-spessartine garnet. For a more satisfactorily discussion of the effect of MnO on mineral stability the reader is referred to the papers by Giaramita & Day (1991) and Dymoke & Sandiford (1992). Additionally, the incorporation of the components TiO_2 in biotite and ZnO in staurolite may also have an influence on the phase relations, but are not considered further here.

Despite the difficulties inherent to the presence of additional components, the petrogenetic grid of the KFMASH system of Spear & Cheney (1989) agrees well with the sequence of mineral reactions and assemblages found in the metapelites of the Stilo unit (Figs 1.8 & 1.9). The grid predicts a stability field of the divariant AFM assemblage Grt-Chl-Bt at low pressures, limited by two univariant reactions to upper (Grt + Chl = St + Bt) and lower (Ctd + Bt = Grt + Chl) temperatures. A series of AFM phase diagrams along a *P-T* array at low pressures, evolving in the andalusite stability field, suggests the stability of Grt-Chl-Bt in subaluminous Fe-rich bulk compositions even in the MnO-free system (Spear & Cheney, 1989). With rising temperatures the latter assemblage should be followed by Grt-St-Bt which is indeed developed in the Stilo unit metapelites of the Aspromonte (Figs 1.8 & 1.9).

A contrasting petrogenetic grid proposed for the KFMASH system, predicts the invariant point with the assemblage Grt-Bt-Chl-Ctd-St either outside the andalusite stability field (*c*. 7 kbar; Droop & Harte, 1995) or near the And/Ky phase transition line (*c*. 4.2 kbar; Mahar *et al.*, 1997). The sequence described in the Stilo unit metapelites with Grt-Bt-St following Grt-Chl-Bt would only occur along a *P-T* array above the invariant point at higher pressures. This would be in contradiction to the stable alumosilicate andalusite at this metamorphic grade of the sequence. At pressures below the invariant point (in the andalusite stability field) in subaluminous Fe-rich bulk compositions the assemblage Grt-Ctd-Bt is expected to be always stable between a Grt-Chl-Bt and a Grt-St-Bt zone. This Ctd-bearing assemblage has not been found in the Stilo unit metapelites. The only described Ctd-bearing rock from that area has been assigned to the chlorite zone. These observations led us to apply the alternative grid proposed by Spear & Cheney (Fig. 1.9).

1.7.1 The biotite-in isograd

At the biotite-in isograd biotite appears only in semipelitic rocks of greywacke and carbonate-rich compositions (up to 50% carbonate). North of the village of Chorio (Fig. 1.2) calcareous sediments reveal relics of ankerite in a matrix of muscovite+calcite+quartz besides Bt+Chl-intergrowth at the margin of muscovite. This texture may relate to the biotite-producing reaction

$$Ms + Qtz + Ank + H_2O = Cal + Bt + Chl + CO_2 \quad (1).$$

This reaction has been described by Ferry (1976) for schists in New England where it occurs at about the same grade as the biotite-in isograd in metapelites. Near the village of San Lorenzo (Fig. 1.2) the appearance of biotite in greywackes with detrital K-feldspar can be explained by the continuous reaction

$$Kfs + Chl = Bt + Ms + Qtz + H_2O \quad (2).$$

This reaction is also proposed by Mather (1970) for pelites of the Scottish Dalradian. Further north, towards deeper sections of the biotite zone, pelites lacking K-feldspar dominate the metasedimentary sequence. In these rocks biotite forms most probably by the continuous reaction

$$Phe + Chl = Bt + \text{Phe-poor Ms} + Qtz + H_2O \quad (3).$$

According to Mather (1970) this reaction involves the progressive replacement of chlorite and the reduction of the phengite component in muscovite. This is in accordance with the observed change of the chemistry of muscovite with increasing grade discussed above.

1.7.2 The garnet-in isograd

The appearance of garnet is most probably related to the two continuous reactions

$$Chl + Qtz = Grt + H_2O \quad (4) \text{ and}$$

$$Chl + Ms + Qtz = Grt + Bt + H_2O \quad (5)$$

deduced from the AFM-phase compatibilities (Fig. 1.8).

Chloritoid as a possible reactant for garnet formation was not observed in the metapelites studied here, either due to the high MnO content of garnet which expands the Grt-Chl stability field to lower temperatures, or to the Al-poor bulk compositions of the pelites preventing the appearance of chloritoid (Spear & Cheney, 1989).

1.7.3 The staurolite-andalusite zone

The first appearance of staurolite is related to two reactions. Textures showing the formation of staurolite at the expense of garnet suggests the discontinuous reaction

$$Grt + Chl + Ms = St + Bt + Qtz + H_2O \quad (6).$$

In garnet-free assemblages, staurolite is probably formed by the continuous reaction

$$Chl + Ms = St + Bt + Qtz + H_2O \quad (7).$$

This reaction can be deduced from AFM-phase compatibilities and from metamorphic textures as well, since staurolite grew mainly in phyllosilicate-rich layers. These reactions account for the disappearance of primary chlorite in the staurolite-andalusite zone (cf. Figs 1.2 & 1.8). The characteristic reaction texture for this zone, andalusite rims surrounding staurolite porphyroblasts, forms due to the continuous breakdown reaction of staurolite+quartz+muscovite (Fig. 1.4c):

$$St + Ms + Qtz = Bt + And + H_2O \quad (8).$$

In many samples with this texture garnet is also present and may have been involved in the reaction.

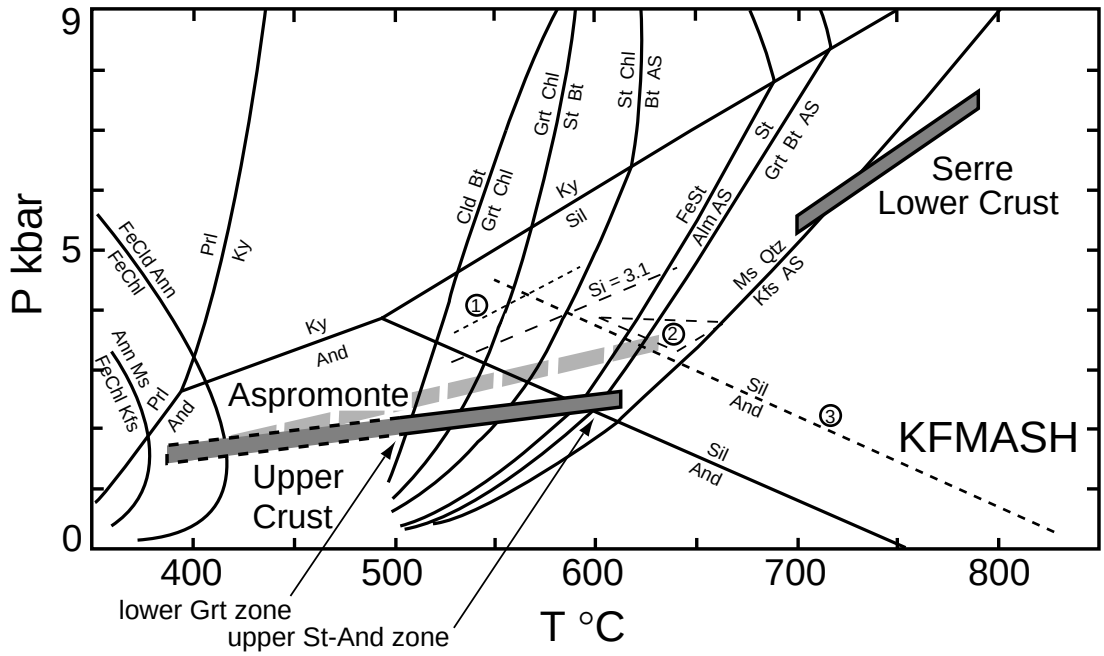

Fig. 1.9 *P-T* grid for pelites in the KFMASH system after Spear & Cheney (1989) with results of the garnet-biotite and garnet-cordierite thermometry for samples of the lower garnet zone and upper staurolite-andalusite zone. Thermal conditions in the lower crustal section of the Serre after Schenk (1990) and in Palaeozoic metasediments of the upper crustal section in the Aspromonte area (this study). Thick dashed upper crust bar shows possible *P-T* conditions in the upper crust if the andalusite-sillimanite phase boundary (reaction 3) after Pattison (1992) is applied. Si=3.1 isopleth for muscovite after Massonne & Schreyer (1987). Reaction 1: garnet-plagioclase-muscovite-biotite equilibrium (Hodges & Crowley, 1985) calculated for sample 47-93 of the staurolite-andalusite zone. Dashed triangle 2: TWEEQU results for garnet-cordierite-andalusite-biotite-muscovite-quartz-H_2O assemblage of sample 5-94 (activity models for garnet, cordierite: Berman & Aranovich, 1996; biotite: unpublished data of Berman & Aranovich, 1997; muscovite: Chatterjee & Froese, 1975).

One analysed sample (5-94) contains cordierite porphyroblasts overgrowing the pre-existing assemblage. Unfortunately, there is no reaction texture enlightening the cordierite forming reaction. The cordierite might not be in equilibrium with the main matrix minerals since cordierite represents the fifth 'AFM-mineral' in this assemblage and is very Fe-rich (Fig. 1.8). Alternatively, the stable coexistence of the five 'AFM-phases' might be due to the presence of MnO in garnet and of ZnO in staurolite.

1.7.4 The sillimanite-muscovite-in isograd

Sillimanite occurs as fibrolitic fibres overgrowing biotite and/or muscovite (Fig. 1.4d). According to the model of Carmichael (1969), the development of fibrolite at the expense of micas may be related to a series of local metasomatic cation-exchange reactions.

Table 1.4 Temperature estimates for different metamorphic zones as obtained with the garnet-biotite and the garnet-cordierite geothermometry at P=2 kbar.

Sample	Met. zone	T(°C) H&S	T(°C) K&R	T(°C) (B)	T(°C) (T)
217-94	Grt	492	527		
44-93	Grt	522	530		
41a-85	Grt	525	540		
47-93	St-And	530	543		
5-94	St-And	590	580	600	580

Grt-Bt: H&S: Hodges & Spear (1982); K&R: Kleemann & Reinhardt (1994)
Grt-Crd: B: Bhattacharya, Mazumdar & Sen (1988); T: Thompson (1976)

1.8 *P-T* CONDITIONS

Estimates of metamorphic temperatures for the garnet and the staurolite-andalusite zones are based on Fe-Mg exchange between garnet and biotite. The calibrations of Hodges & Spear (1982) and Kleemann & Reinhardt (1994) were used as these take into account the influence of high spessartine content in garnet. A problem with some estimates is due to the partial retrograde chloritization of some of the analysed biotite. An additional temperature estimate was made for a sample of the upper staurolite-andalusite zone (5-94) applying the Fe-Mg exchange between garnet and cordierite (Thompson, 1976; Bhattacharya *et al.*, 1988), despite the fact that both phases might not be in equilibrium.

Using the compositions of less altered biotite, of unzoned cordierite and the rim compositions of prograde zoned garnet or the minimum X_{Fe}-values near the rims (Tables 1.2 & 1.3), the thermometry reveals increasing temperatures from the lower garnet zone (*c*. 500 °C) to the upper staurolite-andalusite zone (*c*. 590 °C; Table 1.4). Reaction textures in the latter zone point to the partial breakdown of staurolite (St + Ms + Qtz = Bt + And ± Grt + H_2O) within the stability field of andalusite. This discontinuous reaction (with garnet) indicates maximum temperatures of about 590 °C at low pressures (*c*. 2.5 kbar; Spear & Cheney, 1989; Fig. 1.9) which are the same as for the results of garnet-biotite and garnet-cordierite thermometry from the upper part of this zone. The peak metamorphic temperatures in the sillimanite-muscovite zone must have been lower than *c*. 620 °C with pressures of about 2.5 kbar because there has been no breakdown of Ms + Qtz. If garnet is not invoved, the staurolite-breakdown is a continuous reaction (St + Ms + Qtz = Bt + And + H_2O), commencing at lower temperatures than the discontinuous one discussed previously.

In addition, pressures have been estimated using the garnet-plagioclase-muscovite-biotite barometer (GPMB; Hodges & Crowley, 1985), using garnet and plagioclase rim compositions of zoned minerals. Calculated pressures of about 7-8 kbar for the garnet zone samples are unrealistically high, probably due to the low anorthite content of the plagioclase. These estimates lie in the stability field of kyanite and in the range of values of 5.5-7.5 kbar deduced for the

granulite facies lower crustal part of the section (Schenk, 1990). A reason for the high pressure results might be disequilibrium with respect to CaO for coexisting garnet and plagioclase (e.g. Chernoff & Carlson, 1997), which is enhanced by the low metamorphic temperatures and the scarcity of plagioclase. The sample from the staurolite-andalusite zone (47-93) gives values ranging between 4 and 5 kbar (GPMB equilibrium 1 in Fig. 1.9), which are much lower than those of the garnet zone but are still too high in comparison with pressures deduced from simple phase equilibria in the KFMASH system. When the andalusite-sillimanite phase boundary is shifted to higher *P-T* values as proposed by e.g. Pattison (1992; cf. Fig. 1.9), its intersection with the discontinuous staurolite-breakdown reaction is at *c*. 3.5 kbar. This pressure is still lower than the pressures calculated with the GPMB equilibrium.

Additional pressures were estimated for the staurolite-andalusite zone, using the phengite-content of muscovite (isopleth of Si=3.1 in Fig. 1.9) and the TWEEQU software of Berman (1991, updated 1996) for the assemblage garnet-hydrous cordierite-andalusite-biotite-muscovite-quartz-H_2O of sample 5-94 (dashed triangle 2 in Fig. 1.9). The results for this andalusite-bearing rock are at 3 to 4 kbar falling in the stability field of sillimanite. The pressure estimate on the basis of Si-content in muscovite should theoretically be regarded as a minimum value since the rock lacks K-feldspar and does not contain the limiting assemblage (Massonne & Schreyer, 1987).

Our prefered pressure estimates for the upper crust are shown in Fig. 1.9 as the solid bar. At the sillimanite isograd, this corresponds to a pressure of about 2.5 kbar. By adopting the generally assumed temperature for the biotite-in isograds of about 370 to 400 °C (e.g. Ferry 1984; Yardley, 1989), the whole range of metamorphic temperatures estimated for the Palaeozoic metasediments of the southern Aspromonte area, extending from chlorite to sillimanite-muscovite grade, are in the range from *c*. 370 to 620 °C (Fig. 1.9).

1.9 DISCUSSION

1.9.1 Upper crustal metamorphism

The metamorphosed Palaeozoic rocks in the southern Aspromonte area, representing the uppermost part of the exposed crustal cross section of southern Calabria, have a high-temperature/low-pressure type metamorphic imprint. The zonal sequence of chlorite, biotite, garnet, staurolite-andalusite and sillimanite-muscovite, is the same as that in the Moldanubian zone of the Hercynian fold belt in central Europe (Blümel & Schreyer, 1976), and similar to that at the Saxothuringian-Moldanubian boundary (Wagener-Lohse & Blümel, 1984). However, it differs from other low pressure terranes, like the Abukuma and Buchan areas (Miyashiro, 1973; Hudson, 1980), in that a garnet-zone is developed instead of a cordierite zone. This is attributed to the generally Al-poor and Fe-rich bulk composition of the Calabrian metapelites.

In Calabria, the sequence is cut by a peraluminous granite at its high-temperature end, which is in the stability field of muscovite+quartz. The metamorphic pressure at the sillimanite isograd is

about 2.5 kbar, which is constrained by the breakdown of staurolite+muscovite +quartz within the stability field of andalusite in the adjoining upper part of the staurolite-andalusite zone. A high water activity has to be assumed since the results of the garnet-biotite and the garnet-cordierite thermometry are in perfect agreement with calculated breakdown temperatures for staurolite+muscovite+quartz (at $a_{H2O} = 1$) at these pressures in the KFMASH-system (Spear & Cheney, 1989).

The results of U-Pb monazite dating, which will be published elsewhere, revealed that the regional metamorphism and the intrusion of the granite are part of the same orogenic scenario and are of the same age of *c*. 300 Ma. This suggests a genetic link between the granite ascent from the deep crust and the high-temperature/low-pressure type of metamorphism in the upper crust. This is supported by the textural relationships indicating that prograde metamorphic heating outlasted the deformation (D1-D3) of the schists. For example, andalusite growth started synkinematically with the development of S2 but undeformed andalusite porphyroblasts enclosing folds of the S2 fabric as well as late stage biotite (Bt 2) and muscovite (Ms 2) oriented parallel to S3 also occur. In addition, late stage biotite and muscovite of the biotite and the chlorite zones posttectonically overgrow the S2 fabric. There is no firm petrological evidence for a pressure change either during heating or during retrogression. Therefore, we assume that the peak metamorphic temperatures were achieved during isobaric heating of the crust and that they reflect a transient, unusually high geotherm which was only slightly (if at all) affected by thickening or erosional processes affecting the crust prior to peak metamorphism. From the thermobarometric data given above a geothermal gradient of *c*. 60 °C km^{-1} can be calculated for the upper crustal section. Magmatic heat input into the upper *c*. 10 km of the crust during the Hercynian orogenic event supplied from ascending and crystallizing granitic melts is therefore envisaged as the most likely scenario to account for the metamorphism.

The petrographic report of comparable series along the eastern side of the granitoids of the Sila massif of northern Calabria (Borghi *et al.*, 1992) points to striking similarities with the southern Aspromonte area. However, the geological interpretation is quite different: The lower grade part (biotite and chlorite grade) is considered to form a nappe, the so-called Bocchigliero Complex, on top of the staurolite-andalusite schists of the 'Mandatoriccio Complex' (Borghi *et al*., 1992, p. 323). Because of the simpler deformation history and the higher Si-content of white mica of the lower grade complex, which are similar to those of the biotite zone in the Aspromonte area (cf. Fig. 1.7), compared to muscovite of the underlying staurolite schists Borghi *et al.* (1992) concluded that both units experienced different metamorphic evolutions. Consequently, these authors assumed that the two units came into contact through a post-metamorphic tectonic event presumably of Hercynian age. Also the age of metamorphism is different, with Rb-Sr whole rock dating of meta-volcanics, suggesting it took place at *c*. 330 Ma (Aquafredda *et al*., 1991).

Only systematic petrographic mapping and the application of comparable isotopic dating methods could prove whether the geological evolutions of upper crustal rocks in the Sila and in the

Aspromonte are really different or whether the conclusions drawn here for the Aspromonte section can be extended to a broader regional scale.

1.9.2 Upper crust - lower crust relationship

The metamorphic evolution of the upper crustal rocks may now be compared to that experienced by the lower crustal rocks of the same crustal section (Schenk, 1980, 1984, 1990) cropping out in the northern Serre, some 80 km further north. The granulite facies rocks constitute a 7-8 km thick sequence which, at the time of metamorphism, represented a crustal depth range of *c*. 20-27 km. U-Pb ages of zircon and monazite scatter in the interval 310 to 290 Ma (Schenk, 1980, 1990) which puts the metamorphic event into the same time period as the upper crustal metamorphism and magmatism. The lower crustal rocks are overlain by I-type granitoids (quartz-diorite, tonalite) which were intruded at 295 to 290 Ma. Also within the lower crustal section, mafic sills with a granulite facies mineralogy occur (Figs 1.1 & 1.10). One of these sills has been dated at *c*. 298 Ma which shows that the lower crustal metamorphism is connected in space and time with the overaccretion of very large volumes of magmas suggesting a genetic link between magmatism and metamorphism for the lower crustal section also.

The metamorphic evolution of the lower crustal rocks is characterized by a moderate pressure increase during prograde heating and there is no petrological evidence for substantial tectonic crustal thickening prior to peak granulite facies metamorphism. This is in agreement with the model of magmatic loading on top of the lower crust and is supported by metamorphic textures, e.g. garnet rims around cordierite pointing to a pressure increase. Net-like orthopyroxene porphyroblasts in felsic granulites, pyroxene-plagioclase symplectites replacing hornblende, and, at the uppermost part of the lower crustal section, sillimanite-K-feldspar-biotite pseudomorphs after muscovite are evidence that prograde heating outlasted the deformation (Schenk, 1984, 1990).

From the description given above it is evident that the prograde metamorphic evolutions of the upper and lower crustal sections are similar, the causes of which might originate from the similar type of heat source. The main difference between this prograde evolution is the pressure increase in the lower crustal rocks which is presumably due to magmatic loading, but has not been identified in the upper crustal section.

P-T estimates for the lower crust revealed a geothermal gradient of 30-35 °C km^{-1} (Schenk, 1990) which is much lower than the 60 °C km^{-1} value for the upper crust. The small temperature difference between the base of the upper crustal section (620 °C at *c*. 2.5 kbar) and the top of the lower crust (690 °C at 5.5 kbar) can be explained by the large intrusions into the middle crust which through advective heat transport aligned the temperatures in the different levels of the crust (Fig. 1.10).

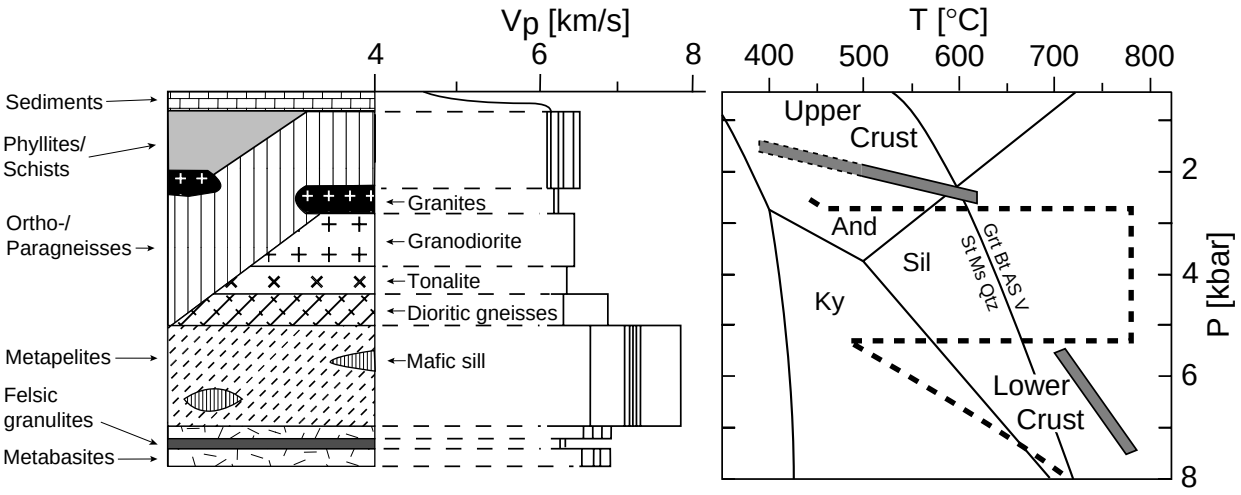

Fig. 1.10 Conjectural lithological section through the Calabrian crust (modified from Schenk, 1990) and *P-T* conditions in different crustal levels (heavy bars) as deduced from metamorphic phase equilibria. Dashed line shows schematical thermal conditions immediately after intrusions. Wave velocity data from Kern & Schenk (1985, 1988).

Future research in Calabria will have to find out to what extent the higher grade amphibolite facies rocks of the central Aspromonte area, which have been sliced into different Alpine nappes, have been affected by the late stage Hercynian metamorphic event as well.

CHAPTER TWO

An exposed Hercynian lower crustal section in the Sila massif of northern Calabria: mineral chemistry, petrology and a *P-T* path of granulite facies metapelitic migmatites and metabasites

2.1 ABSTRACT

In the Sila massif of northern Calabria a continuous section through a segment of a Hercynian lower continental crust is exposed which has been interpreted by previous workers as a stack of basement nappes ('Mt. Gariglione Complex'). The section consists essentially of metapelitic migmatites and subordinate metabasites and marbles which were metamorphosed at medium-pressure/high-temperature granulite facies conditions. A continuous metamorphic gradient through the exposed segment can be deduced from the systematic change in the compositions of ferromagnesian minerals in divariant metapelitic assemblages. This gradient is partly supported by conventional geothermobarometry and by applying the TWEEQU method. Due to partial retrograde re-equilibration of matrix phases, peak metamorphic conditions are best defined by mineral equilibria, especially by dehydration melting reactions. These estimates reveal *c*. 4 kbar and 740 °C at the top and *c*. 6 kbar and 770 °C at the base of the section. Therefore the exposed rocks represent a former crustal depth range of *c*. 14-21 km with a geothermal gradient of *c*. 35-50 °Ckm^{-1} during the highest metamorphic temperatures.

The metamorphic evolution of the former lower crust has been reconstructed from reaction textures. The prograde *P-T* path is characterized by heating accompanied by loading and proceeded in the stability field of sillimanite. The retrograde path is characterized by a stage of isothermal uplift after peak metamorphism into mid-crustal levels (10-15 km) followed by near isobaric cooling to greenschist facies conditions.

The lower crustal section in northern Calabria can be compared to that of the Serre in southern Calabria which represents a deeper part of an exposed tilted cross-section through the Hercynian continental crust. Metamorphic textures and isotopic ages indicate that the thermal conditions in the Calabrian crust during the Hercynian orogeny were mainly controlled by advective heat input through magmatic intrusions. Like in southern Calabria, at the time of regional metamorphism large granitic bodies intruded in-between the granulite-facies lower crust (Mt. Gariglione Complex) and the amphibolite to greenschist facies upper crust.

Mineral abbreviations are from Kretz (1983).

2.2 INTRODUCTION

Exposed cross-sections through the continental crust offer the possibility to study the effect of thermal and tectonic events during orogenic cycles on the lithologies of different crustal levels. In the Sila massif of northern Calabria a large unit (*c*. 900 km^2) of granulite facies, dominantly metapelitic migmatites is exposed, which was metamorphosed during the Hercynian orogeny. This unit ('Mt. Gariglione Complex') represents the lower part of the Alpine 'Sila nappe' which consists in its middle part of a wide range of late-Hercynian granitoids overlain by upper crustal rocks (Dubois, 1970, 1976). The granulite facies metapelites of the Sila resemble those of the lower continental crust in the southern Calabrian massif (Serre). In the latter region, they form part of the 7 to 8 km thick base (5.5 to 7.5 kbar) of an exposed continuous profile through the Hercynian continental crust (Schenk, 1984, 1990). Like in northern Calabria, these lower crustal gneisses are overlain by granitoid intrusions of the middle crust and amphibolite to greenschist facies upper crustal rocks (Graeßner & Schenk, 1999). However, the Sila section differs from the one in southern Calabria in that the metapelites are not underlain by a granulite facies unit dominated by metabasites. This lowermost 'granulite-pyriclasite unit' (Schenk, 1984) is missing in the Sila of northern Calabria.

Until now, modern petrological methods have not been applied to the high-grade gneisses of northern Calabria. Therefore, the first scope of this study is to prove whether mineral chemistry and phase relations of metapelites point to a continuous metamorphic gradient through the Mt. Gariglione Complex. This would support a model of an exposed profile through a part of the former lower continental crust and would be in contrast to the tectonic model of Zanettin Lorenzoni (1980) and Lorenzoni & Zanettin Lorenzoni (1983) who proposed an Hercynian nappe boundary within this granulite facies unit of the Sila massif.

The second scope of this paper is to evaluate the thermal conditions of the granulite facies segment in order to reconstruct its former structural level within the continental crust. Furthermore, the *P-T* path of these rocks are deduced to get information on the geodynamic causes of metamorphism and to compare it with that of the lower crust exposed in southern Calabria.

2.3 GEOLOGICAL SETTING OF NORTHERN CALABRIA

The Calabrian massif is situated in the southern part of the Appenine mountain system and consists of pre-Alpine crust which was involved in the Alpine orogeny. The Alpine mountain system became dismembered due to later movements of microplates in the western Mediterranean (e.g. Alvarez, 1976). Some authors (Amodio-Morelli *et al*., 1976; Scandone, 1979; Bonardi *et al.*, 1982) regard the Calabrian massif as a piece of Adriatic crust that was thrust firstly (Alpidic stage) onto ophiolitic units in the west and later (Apenninic stage), together with its underlying base, backwards onto the Apenninic carbonate platform in the east. In contrast, Dietrich (1988) regards

the Calabrian massif as derived from the European continent, thrust only towards the east, overriding the ophiolitic units and resting now with its ophiolitic base upon the Adriatic platform units.

The tectonically higher units of the Sila massif in northern Calabria (Mt. Gariglione, Bocchigliero and Mandatoriccio Complexes) form the so called 'Sila nappe' of Dubois (1970, 1976) which consists in its deeper part of granulite facies lower crustal gneisses, the Mt. Gariglione Complex. These gneisses are overlain by two cycles of late-Hercynian granitoids, a mesaluminous to calcalkaline and a peraluminous one (D'Amico *et al.*, 1982; Messina *et al.*, 1991a; Messina *et al.*, 1991b; Ayuso *et al.*, 1994; Fig. 2.1). The granites intruded into the overlying amphibolite facies upper crustal gneisses and low-grade Palaeozoic rocks (Bocchigliero and Mandatoriccio Complexes), which are unconformably overlain by a Mesozoic to Caenozoic sedimentary cover. This sequence thus consists of rocks from very different crustal levels and may have stored- if they were part of the same Hercynian crustal segment - valuable information about the former thermal conditions at different levels of that Hercynian crust. The same tectonic structure is observed in the southern Calabrian massif (Serre and Aspromonte), where the most continuous crustal section has been documented. Here, geological mapping and petrological analysis revealed a continuous profile through the granulite facies lower crust and the greenschist to amphibolite facies upper crust (Schenk, 1984, 1989, 1990; Graeßner & Schenk, 1999).

The relatively simple tectonic model for the Sila nappe described above, attributing the granulite facies rocks which are the subject of this paper to only one Hercynian unit (Mt. Gariglione Complex) is a matter of debate in the literature (e.g. Dubois, 1970, 1976; Messina *et al.*; 1991a; Borghi *et al.*, 1992; and references therein). According to e.g. Amodio-Morelli *et al.* (1976), Zanettin Lorenzoni (1980) and Lorenzoni & Zanettin Lorenzoni (1983) the high-grade metamorphic rocks are subdivided into two Alpine units of which only the upper one is characterized by a considerable amount of migmatites. Furthermore Zanettin Lorenzoni (1980) and Lorenzoni & Zanettin Lorenzoni (1983) propose an Hercynian nappe boundary within this migmatitic unit separating high-grade metamorphic rocks from overlying intermediate-grade rocks. Both units were intruded by the late-Hercynian granitoids. As will be discussed below, according to metamorphic phase equilibria and mineral chemistry of the granulite facies rocks the authors of the present study favour the relatively simple tectonic model for the Mt. Gariglione Complex.

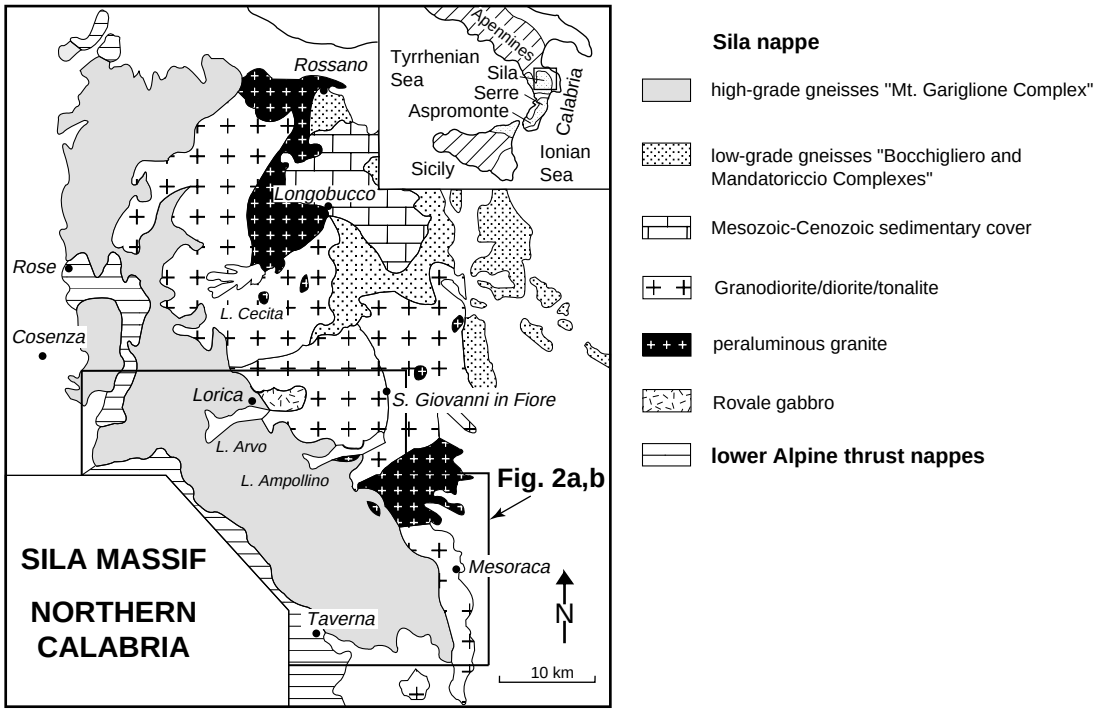

Fig. 2.1 Simplified geological map of the Sila massif in northern Calabria (modified after Ayuso *et al.*, 1994). Box shows area of Fig. 2.2a,b.

2.4 FIELD RELATIONS AND MINERAL ASSEMBLAGES

To evaluate the metamorphic gradient and peak metamorphic conditions in the high-grade rocks of the Sila nappe nearly 200 thin sections of metapelitic and metabasic rock samples of the southern part of the Mt. Gariglione Complex ('Sila Piccola') have been petrographically analysed. Most of these rock samples were collected along two southwest-northeast running profiles through the southern and northern part of the study area. Additional rocks were sampled in-between the two profiles around the villages of Villaggio Mancuso and to the east of Mesoraca (Fig. 2.2a,b). Some additional thin sections were supplied by N. Le Breton (cf. Le Breton, 1983).

The Mt. Gariglione Complex (Fig. 2.2a,b) comprises dominantly metapelites as well as some garnet-biotite gneisses and interlayered quartzofeldspathic leucosomes which account for roughly estimated 10-20 vol.% of the exposed rocks. These leucosomes form lenses and bands mostly parallel to the foliation (stromatitic leucosomes) and are interpreted as partial melts of the host metapelites. Silica-undersaturated aluminous restitic rock compositions are found as small layers in thin section scale but only rarely in hand specimen scale. They are characterized by the occurrence of retrograde spinel inclusions in cordierite formed during decompression after peak metamorphism. In most of the coarse grained gneisses a well developed foliation affected by isoclinal folding is recognizable. It dips approximately 20-30° towards the east. Some massif rock types do also occur in which a foliation is not visible.

The *metapelites* have been metamorphosed at sillimanite+K-feldspar grade, so that prograde muscovite+quartz was not stable during peak metamorphism. 14 different mineral assemblages have been formed in the metapelites, among which the most common ones are Grt-Sil-Crd and Grt-Sil-Kfs both in equilibrium with Qtz-Bt±Pl. The 'univariant' assemblage Grt-Bt-Crd-Kfs-Sil-Qtz (forming an isograd in the Serre further to the south (Schenk, 1990) occurs at 24 localities and at very different structural levels of the Sila Piccola studied here. A jump in metamorphic grade from high-grade granulite facies to intermediate-grade rocks, which would support the model of tectonic slices in the Mt. Gariglione Complex as proposed by Zanettin Lorenzoni (1980) and Lorenzoni & Zanettin Lorenzoni (1983), has not been found. Plagioclase-quartz symplectites replacing K-feldspar (myrmekites) are intensively developed in the studied samples, not only in melanosomes but more often in leucosomes. In samples of the upper part of the unit, retrograde muscovite-quartz intergrowth replacing Sil-Kfs is found in addition to the symplectites. In this part retrograde fibrolitic sillimanite and andalusite is also common. Retrograde kyanite+chlorite formed at the expense of cordierite is found only in one sample of the western part of the study area (Colle d'Ascione, east of Mt. Paganella; Fig. 2.2a). Staurolite is found in several rocks independent of their former structural level and is interpreted as being of retrograde origin (Fig. 2.2a).

Metabasites and some *intermediate rock* types of enderbitic composition are mainly restricted to two larger bodies near the village of Villaggio Mancuso and to few small lenses and layers within the metapelites (41 samples, Fig. 2.2b). Leucosomes in metabasites have not been observed in thin section scale or in the field but cannot strictly be ruled out due to the scarcity of outcrops. In metabasic rocks 7 different mineral assemblages have been distinguished, not considering amphibole as a critical mineral (Fig. 2.2b). The granulite facies assemblage Opx±Grt+Pl+Qtz is found next to retrogressed Amp-Pl±Grt bearing rocks which occur in all parts of the study area. Since the assemblage Grt-Cpx-Qtz is missing the granulites are assigned to the medium pressure type of Green & Ringwood (1967).

Olivine metagabbros are common as river pebbles in the southwestern part of the study area (Fig. 2.2b). They comprise the primary magmatic assemblage Ol+Pl+Opx±Cpx and late-stage reaction rims of Opx+Cpx+Spl and Prg-Hbl+Spl which developed during near isobaric cooling to the medium pressure granulite facies conditions prevailing in the surrounding lower crustal rocks. This rock type is similar to the Rovale Gabbro (Acquafredda *et al.*, 1992; Caggianelli *et al.*, 1994) in the northern part of the study area and resembles rocks described by Dubois (1976) from a small outcrop near the village of Cellara in the west of the Mt. Gariglione Complex. With respect to this undersaturated olivine-bearing rock types the lower crustal sections of the Sila and the Serre are different since it seems to be absent from the latter region (Schenk, 1984).

Marbles occur as lenses and layers (100 m to km scale; Fig. 2.2a,b) within the metapelites but were not collected systematically for this study. In one sample of the lower part of the unit the assemblage Fo±Di-Cal-Dol is found refering to granulite facies or upper amphibolite facies conditions.

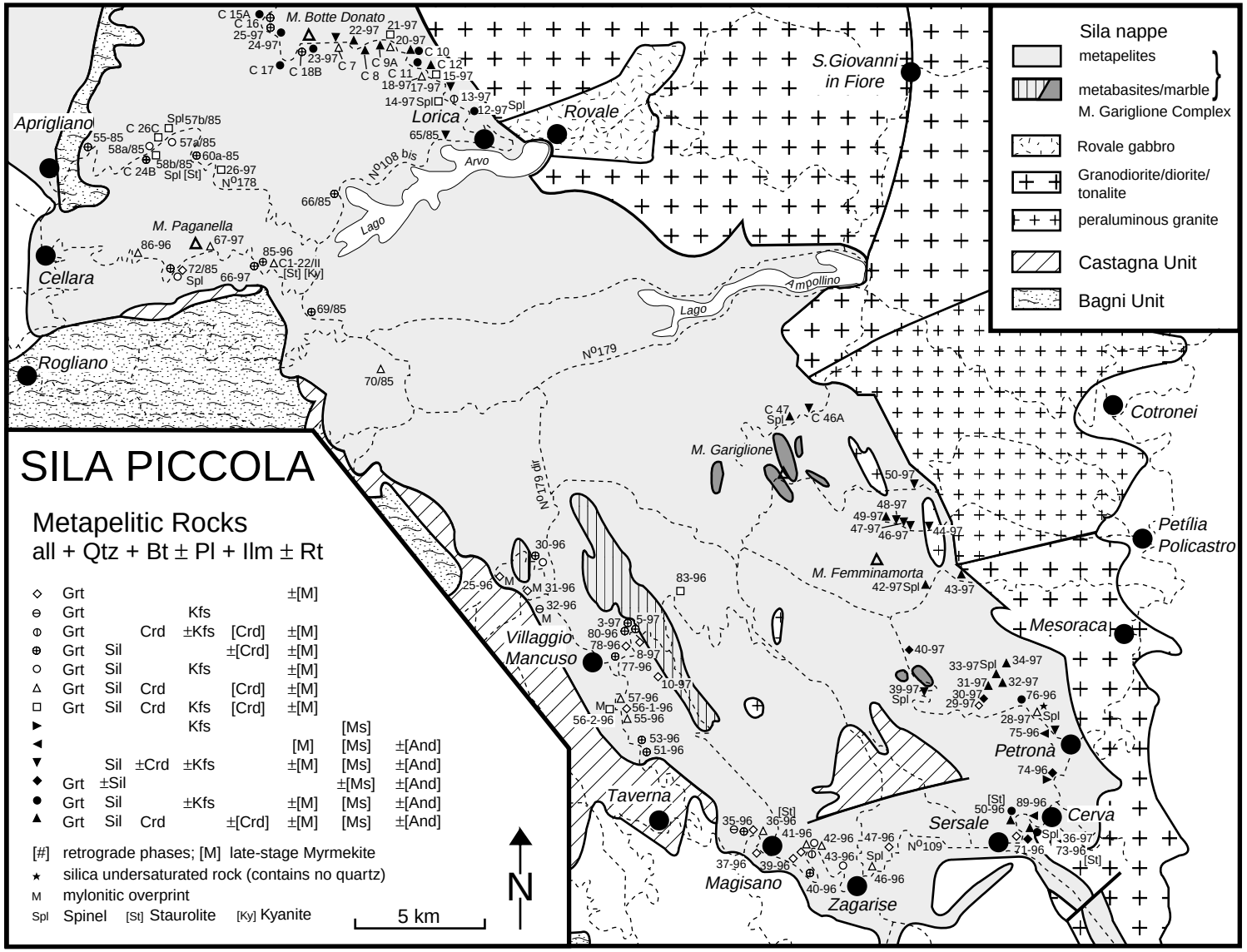

Fig. 2.2 (a) Regional distribution of mineral assemblages of metapelitic rocks of the Mt. Gariglione Complex in the southern part of the Sila ('Sila Piccola'). The outlines of the main geological units are modified after Ayuso et al. (1994) and Lorenzoni & Zanettin Lorenzoni (1983). Map area is given in Fig. 2.1.

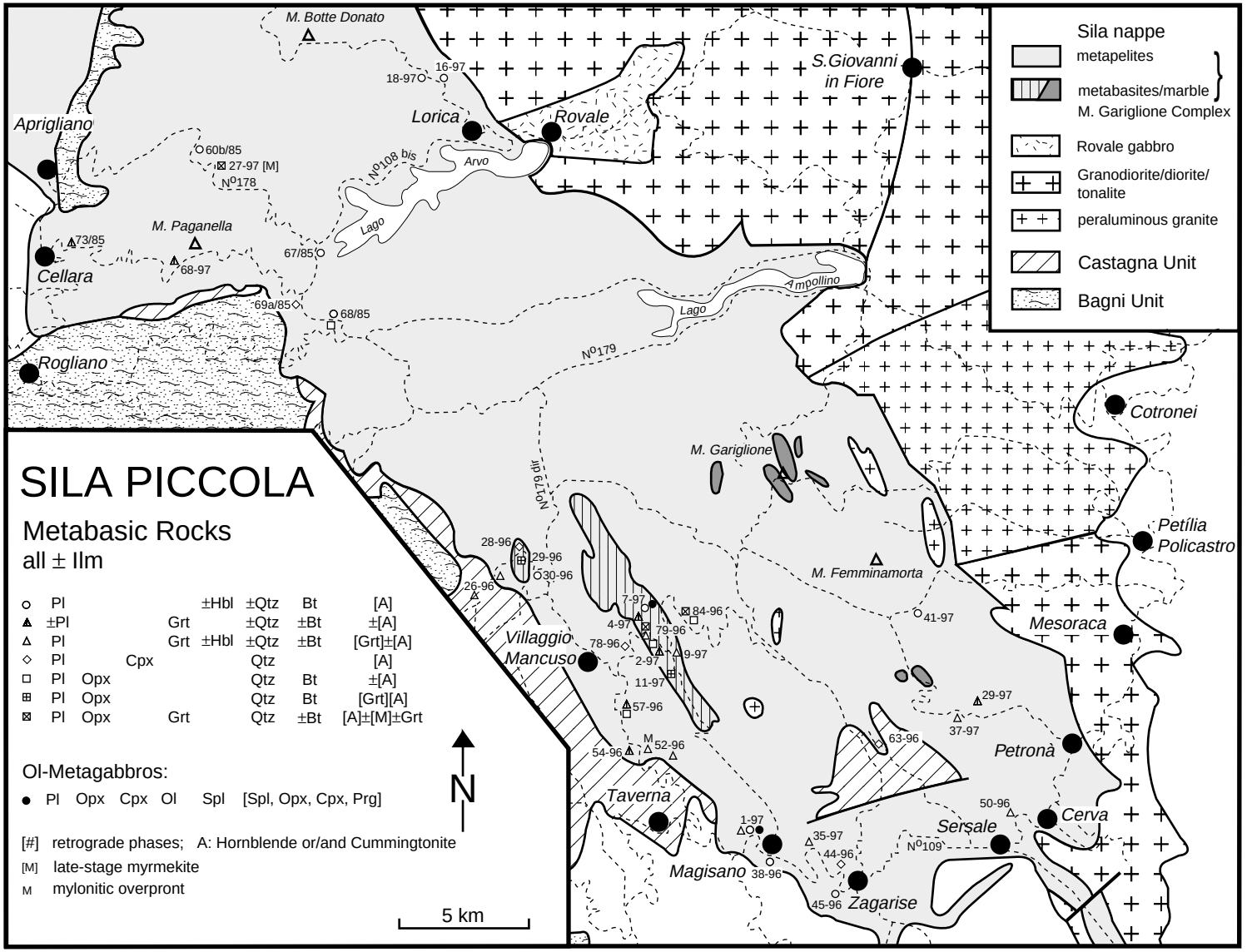

Fig. 2.2 (b) Regional distribution of mineral assemblages of metapelitic rocks of the Mt. Gariglione Complex in the southern part of the Sila ('Sila Piccola'). The outlines of the main geological units are modified after Ayuso et al. (1994) and Lorenzoni & Zanettin Lorenzoni (1983). Map area is given in Fig. 2.1.

2.5 PETROGRAPHY AND MINERAL CHEMISTRY

To constrain the *P-T* conditions of metamorphism of the Mt. Gariglione Complex, minerals of nine metapelites and four metabasic rocks were studied with the electron microprobe (see Table 2.1 for assemblages), using the CAMECA CAMEBAX microprobe at the University of Kiel in the wavelength-dispersive mode with 15 kV acceleration potential and 15 nA beam current. Corrections were carried out with the PAP correction program (Pouchou & Pichoir, 1984). Representative analyses are presented in Tables 2.2 to 2.6.

2.5.1 Metapelitic migmatites

Texturally two types of *garnet* can be distinguished in melanosomes: coarse 1-5 mm anhedral to sub-hedral grains and small euhedral ones (0.1-0.5 mm). Both types display the same chemical composition (except for small euhedral garnet of sample 33-97 showing strong retrograde Fe and Mg homogenization). The larger grains contain inclusions of biotite, quartz, ilmenite, sometimes plagioclase in the core and sillimanite and minor cordierite near the rims (Fig. 2.3a). This suggests growth of garnet during increasing temperatures and pressures due to reactions like Bt + Sil + Qtz = Gr + Kfs + L/V and Crd = Grt + Sil + Qtz. Retrograde reaction textures like coronae of cordierite (Fig. 2.3a) or cordierite-spinel symplectites replacing garnet (rare) and the breakdown of garnet to aggregates of biotite±sillimanite±plagioclase (Fig. 2.3b,c) indicate decompression followed by decreasing temperatures.

The garnet cores are essentially unzoned pointing to intracrystalline diffusional homogenization due to the high metamorphic grade (Fig. 2.4a-d; Table 2.2). Garnet core compositions are in the range $Alm_{63\text{-}82}$, $Prp_{13\text{-}32}$, $Grs_{2\text{-}4}$, $Sps_{1\text{-}3}$. Growth zoning pattern is only preserved in garnet of sample 33-97 from the eastern part of the Mt. Gariglione Complex. In this sample clouded cores show a slightly higher grossular content which decreases towards a wide marginal zone. The X_{Fe}-values are in the range of 0.66-0.86, decreasing from east to west of the study area, which is towards the structurally lower part of the complex. All analysed garnets (except that from sample 57-1-96) show retrograde zoning patterns along fractures, biotite inclusions and near the rims. This is indicated by increasing X_{Fe}-values due to retrograde Fe-Mg exchange (Fig. 2.4b,c). Garnet of the structurally higher part of the unit is characterized by a wider seam of retrogression (c. 1-1.5 mm; Fig. 2.4a) than that from the structurally deeper part (<0.25 mm; Fig. 2.4c,d). Increasing spessartine content at the rims suggests resorption during retrogression (Fig. 2.4b). The outermost rims of some garnet grains of the western part are additionally characterized by an increase of grossular component (e.g. sample 42-96; Fig. 2.4c).

Garnet of leucosomes has only been analysed in sample 50-4-96. The unzoned, small anhedral, ellipsoidally shaped grains (*c*. 0.1 mm) display X_{Fe}-values in the core similar to those of rims of garnet in melanosomes (X_{Fe}=0.87-0.89). The spessartine content (Sps_{11}) is slightly higher.

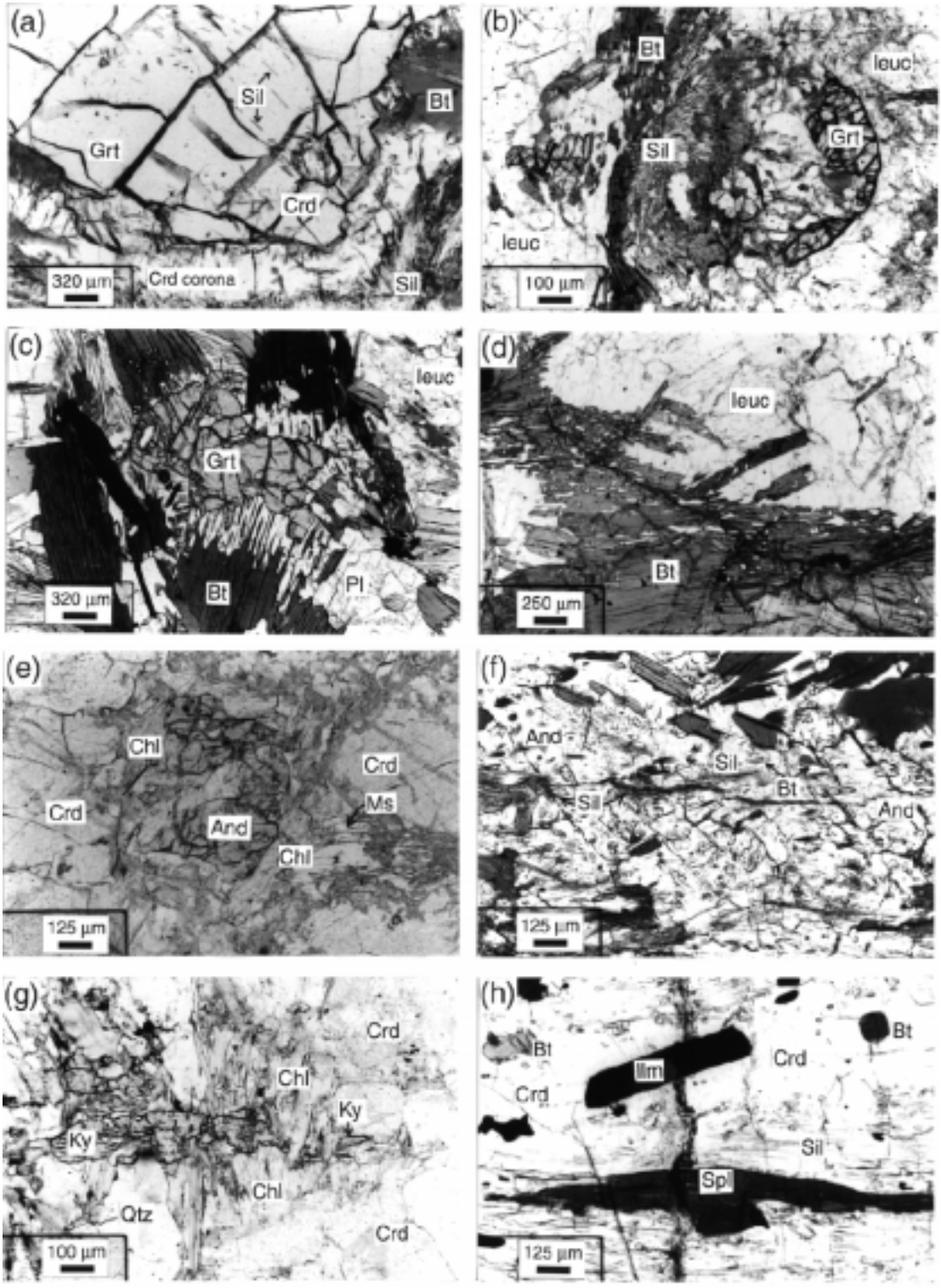

Fig. 2.3. (a) Prograde sillimanite and cordierite inclusions in garnet rim. Garnet is surrounded by a late-stage corona of cordierite formed during decompression (sample 21-1-97). (b) Retrograde decomposition of garnet to an aggregate of biotite, sillimanite and quartz in leucosome (leuc) (sample 69c/85). (c) Garnet at the edge of a melanosome partly replaced by biotite-quartz symplectites and plagioclase (sample 49-97). (d) Biotite dehydration melting: skeletal biotite at the margin of leucosome (leuc), partly rotated into the former melt (sample 69c/85). (e) Andalusite+chlorite grown at the expense of cordierite during cooling (C 47 B). (f) Undeformed late-stage andalusite overgrowing foliated matrix of fibrolitic sillimanite and biotite (sample 12-1-97). (g) Late-stage kyanite+chlorite embaying cordierite (sample C1-22 II). (h) Inclusions of sillimanite, spinel and rounded relics of biotite in cordierite. Spinel has overgrown the sillimanite inclusions (sample 14-1-97).

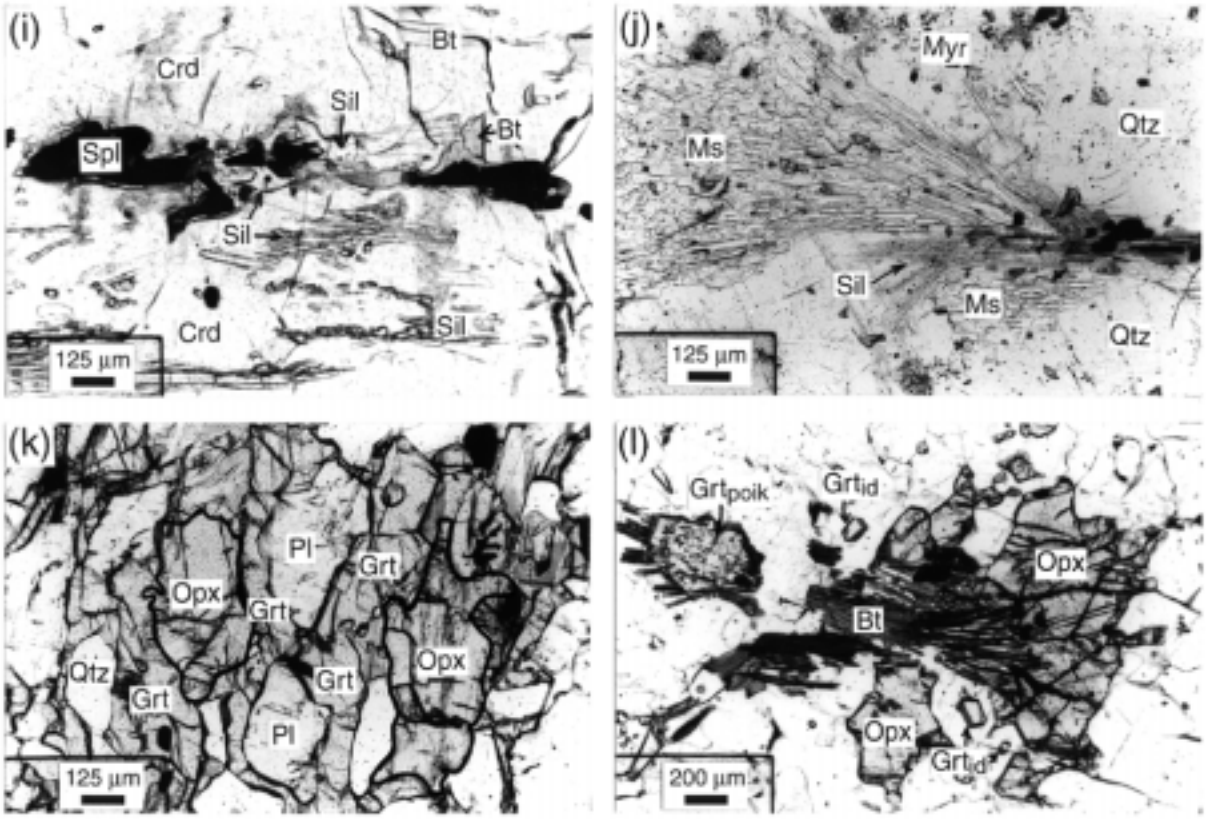

Fig. 2.3 continued (i) Late-stage sillimanite seams and retrograde biotite formed between spinel and cordierite during near isobaric cooling. Reverse of reaction seen in (h) (sample C47 B). (j) Coarse grained randomly oriented muscovite-quartz pseudomorphs after sillimanite, next to myrmekite in leucosome. Knots of fibrolite possibly formed during dehydration melting of muscovite (sample 76-1-96). (k) Retrograde reaction rims of garnet developed between orthopyroxene and plagioclase during nearly isobaric cooling (sample 29-96). (l) Biotite-quartz symplectites replacing net-like orthopyroxene, and are overgrown by late-stage poikilitic garnet (Grt_{poik}). Small euhedral garnet grains (Grt_{id}) and orthopyroxene are interpreted as the peak metamorphic assemblage (sample 84-96).

Table 2.1 Mineral assemblages of the analysed samples; sample locations are given in Fig. 2.2a,b.

Metapelites															
Sample	Qtz	Pl	Bt	Grt	Sil	Crd	Kfs	Ilm	Rt	Spl	[Crd]	[Myrm]	[St]	[And]	[Ms]
21-97	x	x	x	x	x	x	x	x			x	x			x
33-97	x	x	x	x	x	x		x		x		x			
42-96	x	x	x	x	x	x		x	x		x				
46-3-96	x	x	x	x	x	x		x		x	x	x			
50-4-96	x	x	x	x	x					x		x	x	x	x
57-1-96	x	x	x	x	x	x		x	x		x				
57b/85	x	x	x	x	x	x	x	x		x	x	x			
86-96	x	x	x	x	x	x		x			x				
C8F	x		x	x	x	x		x			x				x

Metabasites													
Sample	Qtz	Pl	Bt	Grt	Opx	Ilm	Hbl	Cum	[Grt]	[Hbl]	[Cum]	[Myrm]	[Bt]
29-96	x	x			x	x	x		x	x	x		
27-97	x	x	x	x	x	x		x				x	
79-2-96	x	x	x	x	x	x	x			x	x		
84-96	x	x	x	x	x	x			x				x

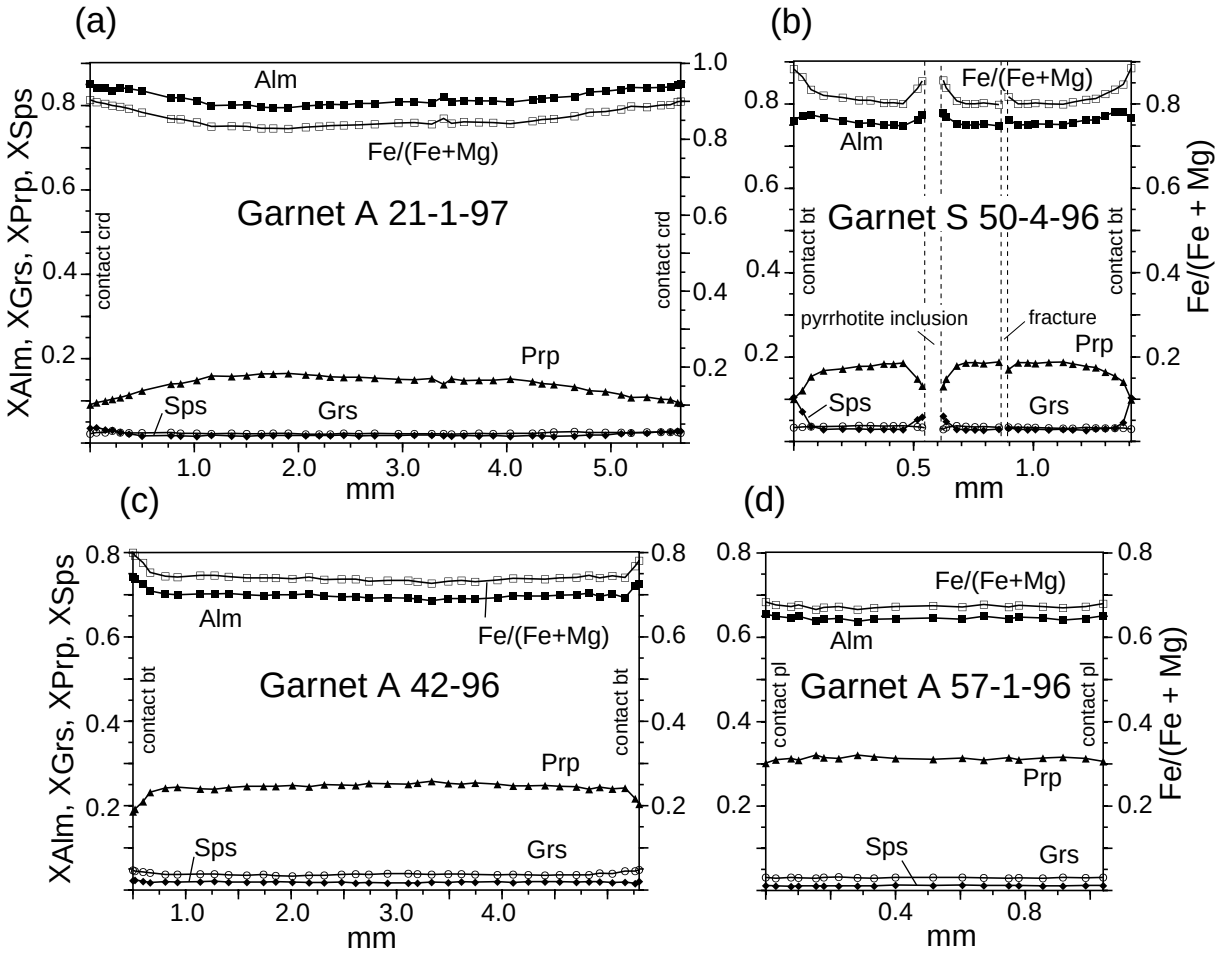

Fig. 2.4 Representative garnet zoning profiles from metapelites of structurally higher (a, b) and deeper parts (c, d) of the Mt. Gariglione Complex. Each profile extends from rim to rim through the core of the garnets. Location of samples is given in Fig. 2.2a.

Three textural types of *biotite* can be distinguished in the melanosomes: inclusions in garnet, matrix grains and grains formed as a breakdown product of garnet. Symplectitic intergrowth of skeletal biotite with quartz surrounding the leucosomes suggests dehydration melting of biotite (Fig. 2.3d). The lowest X_{Fe}-values are found in biotite inclusions in garnet. Compositional differences between matrix biotite and grains in contact with garnet formed during retrogression are only small within a single sample suggesting retrograde re-equilibration of the progressively formed matrix biotite. However, in several samples (e.g. 33-97, 46-3-96, C8F) matrix grains are slightly higher in X_{Fe} than biotite adjacent to garnet affected by retrograde cation exchange. X_{Fe}-values of matrix grains range from 0.34-0.61 (Table 2.3). Figure 2.5 shows the composition fields of matrix biotite from the analysed samples in comparison to findings from other areas (Robinson *et al.*, 1982). Most biotite compositions show lower Ti-contents and X_{Fe}-values than those of biotite in comparable assemblages from New England (except for sample 57-1-96) which can be explained with intensive re-equilibration of the matrix minerals during retrogression. This

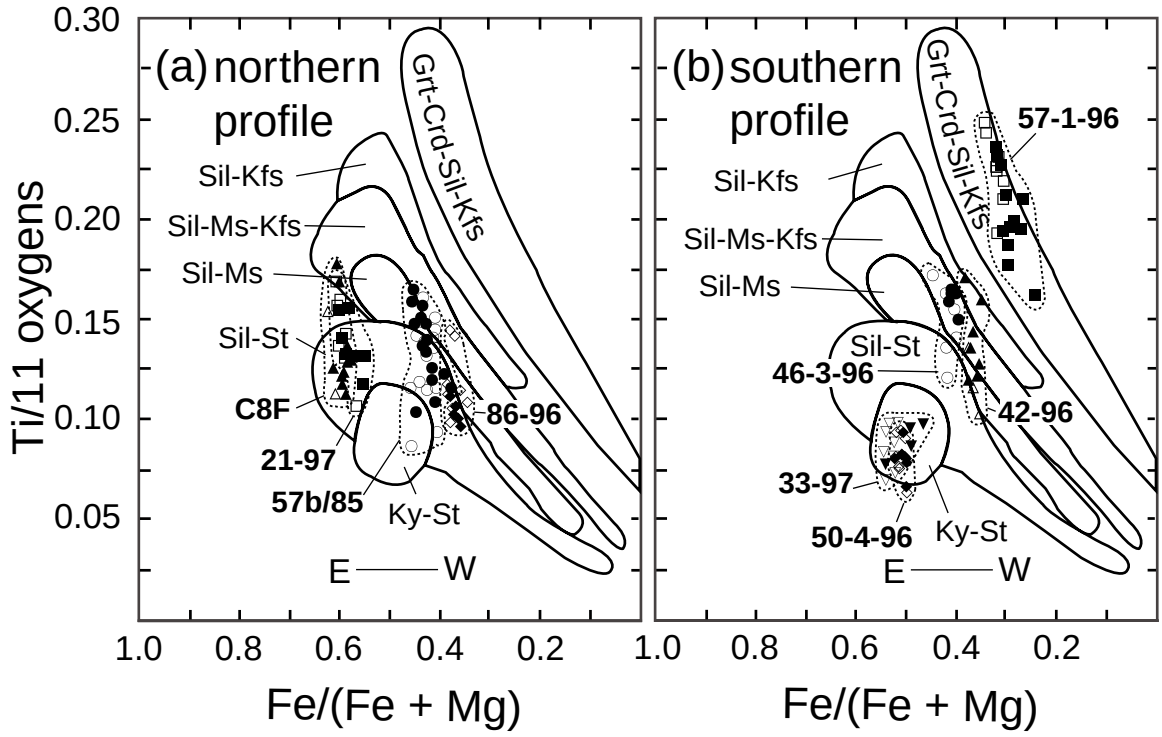

Fig. 2.5 Plot of Ti (per 11 oxygens) as a function of Fe/(Fe+Mg) for metapelitic matrix biotites along the northern (a) and southern profile (b) through the Mt. Gariglione Complex. Unshaded fields: compositional ranges of biotite from metamorphic zones in New England (Robinson *et al.*, 1982). Location of samples is given in Fig. 2.2a.

interpretation is supported by ilmenite coronae around biotite indicating retrograde exsolution of this Ti-phase.

Coarse grained *sillimanite* as a main constituent of the melanosomes shows prefered orientation parallel to the matrix foliation. Sillimanite needles as inclusions in garnet rims (Fig. 2.3a) and in cordierite are evidence that prograde metamorphism proceeded mainly within the stability field of sillimanite. The numerous sillimanite inclusions in the garnet rims are often oriented parallel to the matrix foliation, but inclusions parallel to the outline of the garnet and oblique to the fabric of the matrix are also found in some cases. Retrograde prismatic sillimanite intergrown with biotite and replacing garnet is common within the studied migmatites (Fig. 2.3b). In the eastern part of the Mt. Gariglione Complex fibrolitic sillimanite is much more abundant than in the western part. Fibrolite is interpreted as a late-stage reaction product overgrowing pre-existing prismatic sillimanite and biotite. Mats of fibrolite embay garnet and are often found as knots of tiny fibres within the leucocratic segregations. Retrograde *andalusite* replacing cordierite is also common in the east of the study area (Figs 2.2a, 2.3e) and is formed always later than fibrolitic sillimanite which is found as inclusion (Fig. 2.3f). *Kyanite* occurs in only two thin sections from one sample of the western part of the study area (sample C1-22 II at the road at Colle d'Ascione, east of the M. Paganella). These are the original thin sections from which Dubois (1976) described kyanite and

regarded it as a pre-Hercynian relic phase. However, here it is interpreted as a retrograde mineral formed together with chlorite and biotite at the expense of cordierite (Fig. 2.3g).

In melanosomes two textural types of *cordierite* can be distinguished: matrix grains and late stage coronae around garnet (Fig 2.3a). Additionally, few cordierite inclusions in garnet rims are relics of the prograde metamorphic evolution. The matrix grains show inclusions of sillimanite and biotite and in silica undersaturated rock compositions also of spinel (Fig. 2.3h,i). Retrograde breakdown to biotite+sillimanite+quartz or andalusite+chlorite+quartz is common in the eastern part and to kyanite bearing assemblages rarely in the western part of the Mt. Gariglione Complex (Fig. 2.3e,g). The cores of matrix grains and of coarse grained cordierites at the margin of leucosomes are unzoned and uniform in composition within each sample (Table 2.4). The X_{Fe}-range is 0.21-0.51 decreasing systematically from east towards the west of the Mt. Gariglione Complex, which in assemblage with Grt+Sil+Qtz suggests increasing metamorphic pressures in this direction (e.g. Thompson, 1976; Holdaway & Lee, 1977). Rimward decrease of X_{Fe} is explained by retrograde Fe-Mg exchange with matrix minerals. The Na_2O-content of the unzoned cores decreases to the west of the Mt. Gariglione Complex (from 0.04 to 0.24 wt%) suggesting increasing metamorphic temperatures in this direction (Mirwald, 1986). In some samples the grains show higher Na_2O-content at the rims (<0.39 wt%). X_{Fe}-values of late stage cordierite coronae surrounding garnet are in the range and lower than those of the rims of the matrix grains which is attributed to late-stage cation exchange.

Plagioclase is, like perthitic *K-feldspar*, a main constituent of the quartzofeldspathic leucosomes but volumetrically more important than the latter. In the commonly concordant leucocratic lenses and veins both feldspars crystallize mainly at the margins. Very often K-feldspar is embayed and replaced by late-stage myrmekitic plagioclase-quartz symplectites. This has led in many samples to complete replacement of K-feldspar, mainly in the eastern part of the Mt. Gariglione Complex, near to the overlying granites. The cores of plagioclase are essentially unzoned and uniform within a sample. No compositional difference was found between plagioclase of leucosomes and those from melanosomes. The analysed core compositions range from An_{31-44} (Table 2.5). In most analysed plagioclase grains the rims (<0.1 mm) are characterized by a moderate decrease of Ca suggesting retrograde re-equilibration of the rims during isobaric cooling (Fig. 2.6). This would correspond to the increasing grossular-content at the rims of some garnet if the Pl-Sil-Grt-Qtz equilibrium controls this zonation. Plagioclase in contact with myrmekite shows a sudden decrease of anorthite component at the outermost rim (Fig. 2.6) which may be explained by metasomatic processes leading to the formation of the adjacent myrmekite. Also the myrmekitic plagioclase itself is zoned with decreasing anorthite content from core (An_{33-38}) to rim (An_{23-29}). Only the core compositions may have been formed during near peak metamorphic conditions (Phillips & Ransom, 1970). K-feldspar is commonly perthitic microcline. The composition of the exsolved host is in the range of Kfs_{91-94}.

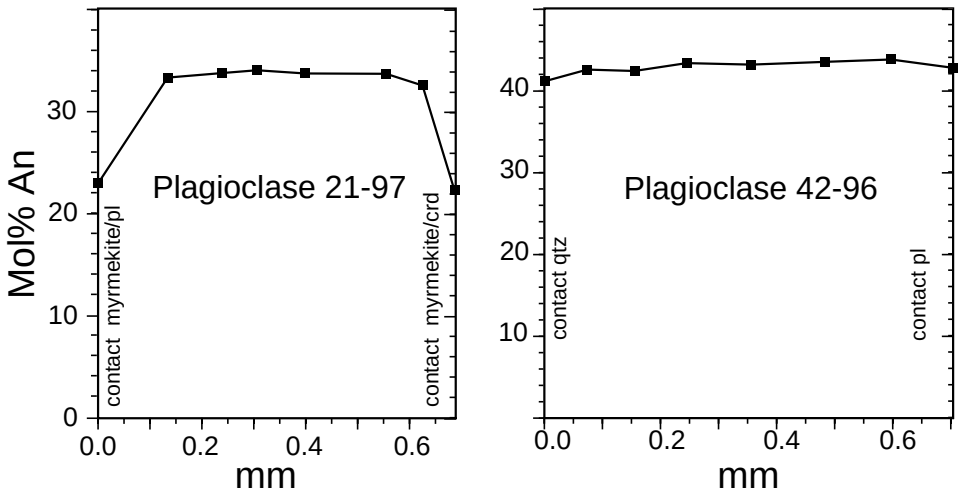

Fig. 2.6 Representative plagioclase zoning profiles of two of the analysed metapelites. Conspicuous is the steeper gradient of decrease of the anorthite component at the rims when in contact with late-stage myrmekite. Location of samples is given in Fig. 2.2a.

Green to brown *spinel* may occur as tiny inclusion in garnet (sample 33-97), as symplectitic intergrowth within large (<5 mm) euhedral sillimanite porphyroblasts or rarely in symplectitic intergrowth with cordierite replacing garnet. More common are inclusions in cordierite in silica undersaturated layers of the migmatites (Fig. 2.3h,i). Spinel is rich in hercynite (Hc_{51-66}) and gahnite (Gh_{10-34}) components. X_{Fe} varies between 0.76 and 0.85, but the compositions are relatively constant in any one specimen. Cr_2O_3-content is generally between 0.25-0.32 wt% but reaches 2.6-4.1 wt% (sample 46-3-96). Site and charge balance calculations indicate a low magnetite component (Fe^{3+}= 0.02-0.12). Zonation trends have not been identified.

Staurolite has only been found as retrograde, commonly tiny reaction products forming spherical to euhedral crystals. It occurs at the margins of biotite or in the vicinity of garnet and as small needles at the seams of cordierite in biotite-sillimanite-rich layers. In the analysed sample 50-4-96 X_{Fe} ranges between 0.80-0.88 and is therefore lower than that of associated garnet rims (X_{Fe}=0.88-0.89). MnO- and ZnO-contents are 0.16-0.28 wt% and 2.6-3.2 wt %. No regular zonation has been identified in individual grains.

Muscovite+quartz was not stable in the Mt. Gariglione Complex rocks during peak metamorphism, but muscovite formed during retrogression is very common. It forms randomly oriented blasts in leucosomes and melanosomes of the structurally higher part of the unit. Its formation after K-feldspar is indicated by the symplectitic intergrowth of muscovite with quartz or by inclusions of fibrolitic sillimanite and/or pseudomorphs after sillimanite (Fig. 2.3j) (Ashworth, 1972). Phengite component is low and uniform in the analysed samples (Si=3.08-3.11 cations per formular unit).

Table 2.2 Representative analyses of garnet from metapelites and metabasites.

Rock type	Metapelite											Metabasite				
Sample no.	21-97 core	33-97 core	33-97 core euhedral	42-96 core	46-3-96 core	50-4-96 core	50-4-96 core leucosome	57-1-96 core	57b/85 core	86-96 core	C8f core	27-97 core	29-96 seam	79-2-96 outer core	84-96 core elongated	84-96 core idiomorph
SiO2	38.02	37.83	37.80	38.54	38.60	38.33	37.62	38.95	37.72	38.58	37.60	38.88	37.96	37.99	38.51	38.71
Al2O3	21.28	21.04	21.17	21.56	21.60	21.37	20.79	21.83	21.32	21.90	21.27	21.71	21.11	21.50	21.55	21.60
FeO	36.89	35.48	37.01	31.86	32.80	34.53	34.64	29.70	34.14	31.47	37.38	29.11	28.47	30.45	30.97	30.17
MgO	4.19	3.95	3.17	6.49	6.25	4.82	2.79	8.43	5.42	7.17	3.21	7.96	3.93	5.22	6.15	6.07
MnO	0.83	1.07	1.51	0.78	0.75	1.27	4.11	0.61	0.86	0.81	0.92	1.10	1.38	1.11	1.50	1.35
CaO	0.76	1.33	1.00	1.40	1.14	1.28	1.16	1.11	1.15	1.53	1.01	1.74	6.89	4.34	2.35	2.84
Total	101.97	100.70	101.66	100.63	101.14	101.60	101.11	100.63	100.61	101.46	101.39	100.50	99.74	100.61	101.03	100.74
Structural formulae on a basis of 24 oxygens																
Si	5.99	6.02	6.006	6.02	6.02	6.02	6.03	6.01	5.97	5.97	5.99	6.01	6.02	5.97	6.00	6.03
Al	3.95	3.95	3.964	3.97	3.97	3.95	3.92	3.97	3.98	3.99	3.99	3.96	3.94	3.98	3.96	3.97
Fe(2+)	4.86	4.72	4.92	4.16	4.28	4.53	4.69	3.83	4.52	4.07	4.98	3.77	3.77	4.00	4.04	3.93
Mg	0.98	0.94	0.75	1.51	1.45	1.13	0.67	1.94	1.28	1.65	0.76	1.84	0.93	1.22	1.43	1.41
Mn	0.11	0.14	0.20	0.10	0.10	0.17	0.56	0.08	0.12	0.11	0.12	0.14	0.19	0.15	0.20	0.18
Ca	0.13	0.23	0.17	0.23	0.19	0.22	0.20	0.18	0.20	0.25	0.17	0.29	1.17	0.73	0.39	0.47
Total	6.09	6.03	6.04	6.01	6.02	6.04	6.12	6.03	6.10	6.08	6.04	6.03	6.06	6.10	6.06	5.99
Fe/(Fe+Mg)	0.83	0.83	0.87	0.73	0.75	0.80	0.87	0.66	0.78	0.71	0.87	0.67	0.80	0.77	0.74	0.74
XAlm	0.80	0.78	0.81	0.69	0.71	0.75	0.77	0.64	0.74	0.67	0.82	0.62	0.62	0.66	0.67	0.66
XGrs	0.02	0.04	0.03	0.04	0.03	0.04	0.03	0.03	0.03	0.04	0.03	0.05	0.19	0.12	0.06	0.08
XPrp	0.16	0.16	0.12	0.25	0.24	0.19	0.01	0.32	0.21	0.27	0.13	0.30	0.15	0.20	0.24	0.24
XSps	0.02	0.02	0.03	0.02	0.02	0.03	0.09	0.01	0.02	0.02	0.02	0.02	0.03	0.02	0.03	0.03

Table 2.3 Representative biotite analyses from metapelites and metabasites and structural formulae.

Rock type	Metapelite									Metabasite		
Sample no.	21-97 matrix	33-97 matrix	42-96 matrix	46-3-96 matrix	50-4-96 matrix	57-1-96 matrix	57b/85 matrix	86-96 matrix	C8f cont.grt	27-97 matrix	79-2-96 matrix	84-96 matrix
SiO2	35.40	36.00	37.90	36.38	36.30	36.45	35.89	37.49	34.84	37.73	35.41	36.51
TiO2	2.96	1.72	2.11	3.04	1.14	4.42	3.12	2.13	2.21	4.06	4.57	5.06
Al2O3	19.52	18.81	18.99	18.62	20.18	16.93	18.98	18.68	20.04	16.00	15.70	15.07
Cr2O3	0.00	0.09	0.08	0.11	0.03	0.27	0.09	0.09	0.03	0.05	0.06	0.14
FeO	20.98	20.41	14.22	16.73	18.97	13.18	17.87	15.18	22.49	12.45	17.39	14.92
MgO	7.62	9.95	13.74	11.60	10.69	14.11	10.24	13.53	7.97	14.99	11.94	13.50
MnO	0.02	0.02	0.00	0.04	0.05	0.00	0.05	0.00	0.06	0.05	0.01	0.05
CaO	0.01	0.00	0.00	0.00	0.00	0.00	0.00	0.02	0.00	0.02	0.00	0.00
Na2O	0.18	0.38	0.21	0.19	0.30	0.16	0.10	0.21	0.11	0.16	0.22	0.03
K2O	9.04	7.36	7.63	7.16	9.00	8.66	9.78	8.67	8.46	9.66	7.92	9.86
Total	95.73	94.74	94.88	93.87	96.66	94.18	96.12	96.00	96.21	95.17	93.22	95.14
Structural formulae on a basis of 22 oxygens												
Si	2.69	2.73	2.78	2.73	2.70	2.72	2.69	2.75	2.65	2.78	2.72	2.74
Al(IV)	1.31	1.27	1.22	1.27	1.30	1.28	1.31	1.25	1.35	1.22	1.28	1.26
Al	0.44	0.42	0.42	0.38	0.47	0.21	0.37	0.37	0.44	0.18	0.14	0.08
Ti	0.17	0.10	0.12	0.17	0.06	0.25	0.18	0.12	0.13	0.23	0.26	0.29
Cr	0.00	0.01	0.01	0.01	0.00	0.02	0.01	0.01	0.00	0.00	0.00	0.01
Fe(2+)	1.33	1.30	0.87	1.05	1.18	0.82	1.12	0.93	1.43	0.77	1.12	0.94
Mg	0.86	1.13	1.50	1.30	1.19	1.57	1.14	1.48	0.90	1.65	1.37	1.51
Mn	0.00	0.00	0.00	0.00	0.00	0.00	0.00	0.00	0.00	0.00	0.00	0.00
Total	2.81	2.94	2.91	2.91	2.90	2.86	2.82	2.90	2.91	2.82	2.90	2.83
Ca	0.00	0.00	0.00	0.00	0.00	0.00	0.00	0.00	0.00	0.00	0.00	0.00
Na	0.03	0.06	0.03	0.03	0.85	0.02	0.02	0.03	0.02	0.02	0.03	0.00
K	0.88	0.71	0.71	0.69	0.04	0.82	0.94	0.81	0.82	0.91	0.78	0.95
Total	0.91	0.77	0.74	0.71	0.90	0.85	0.95	0.84	0.84	0.93	0.81	0.95
Fe/(Fe+Mg)	0.61	0.54	0.37	0.45	0.50	0.34	0.49	0.39	0.61	0.32	0.45	0.38

Ilmenite and *rutile* are common accessory minerals and occur as primary matrix phases and as inclusions in garnet. Measured MnO-contents range between 0.14-1.57 wt% and 0.01-0.08 wt%, respectively. Further accessories are *monazite*, *zircon*, *apatite*, *pyrrhotite* and *graphite*.

2.5.2 Metabasites and intermediate rock types

Garnet is present in 19 of the 41 samples studied. Two textural types can be distinguished: net-like to subhedral porphyroblasts (0.6-3.0 mm) and smaller euhedral grains (<0.3 mm). The net-like grains, enclosing quartz, plagioclase and biotite suggest that no penetrative deformation took place after garnet growth. Both textural types together occur only in two of the analysed samples (79-2-96, 84-96). Formation of late-stage garnet is indicated by coronae around plagioclase separating it from orthopyroxene (sample 29-96, Fig. 2.3k) and from hornblende/cummingtonite. Late-stage poikilitic garnet grows at the expense of biotite+quartz symplectites which replaces orthopyroxene in sample 84-96 of enderbitic composition (Fig. 2.3l).

The cores of both textural garnet types are essentially unzoned and are in the range $Alm_{62\text{-}67}$, $Prp_{19\text{-}30}$, $Grs_{5\text{-}12}$, $Sps_{2\text{-}3}$ (Fig. 2.7, Table 2.2). Only the net-like garnet of sample 79-2-96 in the western part of the study area is weakly zoned and shows a slightly higher grossular content in the core, which decreases towards the inner part of the rim. This is interpreted as a relic of the prograde growth zoning. The X_{Fe}-values are 0.67-0.78 and increase towards the rims due to retrograde Fe-Mg exchange where garnet is in contact with ferromagnesian matrix minerals. The

Table 2.4 Representative cordierite analyses from metapelites and structural formulae.

Sample no.	21-97 core	33-97 core	42-96 core	46-3-96 core	50-4-96 core	57b/85 core	86-96 core	57-1-96 core	C8f core
SiO2	48.46	49.07	50.32	49.56	49.11	49.11	50.00	50.00	47.93
TiO2	0.02	0.01	0.02	0.00	0.00	0.00	0.00	0.00	0.00
Al2O3	32.19	32.23	33.16	32.64	32.91	33.16	33.03	33.29	32.17
FeO	11.17	9.75	5.74	6.43	8.37	8.07	5.72	4.79	11.62
MgO	6.71	7.03	9.74	9.22	8.12	8.56	10.09	10.40	6.29
MnO	0.09	0.11	0.04	0.03	0.25	0.08	0.00	0.00	0.13
CaO	0.01	0.00	0.01	0.00	0.02	0.02	0.02	0.02	0.01
Na2O	0.12	0.22	0.09	0.08	0.21	0.05	0.10	0.04	0.24
K2O	0.00	0.01	0.00	0.02	0.02	0.01	0.00	0.02	0.00
Total	98.77	98.43	99.12	97.98	99.01	99.06	98.96	98.56	98.39
Structural formulae on a basis of 18 oxygens									
Si	5.03	5.07	5.07	5.07	5.02	5.01	5.05	5.04	5.01
Al	0.97	0.93	0.93	0.93	0.98	0.99	0.95	0.96	0.99
Al	2.97	3.00	3.00	3.00	2.99	2.99	2.98	3.00	2.97
Ti	0.00	0.00	0.00	0.00	0.00	0.00	0.00	0.00	0.00
Total	2.97	3.00	3.01	3.00	2.99	2.99	2.98	3.00	2.97
Fe(2+)	0.97	0.84	0.48	0.55	0.72	0.69	0.48	0.40	1.02
Mg	1.04	1.08	1.46	1.41	1.24	1.30	1.52	1.56	0.98
Mn	0.01	0.01	0.00	0.00	0.02	0.01	0.00	0.00	0.01
Total	2.02	1.94	1.95	1.96	1.98	2.00	2.00	1.97	2.01
Ca	0.00	0.00	0.00	0.00	0.00	0.00	0.00	0.00	0.00
Na	0.02	0.04	0.02	0.02	0.04	0.01	0.02	0.01	0.05
K	0.00	0.00	0.00	0.00	0.00	0.00	0.00	0.00	0.00
Total	0.03	0.05	0.02	0.02	0.05	0.01	0.02	0.01	0.05
Fe/(Fe+Mg)	0.48	0.44	0.25	0.28	0.37	0.35	0.24	0.21	0.51

rims of net-like and of subhedral garnet and also of some euhedral ones (sample 79-2-96) are characterized by a rimward increase of the grossular component (only weak in sample 27-97). As it is obvious from the Ca-Fe-Mg ternary in Fig. 2.8 that garnet-orthopyroxene bearing rocks without hornblende as a Ca-buffering phase contain garnet poorer in grossular component than those with hornblende. The compositions of the late-stage garnet coronae between orthopyroxene and plagioclase are nearly the same as those of the matrix grains (Alm_{61-63}, Prp_{15-16}, Grs_{17-20}, Sps_{3}).

Plagioclase is a main constituent of all metabasic rocks. The cores of the anhedral grains (0.1-0.7 mm) are unzoned with compositions normally constant within a thin section (An_{39-85}; Table 2.5). Most of the analysed plagioclase grains are characterized by an increase of anorthite contents at the rims. In sample 27-97 smaller recrystallized matrix grains (<0.3 mm) contain higher anorthite values in the cores (up to 20%) than the larger ones. This may correspond to the higher anorthite contents in rims of matrix plagioclase.

Table 2.5 Representative plagioclase analyses from metapelites and metabasites and structural formulae.

Rock type	Metapelite								Metabasite				
Sample no.	21-97 core	33-97 core	42-96 core	46-3-96 core	50-4-96 core	57-1-96 core	57b/85 core	86-96 core	27-97 core	29-96 rim	29-96 core	79-2-96 core	84-96 core
SiO2	60.16	60.25	58.24	58.92	59.72	60.58	60.85	58.27	57.57	45.57	46.83	50.34	59.07
Al2O3	25.02	25.88	26.65	26.53	26.17	24.72	25.63	26.97	26.83	34.31	33.26	31.59	25.48
Fe2O3	0.08	0.00	0	0.07	0.01	0.02	0.00	0.00	0.06	0.15	0.00	0.09	0.00
CaO	6.78	7.53	9.34	8.32	7.81	6.52	6.72	8.89	9.54	18.34	17.46	14.51	7.99
Na2O	7.54	7.30	6.5	6.85	7.25	7.82	7.41	6.55	6.11	1.14	1.73	3.25	6.71
K2O	0.19	0.05	0.04	0.03	0.04	0.13	0.12	0.07	0.10	0.01	0.01	0.05	0.30
Total	99.77	101.01	100.77	100.72	101.00	99.79	100.73	100.75	100.21	99.52	99.29	99.83	99.55
Structural formulae on a basis of 8 oxygens													
Si	2.68	2.66	2.59	2.61	2.64	2.70	2.68	2.59	2.58	2.11	2.17	2.30	2.65
Al(IV)	1.32	1.35	1.40	1.39	1.36	1.30	1.33	1.41	1.41	1.87	1.81	1.70	1.35
	4.00	4.00	3.99	4.00	4.00	4.00	4.01	4.00	3.99	3.98	3.98	4.00	3.99
Fe(3+)	0.00	0.00	0.00	0.00	0.00	0.00	0.00	0.00	0.00	0.01	0.00	0.00	0.00
Ca	0.32	0.36	0.45	0.40	0.37	0.31	0.32	0.42	0.46	0.91	0.87	0.71	0.38
Na	0.65	0.62	0.56	0.59	0.62	0.68	0.63	0.56	0.53	0.10	0.16	0.29	0.58
K	0.01	0.00	0.00	0.00	0.00	0.01	0.01	0.00	0.01	0.00	0.00	0.00	0.02
Total	0.99	0.98	1.01	0.99	0.99	1.00	0.96	0.99	1.00	1.02	1.02	1.00	0.98
An	32.83	36.22	44.19	40.06	37.26	31.29	33.12	42.68	46.02	89.83	84.74	70.97	39.02
Ab	66.06	63.48	55.61	59.74	62.54	68.01	66.14	56.91	53.37	10.07	15.17	28.73	59.25
Kfs	1.11	0.31	0.20	0.20	0.20	0.70	0.73	0.40	0.60	0.10	0.10	0.30	1.73

Orthopyroxene occurs in nine of the 41 rock samples and only in the western part of the study area. The net-like to anhedral blasts (0.1-0.6 mm) are unzoned in cores (Table 2.6). In the enderbitic sample 84-96 net-like grains, enclosing quartz, plagioclase and small euhedral garnet (Fig. 2.3l) suggest that no penetrative deformation took place after peak metamorphism. The X_{Fe}- and Al(VI)-values are very similar in the analysed samples (0.48-0.49; Fig. 2.8 and 0.02-0.05 cations per 8-oxygen formular unit) with the exception of orthopyroxene of sample 27-97 which has lower X_{Fe}- and higher Al(VI) values (0.42 and 0.08). In contact with garnet orthopyroxene shows narrow rims slightly lower in X_{Fe} due to retrograde Fe/Mg exchange. The combination of the moderate rimward decrease of Al-content in orthopyroxene and the increase of the grossular component in garnet preserves a record of cooling (Bégin & Pattison, 1994; Fitzsimons & Harley, 1994). Common retrograde breakdown products of orthopyroxene are cummingtonite and/or hornblende and biotite+poikilitic garnet (sample 84-96).

Amphibole, occuring in nearly every studied sample, is green *hornblende* and *cummingtonite* and is interpreted as a retrograde formation after pyroxene. Rare brown and dark brown-green hornblende as matrix mineral and as tiny inclusion in plagioclase have been found only in three samples and might be relics of the prograde stage. Common are patchy intergrowths of both amphiboles and, less common, hornblende lamellae within cummingtonite. These textures may be interpreted as formerly homogeneous or coexisting clinoamphiboles which exsolved during cooling (e.g. Klein *et al.*, 1996). Seams of hornblende around cummingtonite do also occur. The calcic amphiboles range in composition from actinolite to mainly magnesiohornblende applying the nomenclature of Leake *et al.* (1997). The generally anhedral grains are unzoned and their Si-, Al- and Ti-values range between 6.8-7.7, 0.56-1.79 and 0.03-0.1 cations per 23-oxygens formular unit, (Table 2.6). The X_{Fe}-values are always lower (0.34-0.43) than the ones of coexisting

Table 2.6 Representative analyses of orthopyroxene, hornblende and cummingtonite from metabasites and structural formulae.

Sample no.	27-97	29-96	79-2-96	84-96	29-96	79-2-96	29-96	79-2-96
Mineral	orthopyroxene core	orthopyroxene core	orthopyroxene core	orthopyroxene core	hornblende core	hornblende core	cummingtonite core	cummingtonite core
SiO2	50.76	51.20	50.98	51.19	47.23	46.23	54.14	54.26
TiO2	0.07	0.07	0.00	0.09	0.86	0.93	0.04	0.02
Al2O3	4.07	0.91	1.37	2.04	9.64	10.53	0.55	0.95
Cr2O3	0.11	0.03	0.00	0.03	0.00	0.00	0.00	0.00
FeO	25.01	28.83	29.53	28.66	14.86	15.45	23.42	24.58
MgO	19.78	17.26	17.59	17.50	12.22	11.54	17.87	17.51
MnO	0.48	0.39	0.31	0.41	0.14	0.05	0.32	0.24
CaO	0.16	0.45	0.43	0.24	11.66	11.42	0.88	1.14
Na2O	0.00	0.00	0.00	0.02	0.77	0.63	0.02	0.04
K2O	0.00	0.00	0.00	0.00	0.23	0.53	0.01	0.00
	100.44	99.14	100.21	100.18	97.61	97.31	97.25	98.74
	Structural formulae on a basis of 6 oxygens (orthopyroxene) and 23 oxygens, ignoring H_2O (amphibole)							
Si	1.90	1.98	1.96	1.96	6.92	6.82	7.94	7.88
Al(IV)	0.10	0.02	0.04	0.04	1.08	1.18	0.06	0.12
Al	0.08	0.03	0.02	0.05	0.59	0.66	0.04	0.04
Ti	0.00	0.00	0.00	0.00	0.10	0.10	0.00	0.00
Cr	0.00	0.00	0.00	0.00	0.00	0.00	0.00	0.00
Fe(2+)	0.79	0.93	0.95	0.92	1.82	1.91	2.87	2.99
Mg	1.11	1.00	1.01	1.00	2.67	2.54	3.91	3.79
Mn	0.02	0.01	0.01	0.01	0.02	0.01	0.04	0.03
Ca	0.01	0.02	0.02	0.01	1.83	1.81	0.14	0.18
Na	0.00	0.00	0.00	0.00	0.22	0.18	0.01	0.01
K	0.00	0.00	0.00	0.00	0.04	0.10	0.00	0.00
Total	2.00	1.99	2.01	1.99	7.28	7.30	7.01	7.04
Fe/(Fe+Mg)	0.42	0.48	0.49	0.48	0.41	0.43	0.42	0.44

cummingtonite (0.36-0.45) and orthopyroxene (0.48). Not exsolved hornblende contains higher X_{Fe}-values than that intergrown with cummingtonite.

Biotite occurs in most of the studied samples, but its modal abundance is normally low (<3 Vol%). Three textural types of biotite can be distinguished: matrix phases, inclusions in garnet and late stage formations after orthopyroxene. The lowest X_{Fe}-values are found in biotite inclusions in garnet. X_{Fe}-value varies from 0.25 to 0.46 and the Ti-content ranges between 0.14 and 0.29 cations per 22-oxygen formular unit (Table 2.3) and is thus higher than in metapelitic biotite. Biotite is unzoned and homogeneous in composition.

Clinopyroxene occurs in five of the 41 metabasites of the western part of the study area. The grains are euhedral to subhedral in the range of 0.4-1.3 mm in diameter. Some grains contain hornblende lamellae that seem to have been formed after exsolved pyroxenes. Larger porphyroblasts (1.1-2.3 mm) show retrograde coronae of poikilitic green hornblende with quartz inclusions.

Ilmenite is a common accessory mineral and occurs as a primary matrix phase and as inclusion in garnet. Measured MnO-contents range between 0.3-0.39 wt%. Further accessories are *sphene*, intergrown with ilmenite in some samples, *apatite*, *allanite* and *zircon*.

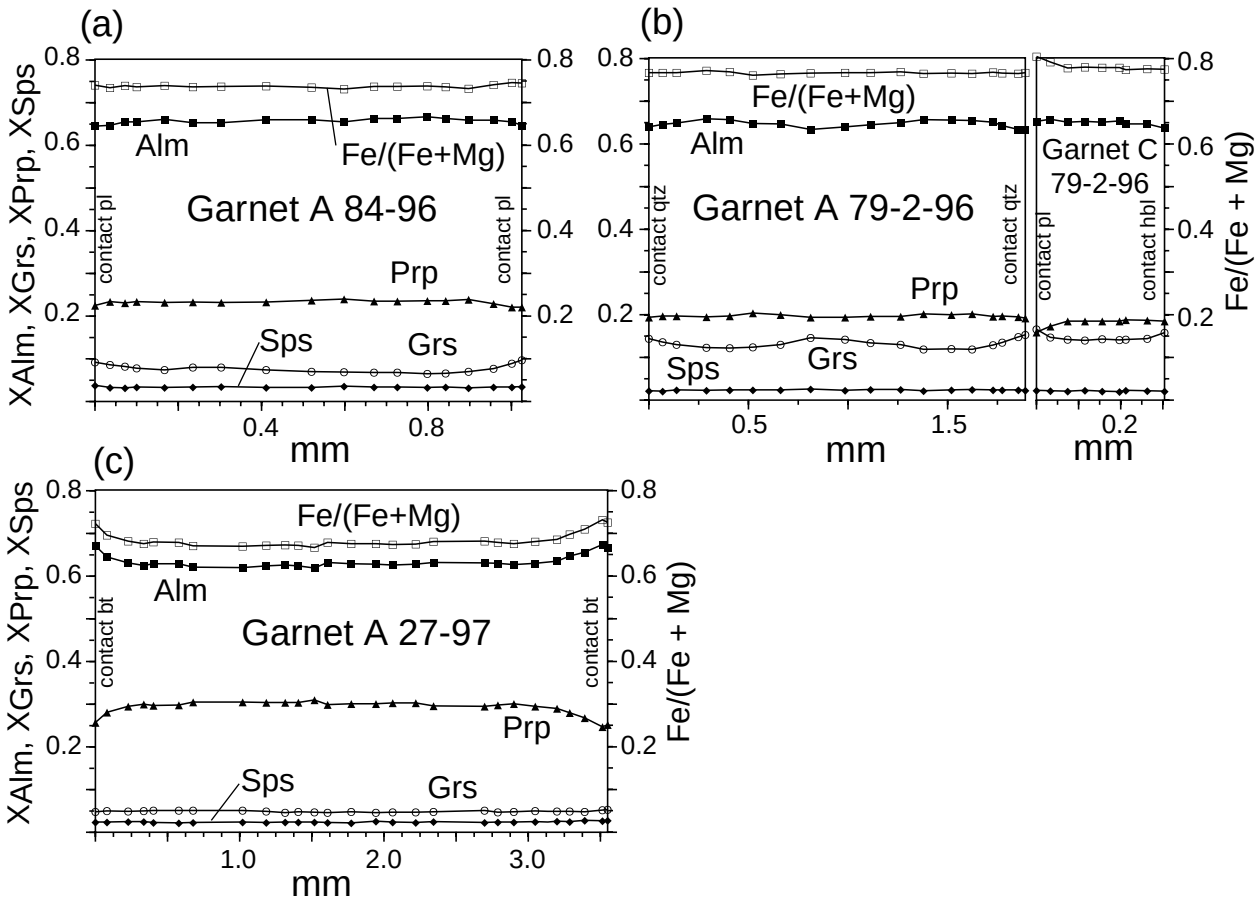

Fig. 2.7 Zoning profiles of garnet porphyroblasts from metabasites of the Mt. Gariglione Complex. Each profile extends from rim to rim through the core of the garnets. Location of samples is given in Fig. 2.2b.

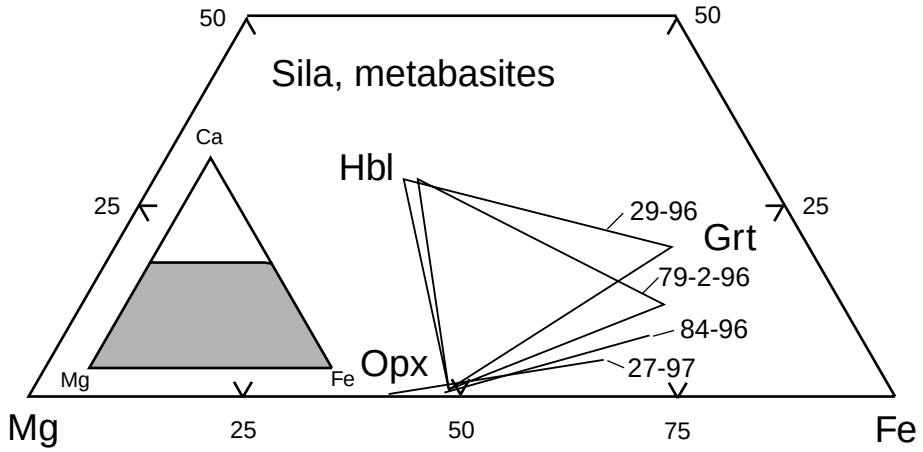

Fig. 2.8 Lower portion of a Ca-Mg-Fe ternary (inset) of coexisting garnet, orthopyroxene and hornblende from the analysed metabasic rock samples. Location of samples is given in Fig. 2.2b.

2.6 MINERAL REACTION HISTORY

2.6.1 Prograde reactions

The prograde reaction history in *metapelites* is best constrained by mineral inclusions in garnet and the presence of quartzofeldspathic leucosomes. Abundant leucosomes in most of the rock samples (*c*. 10-20 vol%) and mineral textures like biotite-quartz symplectites at the margins of the leucocratic segregations (Fig. 2.3d) indicate that dehydration melting has occurred. Sillimanite inclusions in garnet and cordierite are evidence that prograde metamorphism proceeded within the stability field of sillimanite. The absence of muscovite and the overall presence of the assemblage sillimanite+K-feldspar+quartz requires temperature conditions above the dehydration melting of muscovite according to the univariant reaction

$$Ms + Pl + Qtz = Sil + Kfs + L \quad (1).$$

Some of the clots of fibrolitc sillimanite within the leucosomes may be prograde products of the latter reaction. Since many metapelitic rock types may not contain enough muscovite to produce more than 10 vol% of melt due to this reaction (Clemens & Vielzeuf, 1987; Spear *et al.*, 1999) further melt reactions have to be taken into account for the Calabrian metapelites.

Inclusions of biotite and plagioclase in the cores and sillimanite in the rims of garnet point to the divariant garnet-producing melting reaction in assemblage with K-feldspar

$$Bt + Sil + Pl + Qtz = Grt + Kfs + L \quad (2).$$

This biotite-dehydration reaction may produce a large amount of H_2O-undersaturated melt in rocks of pelitic composition (e.g. 20-30 vol%; Clemens and Vielzeuf, 1987; Le Breton & Thompson, 1988) depending on the initial modal amount of biotite and the *P-T* conditions during melting. As described above, garnet rims are characterized by numerous sillimanite-inclusions parallel to the matrix foliation due to an overgrowth of a preexisting sillimanite fabric. In some of the analysed samples this coincides with the part of the garnet which contains slightly higher grossular content. Crossing of the muscovite dehydration melting curve (reaction 1) during prograde metamorphism both plagioclase and melt will become more calcic. When garnet resumes growth due to reaction (2) subsequent to muscovite dehydration melting the Ca in the rim of garnet will be higher in order to adjust to the new plagioclase composition (Spear & Parrish, 1996; Spear *et al.*, 1999).

Some of the studied rocks might be more magnesium-rich since they contain cordierite instead of garnet (Fig. 2.2a). In these rocks cordierite could have been produced by a melting reaction analogous to reaction (2). Further melting proceeds with changing *P-T* condition until the univariant reaction

$$Bt + Sil + Qtz = Grt + Crd + Kfs + L \quad (3)$$

is intersected. This leads to coarse grained peak metamorphic garnet-cordierite-K-feldspar-bearing assemblages in melanosomes coexisting with Bt-Sil-Qtz, an assemblage which is found throughout the study area. In consequence, biotite-dehydration reactions (2) and (3) account for garnet+cordierite-bearing leucosomes. Few cordierite-inclusions in garnet rims (Fig. 2.3a) refect the divariant FMASH-reaction

$$Crd = Grt + Sil + Qtz \quad (4),$$

which points to a pressure increase during prograde metamorphism.

Prograde reaction textures in *metabasites* and *intermediate rock* types are poorly preserved. Dehydration melting of hornblende did not take place since this reaction occurs at higher temperatures than any of those involving biotite (Clemens and Vielzeuf, 1987). In the enderbitic sample 84-96 dehydration which may have taken place at the metamorphic peak led to the formation of large net-like orthopyroxene porphyroblasts together with small euhedral garnet due to a reaction like

$$Bt + Qtz = Opx + Grt_{id} + Kfs + V \quad (5) \text{ (Fig. 2.3l).}$$

A Ti-phase may have contributed to this reaction as described for intermediate and felsic rock types of the Serre in southern Calabria (Schenk, 1984). K-feldspar has not been found in the sample described here, but a K-bearing fluid or potassic feldspar must have been involved in this dehydration of biotite.

2.6.2 Retrograde reactions

The metapelitic and metabasic rocks were strongly affected by retrograde metamorphism. This is most obvious by the many decompression textures and even more common by re-hydration reactions. Decompression after peak metamorphism is documented by textures like cordierite rims around garnet in *metapelites* which have been formed due to the reverse of the continuous reaction (4) (Fig. 2.3a) or due to

$$Grt + Sil + L = Crd + Kfs \quad (6)$$

which has also a flat slope and is therefore nearly independent of temperature (Spear *et al.*, 1999).

In small quartz-deficient domains of metapelites, symplectitic intergrowth of spinel and cordierite besides inclusions of sillimanite and spherical relics of prograde biotite in cordierite, and in some cases also of spinel, accounts for the divariant reaction

$$Bt + Sil = Crd + Spl + Kfs \pm Ilm + L \quad (7) \text{ (Fig. 2.3h).}$$

This reaction has been proposed by Brown (1998) and Whittington *et al.* (1998) for low-pressure rocks of the Ryoke Belt and the Nanga Parbat. Since the reaction has a positive slope the observed textures also indicate decompression after peak metamorphism. In some cases the reverse of reaction (7) took place in the same rock which suggests decreasing temperatures subsequent to decompression. This late-stage reaction is documented by sillimanite seams around spinel inclusions in cordierite and newly grown biotite (Fig. 2.3i). In one silica undersaturated rock decompression is documened by spinel-cordierite symplectites replacing garnet which can be explained by the reaction

$$Grt + Sil = Spl + Crd \quad (8).$$

Again, a temperature decrease is indicated by the replacement of garnet and locally of cordierite by aggregates of biotite+sillimanite±plagioclase. This re-hydration is either due to water released from crystallizing melts or to water that is derived externally. A back reaction involving melt

instead of vapour might also be possible at some higher temperatures. The reverse of reactions (2) and (3) accounts for those textures. Mats of fibrolitic sillimanite intergrown with biotite replacing garnet and/or cordierite may have formed by these reactions (Fig. 2.3b). In aggregates of biotite and plagioclase in which sillimanite is missing garnet is consumed by the reaction

Grt + Kfs + L/V = Bt + Pl + Qtz (9) (Fig. 2.3c).

Some coarse grained randomly oriented muscovite flakes in leucosomes surrounding fibrolite and/or pseudomorphs after sillimanite may have been formed due to the reverse of reaction (1) (Kfs + Sil + L/V = Ms + Qtz ± Pl; Fig. 2.3j). In the western part of the study area, the further temperature decrease is accompanied by the formation of small subhedral to euhedral staurolite grains in the vicinity of garnet and of small needles at the seams of cordierite suggesting the reaction

Crd + Grt + Sil + V = St + Qtz (10).

In rock samples with retrograde muscovite, exclusively in those of the eastern part, staurolite grows at the rims and at the expense of biotite in the vicinity of garnet by the reaction

Bt + Sil ± Grt + V = St + Ms + Qtz (11).

Further cooling leads to the decomposition of cordierite due to the reactions

Crd + Bt = Chl + Ms + Qtz (12) and

Crd = Chl + And + Qtz (13) (Fig. 2.3e) or

Crd = Chl + Ky + Qtz (14) (Fig. 2.3g).

Reactions 12 and 13 are only observed in the eastern part of the study area whereas the kyanite producing reaction (14) is only found in one sample of the western part (Fig. 2.2a). Retrograde andalusite sometimes overgrow fibrolite and sillimanite and is therefore clearly of late-stage origin (Fig. 2.3f). Magnesite instead of chlorite has never been formed among the decomposition products of cordierite. This reflects lower X_{CO2}-values of the fluid phase during retrogression than in metapelites of S-Calabria, where magnesite is very common (Schenk, 1990).

Textures like garnet rims between plagioclase and orthopyroxene in *metabasites* suggest a nearly isobaric cooling path during which the reaction

Opx + Pl = Grt + Qtz (15) (Fig. 2.3k)

has been crossed. This texture was found in the west and in one rock only. Rehydration reactions are widespread in the study area and have commonly affected ortho- and clinopyroxene. Cummingtonite and/or green hornblende surrounding orthopyroxene may have formed due to the reactions

Opx + Pl + Ilm + V = Hbl + Qtz (16) and

Opx + Qtz + V = Cum (17).

Partial replacement of clinopyroxene by hornblende-quartz symplectites reflect the reaction

Cpx + Pl + Ilm + V = Hbl + Qtz (18).

Textural features like garnet seams separating cummingtonite from plagioclase, all in assemblage with biotite and hornblende, could be interpreted as due to the prograde divariant reaction

Cum + Bt + Pl + Ilm = Grt + Hbl + Qtz + V (19).

This reaction has been described by Hollocher (1991) in Fe-rich metabasic rocks of central Massachusetts. However, in the Sila the described garnet coronae are associated with rare relics of orthopyroxene inclusions in cummingtonite, which suggests retrograde formation of cummingtonite by rehydration of the granulite facies orthopyroxene. In this case the garnet reaction rims are presumably formed like cummingtonite at a retrograde stage which might reflect a reaction like

Opx + Pl + V = Grt + Cum + Hbl + Qtz (20) (Hollocher, 1991).

Textures of biotite-quartz symplectites and poikilitic garnet overgrowing orthopyroxene in the enderbitic sample 84-96 record a rehydration reaction like the following

Opx + Kfs + Ilm + V = Bt + Grt_{poik} + Qtz (21) (Schenk, 1984; Fig. 2.3l).

2.7 PHASE RELATIONS OF METAPELITES

The mineral assemblages Grt+Sil+Crd+Qtz and Grt+Sil+Kfs+Bt+Qtz are the most common ones in the studied metapelites (Fig. 2.2a) and can be used to look for regional differences in metamorphic grade within the Mt. Gariglione Complex. In these assemblages the ferromagnesian minerals become more Mg-rich with increasing metamorphic grade (Thompson, 1976). From the variations of the X_{Fe}-values of coexisting minerals a metamorphic gradient along the two E-W profiles through the Sila Piccola can be deduced. This relationship can be shown in an AFM-diagram of the pure KFMASH-system, projected from the appropriate excess components. Since MnO and CaO in garnet are very low (1-3 mol% spessartine, 2-4 mol% grossular) and are also minor in the coexisting minerals, their influence on the plotting positions of the minerals can be ignored.

Figure 2.9 shows two A_2O_3-FeO-MgO-triangles for rocks with the Grt+Sil+Crd+Qtz-assemblage (projected from quartz) from the northern and southern profile. Decreasing X_{Fe}-values in cores of garnet and matrix cordierite from east to west of the study area result in a shift of the three-phase-field Grt-Sil-Crd towards the Mg-side of the triangle. From this a continuous pressure increase from east to west through the Mt. Gariglione Complex can be inferred. The high X_{Fe}-values of cordierite (0.20-0.51) clearly reflect lower metamorphic pressures than in the Serre section, where X_{Fe}-values do not exceed 0.28 (Schenk, 1984; Fig. 2.9).

A corresponding temperature gradient deduced from decreasing X_{Fe} in coexisting garnet-biotite-pairs is not well established by garnet-biotite thermometry due to retrograde equilibration of matrix biotites (see above). The strong retrogression has led to homogeneous composition fields of biotite of any one sample (Fig. 2.5). Nevertheless, like coexisting garnet biotite is shifted towards lower X_{Fe}-values from the east to the west of the Mt. Gariglione Complex, which can be

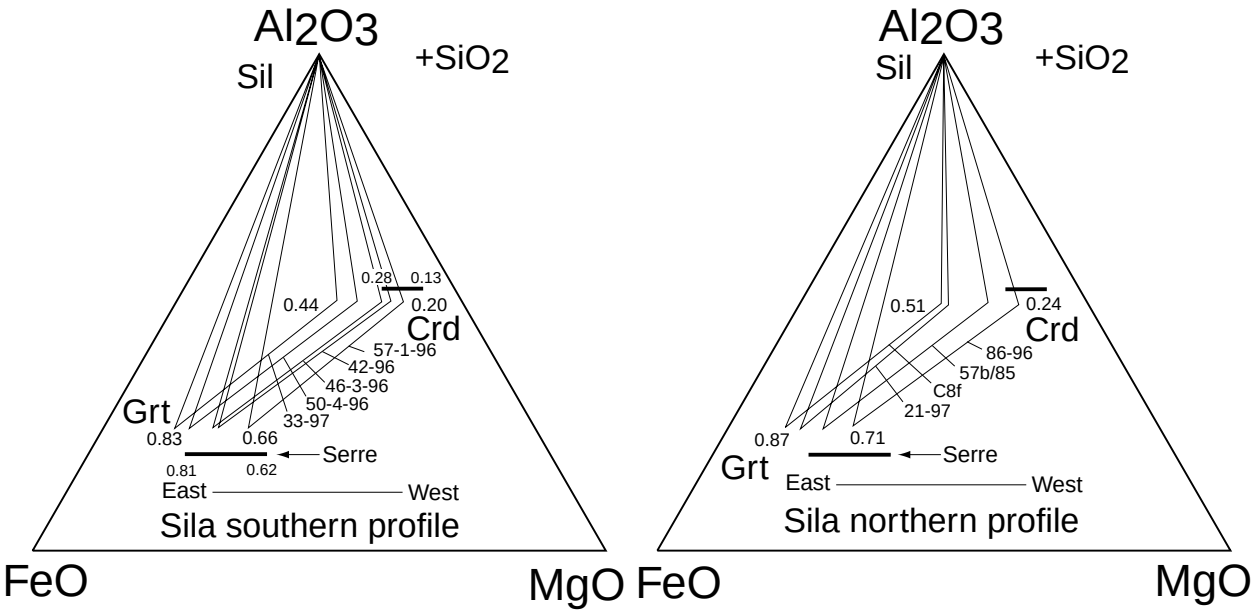

Fig. 2.9. Al_2O_3-FeO-MgO projection from quartz of the assemblage garnet-cordierite-sillimanite-quartz in metapelitic rocks along the two studied profiles through the Mt. Gariglione Complex. In both profiles the three phase fields show a shift towards the Mg-side of the triangle from the top (in the east) towards the base (in the west). For comparison the range of X_{Fe}-values of garnet and cordierite in metapelites of the lower crust in the Serre of southern Calabria are given as heavy bars (Schenk, 1984).

explained by increasing metamorphic temperatures.

2.8 *P-T* CONDITIONS

First indications on the *P-T* conditions during peak metamorphism are obtained from mineral assemblages of the high-grade gneisses in the western part of the Mt. Gariglione Complex. The stability of the assemblage Opx+Pl+Qtz±Grt and the absence of Grt-Cpx-Otz in metabasites points to the *P-T* field for medium pressure granulites (700-850 °C at 5-7 kbar; Green and Ringwood, 1967). The same conditions are revealed by the silica-undersaturated Ol-metagabbros in which magmatic olivine and plagioclase are separated by metamorphic coronae of orthopyroxene+clinopyroxene+spinel. This reaction represents the transition between low- and intermediate pressure granulites (725-880 °C at 5-7 kbar; Green & Ringwood, 1972; Fig 2.12).

In carbonate rocks textures suggest retrograde overstepping of the re-volatilization reaction Fo + Cal + V = Di + Dol during cooling from peak metamorphic temperatures. According to the experiments of Käse & Metz (1980), these must have been higher than 690-720 °C at 5-7 kbar.

All metapelites are metamorphosed at sillimanite-K-feldspar grade and muscovite+quartz was not stable. Further heating has led to biotite dehydration melting recorded by textures pointing to reactions (2) and (3) as discussed above (Fig. 2.17). Peak metamorphic conditions must have been below the Bt+Qtz- or Bt+Grt+Qtz-breakdown (<820-840 °C at 5-7 kbar; Spear *et al.*, 1999; Fig. 2.17) since orthopyroxene is missing in the metapelites of the Sila.

In the following section *P-T* conditions along the two east-west profiles studied here, are first estimated by conventional geothermobarometry applying well calibrated net transfer and cation exchange reactions uniformly at 5 kbar (temperature estimates) and 700 °C (pressure estimates) (Table 2.7). These results will be compared to results calculated with the TWEEQU program (Berman, 1991). For estimating peak metamorphic conditions normally the core compositions of coexisting matrix minerals were used since those are assumed to preserve the highest metamorphic grade and show little alteration by retrograde element exchange. For the enderbitic sample 84-96 peak conditions were estimated using the composition of the small euhedral garnet grains thought to have been formed together with orthopyroxene at the peak of metamorphism. Retrograde conditions were calculated applying rim compositions of matrix minerals that are/or are not in contact with each other (Table 2.8).

2.8.1 Conventional Geothermometry

In *metapelites* calculated peak metamorphic temperatures based on the Fe-Mg partition between coexisting garnet and cordierite (Thompson, 1976; Bhattacharya *et al.*, 1988 and Dwivedi *et al.*, 1998) as well as garnet and biotite (Hodges & Spear, 1982) are similar in both profiles ranging from *c*. 660 to 820 °C and from *c*. 630 to 830 °C (Table 2.7a, Fig. 2.10). Within each analysed rock specimen the calculated garnet-cordierite temperatures scatter for about 20 to 60 °C. The presence of a temperature gradient from east to west through the Mt. Gariglione Complex as deduced from phase relations is not supported by the absolute values obtained by geothermometry. The highest temperatures (e.g. 740 to 830 °C) were calculated in rock samples of the eastern part of the study area, where a lower metamorphic grade than in the western part has been deduced from AFM phase relations. The reason that thermometry yields temperatures that might be too high is that due to retrograde sliding reactions cores of matrix biotite and cordierite may have obtained higher X_{Fe}-ratios than they had at the metamorphic peak, whereas garnet core may not have changed its composition (Fig. 2.11). Peak temperature conditions of 730 to *c*. 770 °C for metapelites of the western part of the study area (samples 57-1-96, 57b/85 and 86-96) might be more realistic than those obtained in the east. In the west some unrealistic low temperatures (*c.* 630-710 °C) were determined, presumably due to intensive late-stage cation exchange.

Retrograde temperatures calculated for garnet rims and adjacent biotite or cordierite seams are 140 to 300 °C and 60 to 130 °C lower than peak estimates for the same sample (Table 2.8a, Fig. 2.10) which can be interpreted with retrograde Fe-Mg exchange between minerals in contact during cooling of the rocks.

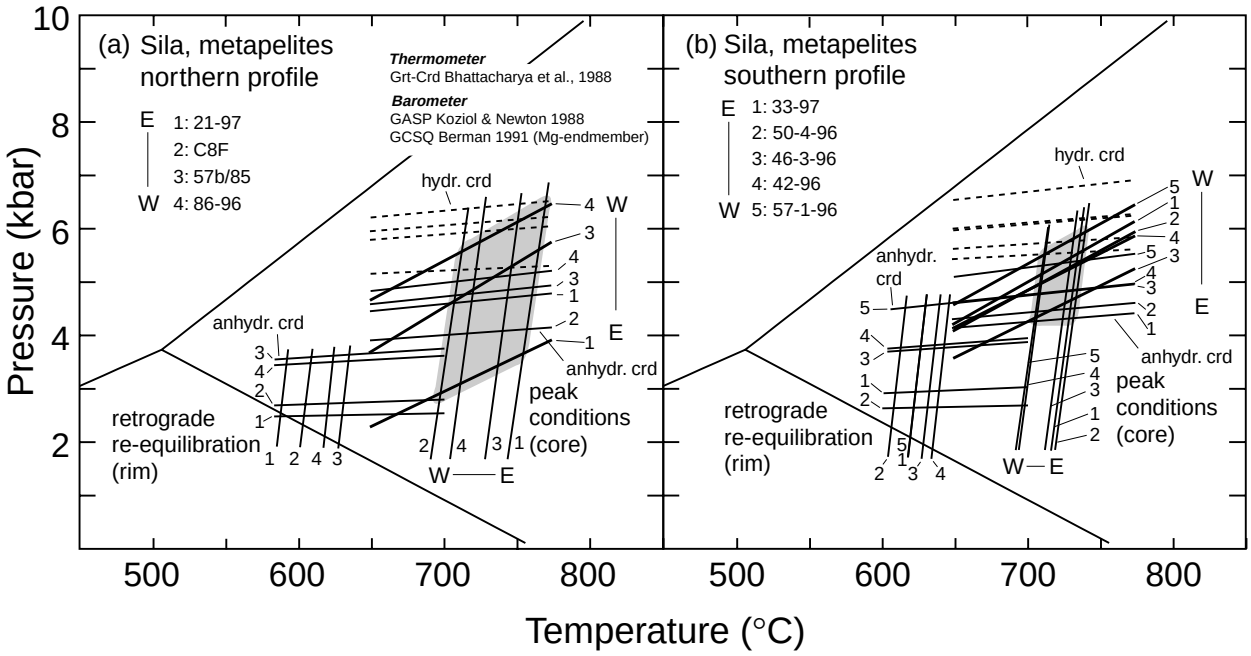

Fig. 2.10 Estimates of peak-metamorphic *P-T* conditions and retrograde re-equilibration calculated for each analysed metapelitic sample of the northern and southern profile through the Mt. Gariglione Complex. Pressures estimated with the GASP (Koziol & Newton, 1988; thick lines) and the GCSQ geobarometers (Berman, 1991, Mg-endmember; thin nearly horizontal lines: with anhydrous cordierite; thin dashed lines: with hydrous cordierite). Temperatures are based on the Mg-Fe partition between garnet and cordierite (Bhattacharya *et al.*, 1988).

In the *metabasites* and *intermediate rocks* temperatures could only be calculated from three samples of the structurally lower, western part of the study area. Temperature estimates are based on the Fe-Mg partition between coexisting garnet and orthopyroxene (Harley, 1984; Lee & Ganguly, 1988; Bhattacharya *et al.*, 1991) as well as garnet and hornblende (Graham & Powell, 1984) and on the Al-solubility in orthopyroxene coexisting with garnet (Harley & Green, 1982). Garnet-orthopyroxene thermometry calibrated by Bhattacharya *et al.* (1991) reveals peak temperatures ranging from *c.* 700-720 °C, which is generally 20 to 50 °C and 30 to 70 °C higher than those determined with the Lee and Ganguly (1988) (*c.* 660-700 °C) and Harley (1984) (*c.* 630-690 °C) calibrations (Table 2.7b, Fig. 2.12). The temperatures based on the Al-content in orthopyroxene (Harley and Green, 1982) lie within the temperatures obtained by Fe-Mg exchange thermometry with the only exception of sample 27-97 (785 °C). Therefore, the calibration of Bhattacharya, *et al.* (1991) yields the highest values among the applied geothermometers for metabasites but the results are still lower than those calculated for metapelites.

Retrograde temperatures (Table 2.8b) calculated for late-stage garnet coronae separating orthopyroxene and plagioclase (sample 29-96) are 573 °C (Harley, 1984), 601 °C (Lee & Ganguly, 1988) and 642 °C (Bhattacharya *et al.*, 1991). Rims of isolated single garnet and orthopyroxene grains as well as rims of grains in contact reveal temperatures in the range of 500-

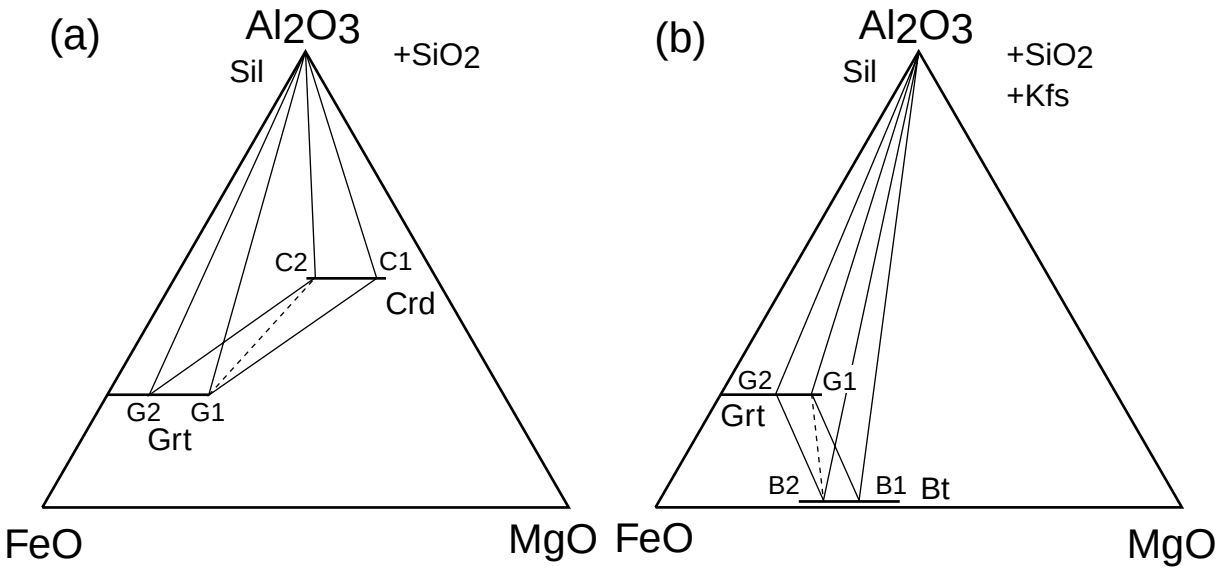

Fig. 2.11 Schematic AFM diagrams illustrating that garnet-cordierite (a) and garnet-biotite thermometry (b) results in temperatures higher than the metamorphic peak if analyses *G1* and *C2* in a and *G1* and *B2* in b are combined. *G1*, *C1* and *B1* are garnet, cordierite and biotite at the peak of metamorphism and *G2*, *C2* and *B2* are compositions after retrograde sliding reactions.

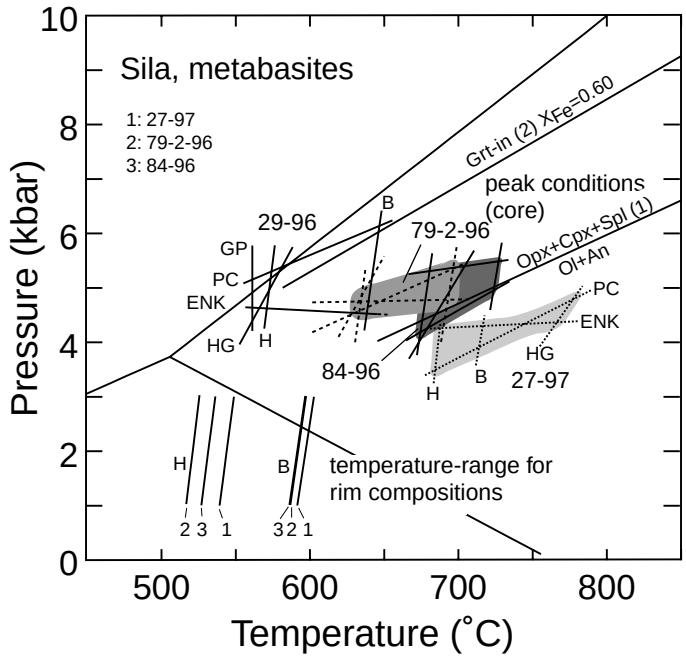

Fig. 2.12 Estimates of peak-metamorphic *P-T* conditions and temperatures for mineral rim compositions of metabasites and intermediate rock types. Pressures estimated with the GOPQ geobarometer (PC: Perkins & Chipera, 1985; ENK: Eckert *et al*., 1991) and the Al-solubility in orthopyroxene (HG: Harley & Green, 1982). Temperatures base on the Fe-Mg partitioning between garnet and orthopyroxene (H: Harley, 1984; B: Bhattacharya *et al.*, 1991) and garnet and hornblende (GP: Graham & Powell, 1984). (1) Green & Ringwood (1972), silica undersaturated rocks; (2) Green & Ringwood (1967), Grt-in for quartz tholeiites.

645 °C (Table 2.8b and Fig. 2.12). For sample 29-96 late-stage garnet and retrograde hornblende give a temperature of 555 °C, similar to that obtained from Al-solubility in orthopyroxene of 574 °C. One garnet-hornblende temperature (sample 79-2-96) of 556 °C calculated for garnet rim and the highest X_{Fe}-ratio of hornblende, which has been formed during retrogression around cummingtonite, is also in the range of the values for retrograde temperatures obtained from garnet-orthopyroxene thermometry. This is supported by the low Ti-content of hornblende (<0.1 pfu), which can be used as a qualitative temperature indicator. Comparable hornblende compositions with low Ti-contents from southern India (Raase *et al.*, 1986) and Sri Lanka (Schumacher *et al.*, 1990) indicate amphibolite facies conditions with temperatures of 570-625 °C and 660 °C. This favours the interpretation that hornblende of the analysed samples is a retrograde mineral.

2.8.2 Conventional Geobarometry

The presence of a pressure gradient during peak metamorphism through the study area of the Mt. Gariglione Complex has been deduced from AFM phase relations and is supported by means of geobarometry on *metapelitic* assemblages. The garnet-cordierite-sillimanit-quartz (GCSQ) geobarometer reveals increasing peak metamorphic pressures from east to west through the study area. Using the TWEEQU program of Berman (1991) with thermodynamic data and the garnet activity model of Berman (1988, 1990; assuming ideal mixing of anhydrous Mg-cordierite) pressures range between 4-5 kbar (northern profile) and 4.2-5.3 kbar (southern profile; Table 2.7a, Fig. 2.10). Using the calibration of Martignole & Sisi (1981) of the GCSQ barometer gives slightly lower pressures for the northern (3.2-4.7 kbar) and southern profiles (3.6-4.9 kbar; Table 2.7a). Since volatiles (mainly H_2O and CO_2) may be important constituents of cordierite in granulite terrains (Vry *et al.*, 1990) pressures were also calculated with the TWEEQU program assuming H_2O-saturated cordierite (ideal mixing model of hydrous Mg-cordierite; Berman, 1988). These estimates yield pressures of 5.2-6.4 kbar (northern profile) and 5.5-6.7 kbar (southern profile; Table 2.7a, Fig. 2.10), which is about 1 kbar higher than those calculated with anhydrous cordierite.

Rutile besides ilmenite has only been observed in two of the analysed metapelites (42-96, 57-1-96) of the southern profile. In these the GRAIL-calibration of Bohlen *et al.* (1983) gives pressures of 4.8 and 5.7 kbar similar to the GCSQ estimates for the same samples.

Calculations with the GASP barometer, using the calibration of Koziol & Newton (1988), reveal peak metamorphic pressures in the range of 2.9 to 5.3 kbar (northern profile) and of 4.2 to5.3 kbar (southern profile). These pressure results support only partially those of the GCSQ-barometry of increasing pressures from east to west through the study area since particularly in the southern profile GASP pressure estimates do not vary distinctively between the structurally upper and lower part (Fig. 2.10, Table 2.7a).

Table 2.7 (a) Peak-metamorphic pressure and temperature estimatesfor metapelites at 700°C and 5 kbar, respectively, and TWEEQU results (all core compositions and matrix biotite).

Sample	Grt-Bt	Grt-Crd Fe-Mg exchange			TWEEQU	GASP	GCSQ	GCSQ	GCSQ	GRAIL	TWEEQU	TWEEQU
	T(°C) HS	T(°C) T	T(°C) B	T(°C) D	T(°C)	P(kbar) KN	P(kbar) Be hydr. crd	P(kbar) Be anhydr. crd	P(kbar) MS anhydr. crd	P(Kbar) Bo	P(kbar)	aH_2O
northern profile												
21-97	833	821	762	816		2.9	5.9	4.6	3.3			
C8F	707	751	711	768			5.2	4	3.2			
57b/85	769	729	745	751	769±7	4.9	6.1	4.8	4		5±0.1	0.43-0.5
86-96	730	679	722	714		5.3	6.4	5	4.7			
southern profile												
33-97	683	740	732	765		5	5.5	4.2	3.6			
50-4-96	720	716	736	743	743±12	4.8	5.7	4.4	3.9		4.7±0.2	0.38-0.45
46-3-96	694	689	726	717		4.2	6	4.7	4.2			
42-96	628	656	710	694		4.8	6.1	4.8	4.6	5.7		
57-1-96	746	683	710	708		5.3	6.7	5.3	4.9	4.8		

HS: Hodges & Spear, 1982; T: Thompson, 1976; B: Bhattacharya *et al.,* 1988; D: Dwivedi et al., 1998 (Berman, 1990 garnet mixing model); KN: Koziol & Newton, 1988; Bo: Bohlen *et al.,* 1983 (Hodges & Spear, 1982 garnet mixing model); Be: Berman, 1991, Mg-endmember reaction; MS: Martignole & Sisi, 1981; TWEEQU results for 1.5 standard deviation calculated with INTERSX program (Berman, 1991); activity models are: grt (Berman, 1990), crd (ideal), bt (McMullin at al., 1991), pl (Fuhrman & Lindsley, 1988); outlier is reaction 8 in samples 50-4-96 and 57b/85 of Fig. 2.13c, d (see Table 2.9).

Table 2.7 (b) Peak-metamorphic pressure and temperature estimates for metabasites and intermediate rock types at 700°C and 5 kbar, respectively, and TWEEQU results (all core compositions).

Sample	Grt-Opx Fe-Mg exchange			TWEEQU	Grt-Opx Al-solubility	GAES		TWEEQU	TWEEQU
	T(°C) H	T°C) LG	T(°C) B	T(°C)	T(°C) HG	P(kbar) E	P(kbar) PC	P(kbar)	aH_2O
27-97	691	703	722	655±6	785	4.4	3.7	4.4±0.09	
79-2-96	634	658	702	653±22	636	4.8	5.4	5±0.005	0.32
84-96	679	704	724	678±8	696	5.4	4.6	5.5±0.1	

H: Harley, 1984; LG: Lee & Ganguly, 1988; B: Bhattacharya *et al.* , 1991; E: Eckert et al., 1991 (Mg-endmember); PC: Perkins & Chipera, 1985 (Fe-endmember); HG: Harley & Green, 1982;
TWEEQU results for 1.5 standard deviation calculated with INTERSX program (Berman, 1991); activity models are: grt (Berman, 1990), opx (ideal), pl (Fuhrman & Lindsley, 1988), hbl (Mäder et al., 1994); bt (McMullin et al., 1991), outlier are reactions 3+6 in sample 79-2-96 and reaction 2 in 84-96 (see Fig. 2.14, Table 2.9).

Table 2.8 (a) Retrograde metamorphic temperature and pressure estimates for metapelites at 5 kbar and 700°C, respectively (all rim compositions of grains in contact).

Sample	Grt-Bt	Grt-Crd	GCSQ
	Fe-Mg exchange		
	T(°C) HS	T(°C) B	P(Kbar) Be anhydr. crd
northern profile			
21-97	538	600	2.55
C8F	520	617	2.8
57b/85	468	641	3.8
86-96	477	630	3.7
southern profile			
33-97	428	633	3
50-4-96	521	619	2.7
46-3-96	516	642	3.9
42-96	481	648	3.95
57-1-96	535	632	4.75

HS: Hodges & Spear, 1982; B: Bhattacharya *et al* ., 1988;
Be: Berman, 1991, Mg-endmember reaction

Table 2.8 (b) Retrograde metamorphic temperature and pressure estimates for metabasites and intermediate rock types at 5 kbar and 700 °C, respectively, and TWEEQU results (all rim compositions).

Sample	Grt-Opx			Grt-Hbl	TWEEQU	Grt-Opx	GAES		TWEEQU	TWEEQU
	Fe-Mg exchange					Al-solubility				
	T(°C) H	T(°C) LG	T(°C) B	T(°C) GP	T(°C)	T(°C) HG	P(kbar) E	P(kbar) PC	P(kbar)	aH_2O
rims of isolated single grains										
27-97	560	500	614			730				
79-2-96	535	526	607	556		541				
84-96	584	567	645			650				
rims of garnet and orthopyroxene in contact										
84-96	545	497	607			605				
retrograde garnet between orthopyroxene and plagioclase										
29-96	573	601	642	555	573±5	574	4.4	6.7	5.1±0.04	0.04

H: Harley, 1984; LG: Lee & Ganguly, 1988; B: Bhattacharya *et al* ., 1991; HG: Harley & Green, 1982; GP: Graham & Powell, 1984;
E: Eckert et al., 1991 (Mg-endmember); PC: Perkins & Chipera, 1985 (Fe-endmember);
TWEEQU results for 1.5 standard deviation calculated with INTERSX program (Berman, 1991); activity models are:
grt (Berman, 1990), opx (ideal), pl (Fuhrman & Lindsley, 1988), hbl (Mäder *et al* ., 1994)

Retrograde pressures were calculated with the TWEEQU program (Berman, 1991) for garnet rims and cordierite coronae giving 2.6-3.7 kbar (northern profile) and 2.7-4.8 kbar (southern profile; Table 2.8a and Fig. 2.10), which is about 1-2 kbar lower than the peak pressures.

In *metabasites* and *intermediate rocks* peak metamorphic pressures were calculated with the garnet-orthopyroxene-plagioclase-quartz (GOPQ) geobarometer of Eckert *et al.* (1991; Mg-endmember reaction) and Perkins & Chipera, 1985; Fe-endmember reaction). The results give lower values for sample 27-97 (3.7-4.4 kbar) than for the other ones of 4.8-5.4 kbar (79-2-96) and 4.6-5.4 kbar (84-96) (Table 2.7b, Fig. 2.12) which is consistent with the structural position of this rock sample. The peak metamorphic pressure estimates of the metabasites agree well with those of the GCSQ barometer using the thermodynamic data of Berman (1988) and those of the GASP barometer.

Retrograde pressures were only calculated for sample 29-96 in which late-stage garnet coronae separate orthopyroxene and plagioclase. The results of the GOPQ geobarometer range between 4.4 and 6.7 kbar depending on the calibrabration used (Table 2.8b, Fig. 2.12). This is not significantly different from estimates of peak pressures.

2.8.3 TWEEQU thermobarometry

Pressure-temperature estimates for metapelites and metabasites were also obtained using the multi-equilibrium technique performed with the TWEEQU computer program (version 1.02) of Berman (1991). Using an internally consistent thermodynamic dataset (Berman, 1988; Mäder *et al.*, 1994), all possible equilibria (stable and metastable) are simultaneously calculated for a given set of end-member phases and their activities within a simplified chemical system applicable for the specified rock. On the basis of the intersections of all equilibria and a weighting scheme that favours reactions with large volume and entropy changes, the extension program INTERSX computes an average value of *P-T* with a 1.5 sigma standard deviation for each rock (Berman, 1988). Activities of end-member mineral components were calculated using the following models: garnet (Berman, 1990); feldspar (Fuhrman & Lindsley, 1988); amphibole (Mäder et al., 1994); biotite (McMullin *et al.*, 1991); and ideal mixing models for orthopyroxene and anhydrous cordierite.

Phase relations in the metabasites and metapelites were investigated in the simplified chemical system K_2O-CaO-FeO-MgO-Al_2O_3-SiO_2-H_2O (KCFMASH). Within these systems the following end-member phases were used in the calculations: almandine, grossular, pyrope, enstatite, ferrosilite, ±tremolite, ±tschermakite, anorthite, ±annite, ±phlogogite and beta-quartz (metabasites) and almandine, grossular, pyrope, Fe-cordierite, Mg-cordierite, ±annite, ±phlogogite, anorthite, ±K-feldspar, sillimanite and beta-quartz (metapelites) (see Table 2.9 for used end-member phases for each sample). The calculations were restricted to H_2O-absent equilibria which provides a method to constrain the *P-T* conditions independently of water activity (the latter is considered in the next section).

Among *metapelites* only two of the analysed samples (50-4-96, 57b/85) show a tightly constrained set of intersections suggesting nearly equilibrium (Fig. 2.13). The observed scatter of equilibria in the other metapelitic samples might be explained by retrograde exchange among cordierite and biotite with garnet (see discussion above in 'conventional geothermometry'). Figures 2.13a to c show improving convergence for equilibria in sample 57b/85 with a decreasing amount of equilibria due to continuing exclusion of endmembers (Fig. 2.13a: no exclusion of phases, not independent of water in sensu stricto; b: excluding K-feldspar; c: excluding K-feldspar and biotite; see Table 2.9 for computed equilibria). An equivalent figure is shown for sample 50-4-96 but only the equilibria excluding the phases biotite and K-feldspar are given (Fig. 2.13d). Conspicuous in both samples is the shift of the garnet-cordierite Fe-Mg exchange reaction (8) to the low temperature side of most intersections. The *P-T* estimates of 743 ± 12 °C at 4.7 ± 0.2 kbar (50-4-96) and 769 ± 7 °C at 5 ± 0.1 kbar (57b/85) agree with those derived from conventional thermobarometry (Table 2.7a).

Table 2.9 Mineral equilibria plotted in *P-T* diagrams of Figs 2.13, 2.14, 2.16.

Metapelites: 50-4-96, 57b/85	Metabasites: 27-96, 29-96, 79-2-96, 84-96
1: 4 Si + 5 Qtz + 2 Alm = 3 Fe Crd	1: 3 Qtz + Grs + 2 Alm = 3 An + 3 Fsl
2: 2 Si + Qtz + Grs = 3 An	2: 3 En + 2 Alm = 3 Fsl + 2 Prp
3: 3 Mg Crd + 2 Ann = 3 Fe Crd + 2 Phl	3: Tr + 2 Alm = En + 3 Fsl + Tsc
4: 4 Si + 5 Qtz + 2 Prp = 3 Mg Crd	4: Grs + 2 Prp + 3 Qtz = 3 En + 3 An
5: 6 Si + 5 Grs + 3 Fe Crd = 2 Alm + 15 An	5: Tsc + 3 Qtz + Grs + En = 3 An + Tr
6: 2 Alm + 6 An + 3 Qtz = 2 Grs + 3 Fe Crd	6: 3 Tr + 8 Alm = 12 Fsl + 2 Prp + 3 Tsc
7: 4 Si + 5 Qtz + 2 Phl + 2 Alm = 2 Ann + 3 Mg Crd	7: 2 Prp + Tr = Tsc + 4 En
8: 2 Alm + 3 Mg Crd = 2 Prp + 3 Fe Crd	8: 3 Tsc + 12 Qtz + 2 Prp + 4 Grs = 12 An + 3 Tr
9: 3 Mg Crd + 5 Grs + 6 Si = 2 Prp + 15 An	9: 3 En + 2 Ann = 3 Fsl + 2 Phl
10: 3 Qtz + 2 Prp + 6 An = 3 Mg Crd + 2 Grs	10: 2 Alm + Grs + 2 Phl + 3 Qtz = 3 En + 3 An + 2 Ann
11: 4 Si + 5 Qtz + 2 Prp + 2 Ann = 3 Fe Crd + 2 Phl	11: Alm + Phl = Prp + Ann
12: 2 Ann + 3 Mg Crd + 5 Grs + 6 Si = 2 Phl + 15 An + 2 Alm	12: 3 Qtz + 2 Prp + Grs + 2 Ann = 3 An + 3 Fsl + 2 Phl
13: 2 Alm + 6 An + 2 Phl + 3 Qtz = 2 Grs + 3 Mg Crd + 2 Ann	
14: Phl + Alm = Ann + Prp	
15: 3 Fe Crd + 5 Grs + 2 Phl + 6 Si = 2 Prp + 15 An + 2 Ann	
16: 3 Qtz + 2 Prp + 6 An + 2 Ann = 3 Fe Crd + 2 Grs + 2 Phl	
17: 2 Alm + Grs + 2 Kfs + 2 W = 3 Qtz + 3 An + 2 Ann	
18: Kfs + Alm + W = Ann + 2 Qtz + Si	
19: Grs + 2 Kfs + 2 Prp + 2 W = 3 Qtz + 2 Phl + 3 An	
20: 3 Si + Kfs + 2 Grs + Alm + W = Ann + 6 An	
21: Kfs + Prp + W = Si + 2 Qtz + Phl	
22: 3 Si + Prp + Kfs + 2 Grs + W = 6 An + Phl	

For the *metabasites* and *intermediate rocks* the TWEEQU software computed seven (samples 27-97, 84-96; Fig. 2.14c, d) and eight (samples 29-96 and 79-2-96; Fig. 2.14a, b) anhydrous equilibria (see Table 2.9 for reactions). All analysed samples show a good convergence of calculated equilibria with pressure estimates (4.4-5.5 kbar) falling in the range of those obtained by conventional geobarometry (Tables 2.7b, 2.8b). This is also true for sample 79-2-96 where it has been concluded previously that hornblende and garnet core might not be in equilibrium because of the late-stage formation of hornblende. The calculated low temperatures (560-680 °C) correspond to the results determined with the garnet-orthopyroxene thermometer of Harley (1984) or are even lower (sample 27-97). Despite of the good convergence of the calculated equilibria the *P-T* estimates for peak metamorphism (samples 27-97, 79-2-96, 84-96) are lower than those of the metapelites and are also too low for the peak of the granulite facies metamorphism. The only reasonable explanation seems to be that minerals re-equilibrated during the slow isobaric cooling.

2.8.4 Calculation of water activity

In *metabasites* the water activities were calculated at the anhydrous multi-equilibrium pressure results derived above. In the calculations, the anhydrous pressure determination is taken as a fixed reference and H_2O-dependent mineral equilibria are plotted in a *T*-$a$$H_2O$ diagram. Equilibria that do not involve hydrous phases plot as isothermal lines, whereas dehydration reactions remain temperature and $a$$H_2O$ dependent. The phase diagrams were calculated with the TWEEQU

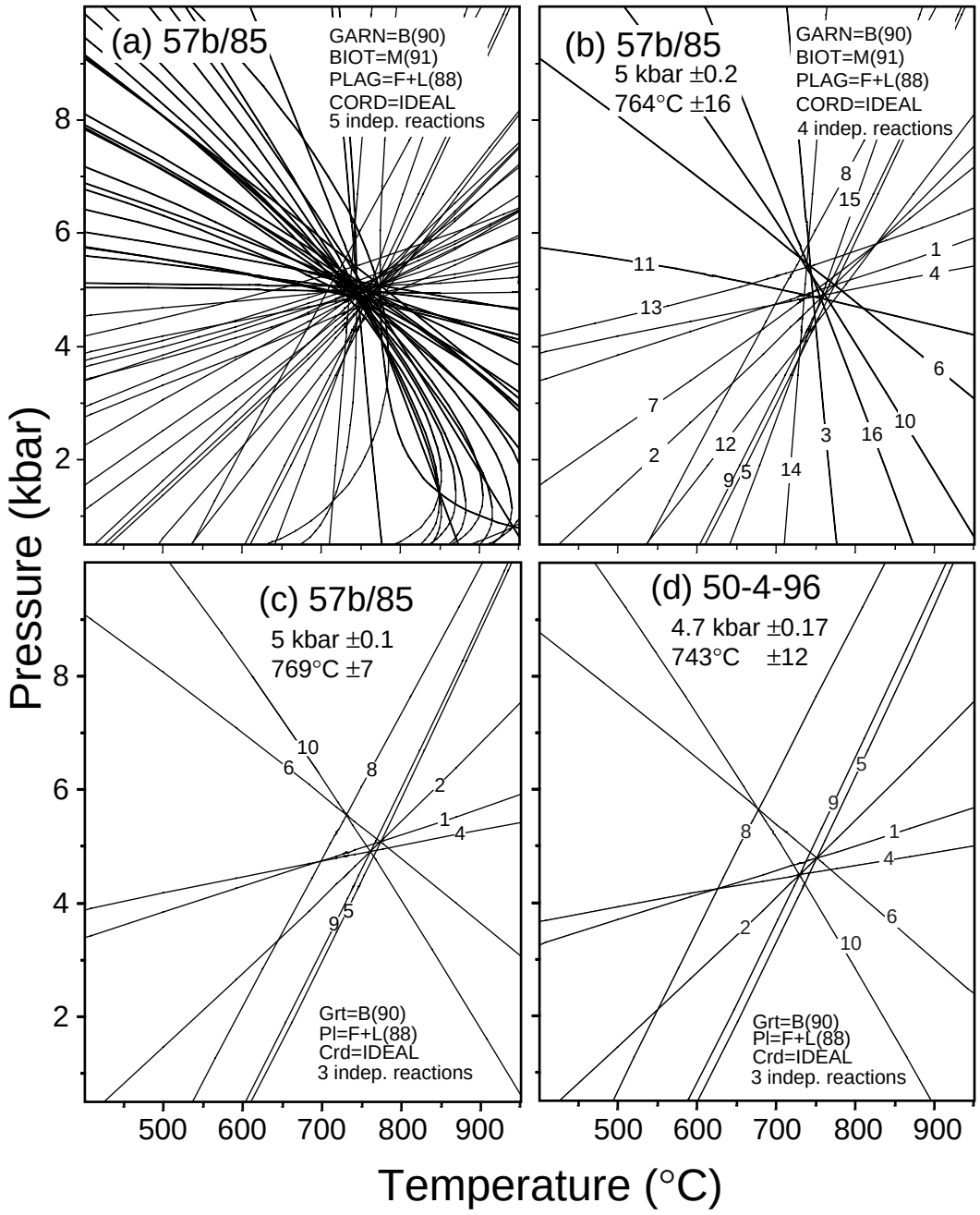

Fig. 2.13 TWEEQU results for two of the analysed metapelitic samples (50-4-96, 57b/85). Sample locations are given in Fig. 2.2a. The plotted mineral equilibria are listed in Table 2.9. Explanations are given in the text.

program using the internally consistent dataset of Berman (1988), along with the data of amphibole from Mäder *et al*. (1994). Figure 2.15 shows two *T*-aH_2O diagrams derived for samples 29-96 and 79-2-96 for the simplified chemical system CaO-MgO-Al_2O_3-SiO_2-H_2O (CMASH) at the obtained pressures. The following endmember phases were used: pyrope, grossular, tremolite,tschermakite, enstatite, anothite and beta-quartz. Activity models are the same as those used for *P-T* calculations. The results of water activity estimates for sample 29-96, showing late-stage garnet rims and retrograde hornblende, and sample 79-2-96 are 0.04 and 0.32. Despite the evidence for late-stage fluid infiltration in both samples suggested by abundant

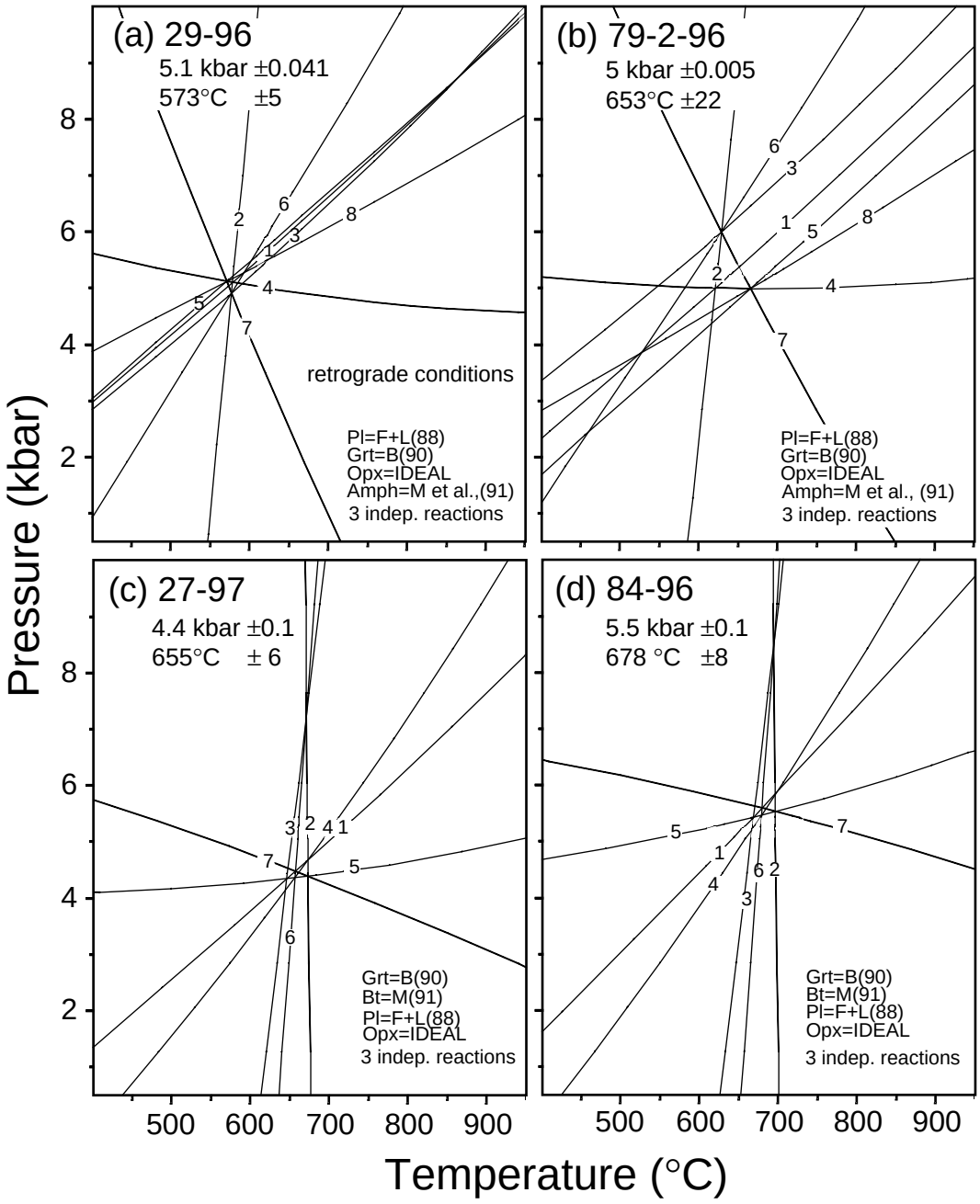

Fig. 2.14. TWEEQU results for metabasic samples. Sample locations are given in Fig. 2.2b. The plotted mineral equilibria are listed in Table 2.9. Explanations are given in the text.

retrograde growth of hornblende/ cummingtonite at the expense of orthopxyroxene, the calculated water activity estimates, particularly that of sample 29-96, are very low.

The water activities for the two *metapelitic* samples (50-4-96, 57b/85) were also calculated with the TWEEQU program, however the procedure was different to that described above. All possible equilibria were calculated in the simplified chemical system KCFMASH using the endmembers almandine, pyrope, grossular, K-feldspar, anorthite, annite, phlogopite, sillimanite, beta-quartz and water. Seven possible equilibria were computed including dehydration reactions which are dependent on water activity (Fig. 2.16, Table 2.9). The diagrams were calculated by successively

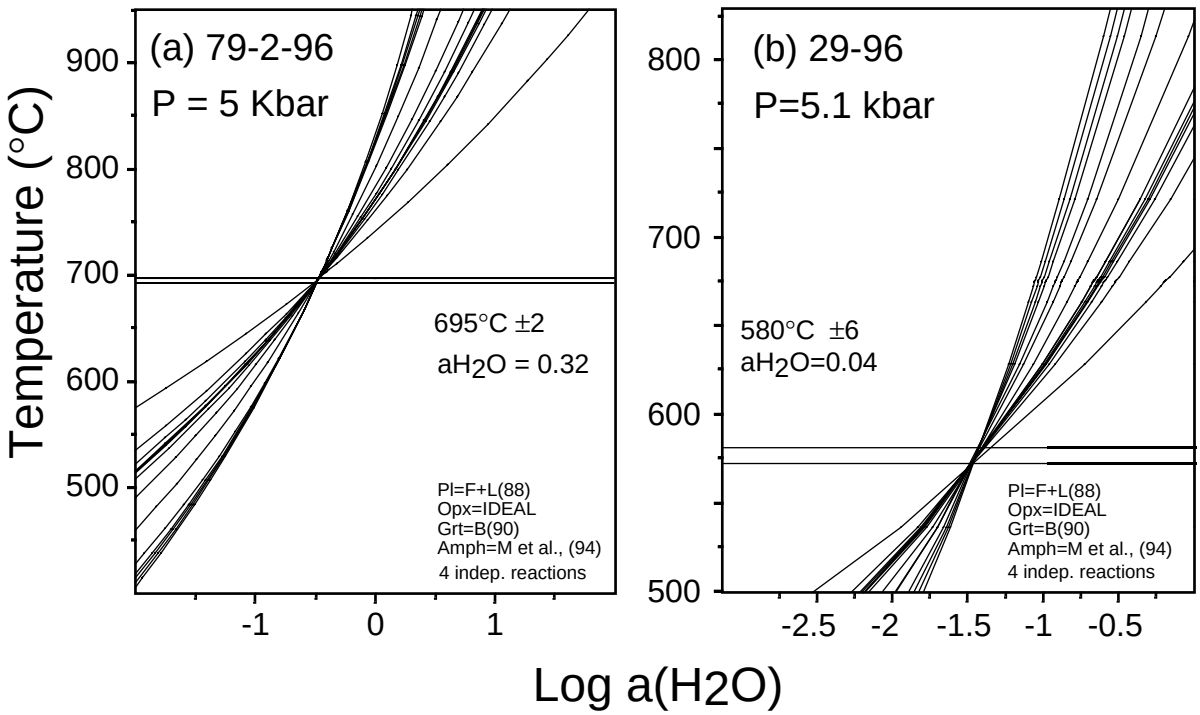

Fig. 2.15 *T-aH$_2$O* plots for two of the analysed metabasites (29-96, 79-2-96). Sample locations are given in Fig. 2.2b. The plots are calculated at the appropriate sample pressure as determined in Fig. 2.14. The plotted mineral equilibria are listed in Table 2.9.

lowering the water activity untill a range of intersections was attained whose *P-T* results correspond to those calculated by H_2O-absent equilibria. The water activities of the samples 50-4-96 and 57b/85 range from 0.38-0.45 and from 0.43-0.50. These low aH_2O combined with the existence of abundant quartzofeldspathic leucosomes support the interpretation that dehydration melting has occurred in the metapelites. A sequence of melting reactions may have lowered the water activity in the rock since the H_2O component of the fluid phase has been partitioned into the generated melt (e.g. Clemens and Vielzeuf, 1987; Lamb & Valley, 1988; Stevens & Clemens, 1993). The calculated water activities in the fluid phase of both metapelitic samples agree relatively well with experimentally determined solidus curves of the haplogranitic system (Qtz-Ab-Or-H_2O±CO_2) for aH_2O=0.46-0.53 at 740-770 °C and 5 kbar (Ebadi & Johannes, 1991; Holtz & Johannes (1994); Vielzeuf & Montel, 1994).

2.9 DISCUSSION

2.9.1 *P-T* path reconstruction and peak metamorphic conditions

The main part of the prograde metamorphic *P-T* path which is characterized by heating accompanied by loading proceeded in the stability field of sillimanite. This is indicated by inclusions of sillimanite and of cordierite in garnet rims and by calculations of the maximum *P-T* conditions. The details of the prograde path are not known but a clockwise *P-T* path is very likely. The high peak metamorphic temperatures and textural evidences suggest that crustal melting has

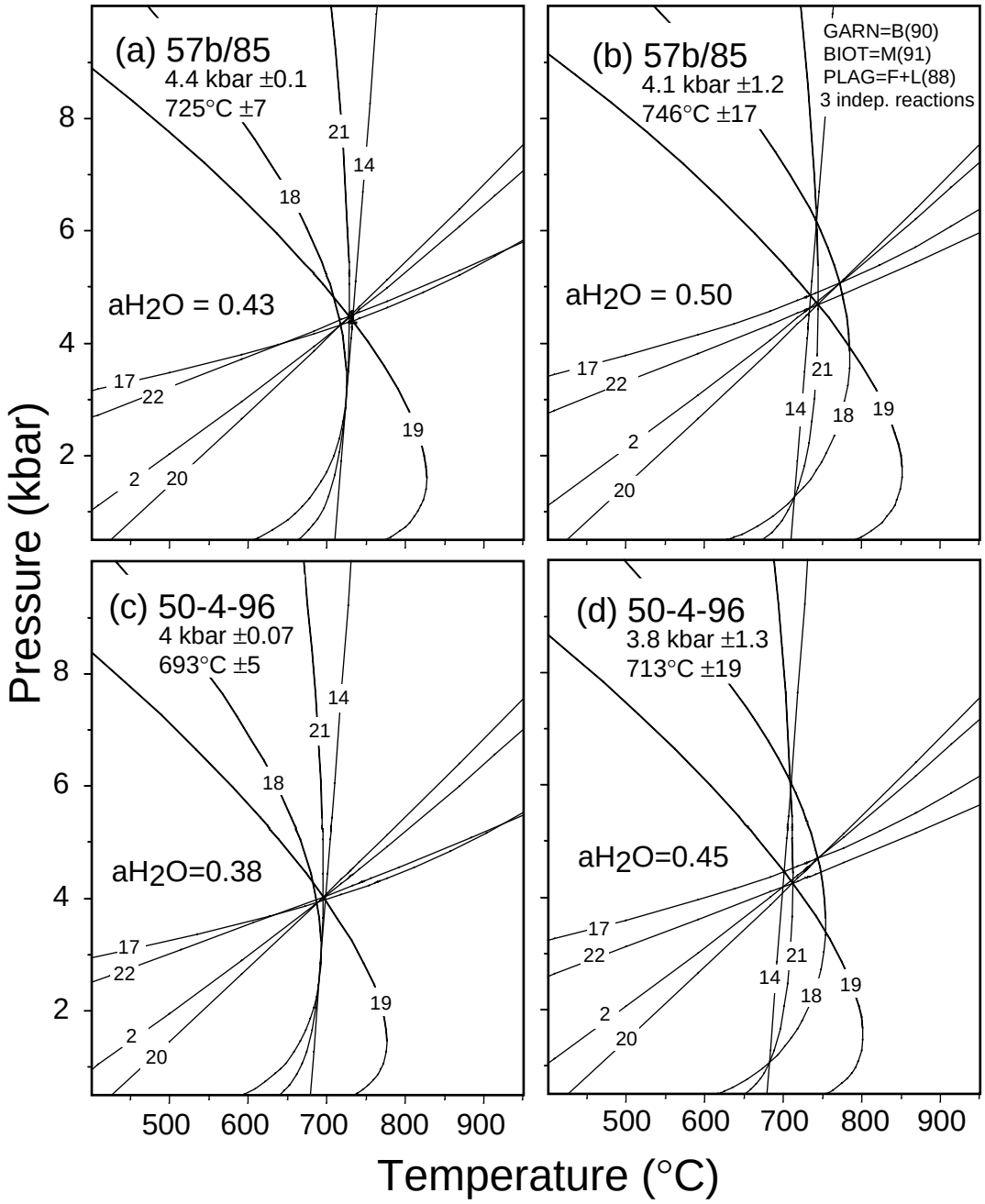

Fig. 2.16 TWEEQU results for the metapelitic samples 50-4-96 and 57b/85 including equilibria dependent on variable aH_2O. For further explanations see text.

occurred during prograde metamorphism due to crossing a sequence of deyhdration melting reactions.

The peak metamorphic conditions for the rocks of the study area have been deduced by combining *P-T* calculations (conventional thermobarometry and TWEEQU method) with AFM-phase relations. Due to partial retrograde re-equilibration of matrix phases of some of the analysed rocks, the peak temperature conditions are best defined by mineral reactions in the NaKFMASH system (Fig. 2.17). *Peak temperatures* for the upper and lower part of the Mt. Gariglione Complex are quite close to each other and must have been in the range of the univariant

dehydration melting reaction (3) in metapelites which is above 740 and 770 °C, respectively, and below the final breakdown reaction of Bt+Grt+Qtz or Bt+Qtz (<800-820°C, Spear *et al.*, 1999; Fig. 2.17). These temperatures coincide with results using the TWEEQU method in two of the metapelites and the occurrence of the mineral assemblage Fo-Cal-Dol in carbonate rocks in the structurally lower part of the study area. *Peak metamorphic pressure* estimates for the temperatures discussed above range between 4 and 5.5 kbar (GCSQ and TWEEQU barometry) and 4.4 to 6.5 kbar (GASP equilibrium) increasing from the upper to the lower part of the section (Fig. 2.10). Comparable *P-T* data for peak metamorphism were determined by Le Breton (1983; T>650 °C and P>4.5-5 kbar) and Althaus & Istrate (1990; T= 690-740 °C and P= <6-8 kbar). The higher pressures of the latter authors are deduced from studies of CH_4- and N_2-rich fluid inclusions in gneisses of the western part of the Mt. Gariglione Complex.

The identification of the Mt. Gariglione Complex as a continuous section through a part of a former lower crust, leads to the reconstruction of two retrograde *P-T* paths, one for the upper and the other for the lower structural level of the section. However, the retrograde *P-T* paths seem not unanimous, since textures and thermobarometric calculations performed on late-stage mineral assemblages in metapelites reveal decompression that is followed by cooling whereas those in metabasites indicate only near isobaric cooling but no textures indicating decompression prior to it have been developed. The combination of the different metamorphic textures in all metapelitic and metabasic rock types leads to retrograde paths characterized by more or less isothermal uplift after peak metamorphic conditions into mid-crustal levels (10-15 km) followed by a stage of near isobaric cooling (Fig. 2.17). Decompression from *c.* 4-6 kbar to 2.4-4.8 kbar is supported by cordierite coronae around garnet in metapelites and silica-undersaturated aluminous rocks as well as cordierite-spinel symplectites replacing garnet and textures suggesting growth of cordierite+K-feldspar+spinel at the expense of biotite+sillimanite. Textural support in metapelites for isobaric cooling subsequent to decompression includes the reversal of the latter reaction indicated by newly grown sillimanite and biotite between cordierite and spinel and the reversal of dehydration melting reactions (2) and (3) additional to reaction (9), which consume garnet or form muscovite at the expense of sillimanite/fibrolite+K-feldspar+melt/vapour (reversal of reaction 1 in Fig. 2.17). The latter reaction is only observed in rocks of structurally high levels. Since the retrograde *P-T* trajectory of this part crosses the reaction (1) below the invariant point IP1 (Fig. 2.17) retrograde muscovite may not form if the water released during crystallization of melts has already left the rock before the stability field of Ms+Qtz has been reached (Spear *et al*., 1999). However, in the Sila massif, water either remained in the rocks during retrogression or may have been introduced from outside. In the lower part of the section the reversal of the muscovite dehydration melting reaction (1) is not observed although the *P-T* trajectory crosses the reaction above IP1. Since the estimate of 10-20 vol% leucosomes in the metapelites is very rough it might be that in the lower part of the crust leucosomes account for a lesser extend of the exposed rocks than the estimates above. In this case a major part of the melt released during prograde metamorphism may have

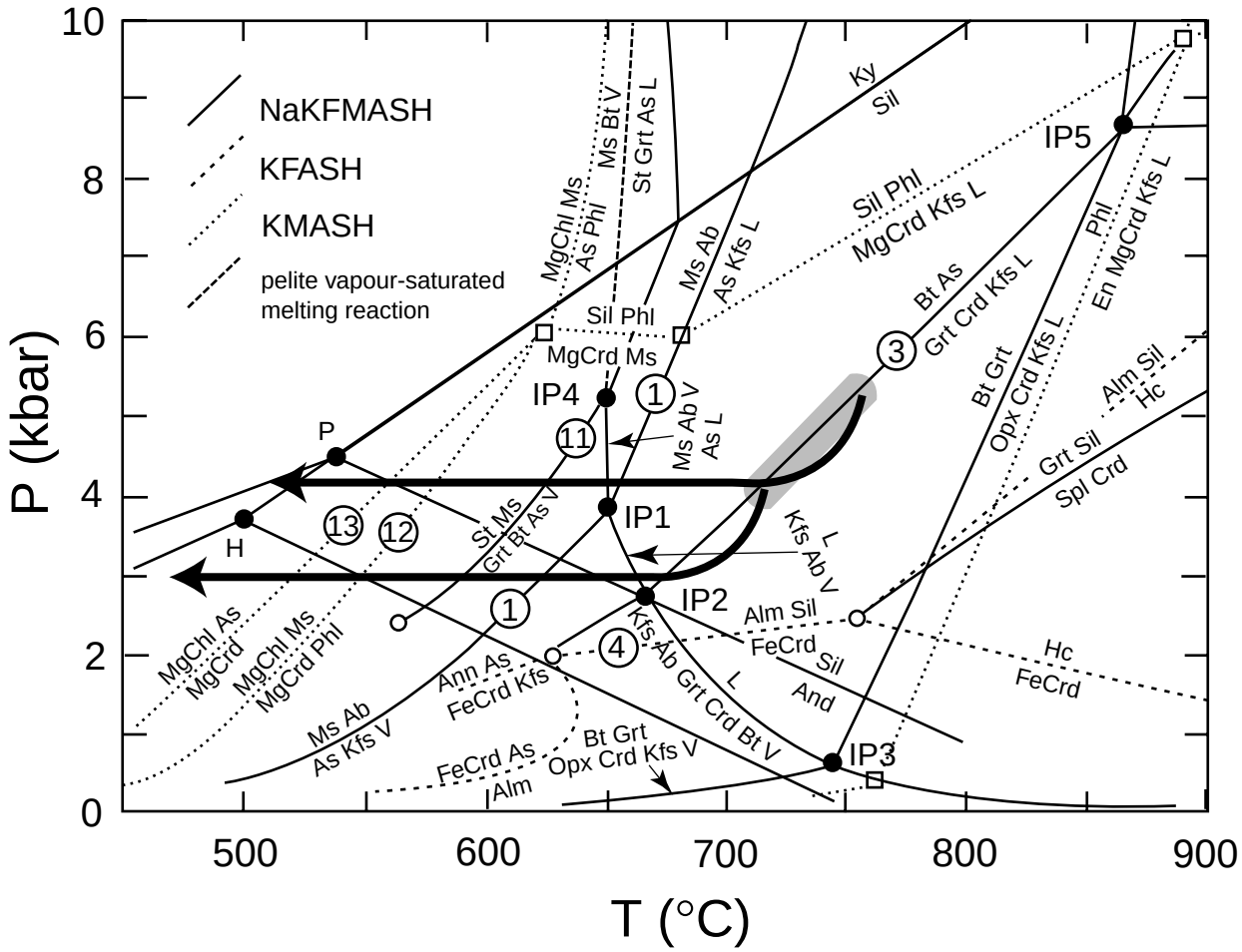

Fig. 2.17 *P-T* grid of the NaKFMASH systemwith relevant curves for pelites of the Mt. Gariglione Complex (finely dashed lines: KFASH system; dotted lines: KMASH system; dashed line: pelite vapour-saturated melting reaction). Arrows show infered *P-T* evolution of the upper and lower part of the former lower crustal section of the Sila massif. Melting and dehydration equilibria are from Spear *et al.* (1999) and references therein. Alumosilicate triple point after Holdaway (1971; H) and Pattison (1989; P). The triple point of Holdaway (1971) is preferred in this study since in the lower part of the crustal section no retrograde andalusite but kyanite is observed. Grey field: *P-T* conditions in the lower crustal section during peak metamorphism. Numbers refer to reactions dicussed in the text.

risen to higher levels of the crust and the remaining melt had been consumed by the retrograde reversal of biotite dehydration melting reactions (2, 3, 9). Further cooling is petrologically documented by textures of andalusite and kyanite (+Chl+Qtz) overgrowing even late-stage cordierite in metapelites of the upper and lower part of the study area, respectively (Fig. 2.3e,g). In metabasites textural support for near isobaric cooling at 4-5 kbar is the formation of late-stage garnet rims between orthopyroxene and plagioclase (sample 29-96; Fig. 2.3k). Secondary seams of Opx+Cpx+Spl and further Prg-Hbl+Spl around Ol+Pl in olivine-metagabbros are in agreement with this interpretation. The stage of isobaric cooling is also supported by garnet zoning patterns in metabasites and metapelites which is characterized by a rimward increase of grossular content and by a corresponding rimward Al-decrease in orthopyroxene and a slight decrease of anorthite

component at the rims of plagioclase in metapelites. The very low Grt-Opx temperatures obtained from the metabasic rock sample 29-96 support the late-stage formation of garnet rims between orthopyroxene and plagioclase during the near isobaric cooling stage.

2.9.2 The lower crustal sections in northern and southern Calabria: a comparison

The striking similarities between the lithostratigraphic sequences exposed in the Sila (north) and the Serre (south) of the Calabrian massif are well known at least since the pioneering work of Quitzow (1935) who compiled a geological map of the Calabrian massif and adjoining areas. In both massifs, high-grade gneisses ('kinzigites') are overlain by granitoids (Qtz-diorites, tonalites, granites) which display a clear intrusive contact with the overlying low-grade rocks of the upper crust. Despite these far reaching similarities, different geological histories and internal tectonic subdivisions have been proposed for both parts of the Calabrian massif. The tectonic models of the Sila massif assuming that this lithological sequence is part of an Alpine nappe pile, composed of Hercynian basement slices thrusted onto Mesozoic ophiolitic rocks, are undisputed in the literature. However, the internal tectonostratigraphic subdivision of the highest unit, the so-called 'Sila nappe', which consists in its deeper parts of granulite facies rocks ('kinzigites' of the 'Mt. Gariglione Complex'), is a matter of debate. Dubois (1970, 1976), resumed by Messina *et al.* (1991a), favours a relatively simple tectonic model for this unit attributing all Hercynian rocks of different crustal levels to a single Alpine nappe. However, according to e.g. Amodio-Morelli et al. (1976), Zanettin Lorenzoni (1980) and Lorenzoni & Zanettin Lorenzoni (1983) the high- and low-grade rocks define distinct Alpine units which both were intruded by Hercynian granitoids. Even more complicated is the tectonic subdivision accordimg to the latter two studies which propose in addition Hercynian nappe boundaries within the Alpine units.

The tectonic model of a stack of Alpine nappe slices has also been inferred to the Serre massif of southern Calabria (Amodio-Morelli *et al.,* 1976). However, within the high-grade gneisses no further tectonic subdivision has been made, but in-between the lower crustal rocks and the overlying tonalites an Alpine nappe boundary has been proposed. Based on petrological analyses, geological mapping and isotopic dating an alternative model for the Serre has been proposed by Schenk (1980, 1984, 1990). According to these data, a continuous profile (~8 km) through an Hercynian granulite facies lower crust is exposed in the Serre on top of which the overlying Hercynian granitoids intruded. Petrology is a powerful tool in distinguishing between different or common tectonic histories of lithological units in high-grade gneiss terrains and thus in recognizing tectonic units. Thus, our present study on the high-grade gneisses of the Sila nappe was partly aimed to prove whether the Mt. Gariglione Complex of the Sila represents a single lithological unit characterized by continuous change in metamorphic grade or whether units of different metamorphic histories or grade can be distinguished.

The data presented in this paper show that from the systematic change in compositions of ferromagnesian minerals a continuous metamorphic gradient through the Mt. Gariglione Complex

can be deduced. The situation is thus similar to the one described for the Serre (Schenk, 1984). However, in metapelites of the Sila the coexisting minerals garnet and cordierite are higher in X_{Fe} (0.87-0.66 and 0.51-0.20) than the ones in the Serre section (0.81-0.62 and 0.28-0.13; Schenk, 1984) indicating that in the lower part of the Sila nappe a shallower crustal level (4-6 kbar) is exposed than in the Serre (5.5-7.5 kbar). These petrological results are in agreement with the observation, that in the Serre below the unit of migmatitic metapelites an even deeper lithostratigraphic unit, the 'granulite-pyriclasite unit' (Schenk, 1984), is exposed, which is missing in the Sila nappe. The 'univariant' assemblage Grt-Bt-Crd-Kfs-Sil-Qtz which forms an isobar in the Serre (5.5-6 kbar), and which therefore supports the model of a continuous cross-section through a lower crust, occurs in the Mt. Gariglione Complex at all structural levels, possibly due to regional variations in aH_2O. The peak metamorphic temperatures in both crustal sections are nearly the same with 800-770 °C at the base and 740-700 °C at the top. Slightly different temperature values obtained in both areas are mainly due to the application of different methods in both studies. However, an unusual high geothermal gradient at the time of Hercynian metamorphism in the range of 50-35 °Ckm^{-1} is obvious from both sections.

Both lower crustal sections in northern and southern Calabria experienced similar *P-T* paths. After prograde metamorphism, characterized by strong heating accompanied by a moderate pressure increase, a stage of isothermal uplift of the granulite facies lower crustal rocks into mid-crustal levels was followed by nearly isobaric cooling. The geodynamic causes for decompression after peak metamorphism might be extensional tectonics, which occurred between the Adriatic crust and the European continent due to Mesozoic rifting. This scenario has been envisaged by Brodie & Rutter (1987) and Handy & Zingg (1991) to explain the post-Hercynian uplift of the Ivrea zone which was in a similar paleogeographic position as Calabria. The present authors, however, prefer for Calabria a crustal thickening event prior to peak metamorphism as the cause of metamorphic heating and the subsequent lower crustal uplift and isobaric cooling. The large calcalkaline (Qtz-diorite and tonalite) to mesaluminous granitoid intrusions into the middle crust of the Sila and Serre certainly provoked metamorphic heating, loading and crustal thickening which proceeded synchronous with Hercynian granulite facies metamorphism (Schenk, 1980, 1990; Graeßner & Schenk, 1999). An ancient geotectonic setting of the Calabrian massif as a continental arc above a subduction zone would satisfy the petrological and isotopic data (Schenk, 1990). Metamorphic textures like net-like orthopyroxene and garnet porphyroblasts (in both sections) and pyroxene-plagioclase symplectites replacing hornblende (in the south) in metabasites, and, only at the uppermost part of the lower crustal section in southern Calabria, sillimanite-K-feldspar-biotite pseudomorphs after muscovite are strong evidence that prograde heating outlastet the deformation. We attribute this textural relationship to the magmatic heat source inducing the unusual high temperatures in the crust of the Calabrian continental arc.

CHAPTER THREE

Geochronological constraints on the timing of granitoid magmatism, metamorphism and post-metamorphic cooling in the Hercynian crustal cross-section of Calabria

3.1 ABSTRACT

The U-Pb, Rb-Sr and K-Ar geochronlogy of granulite facies metapelitic migmatites, peraluminous granites and amphibolite facies upper crustal gneisses reveal constraints on late-Hercynian peak metamorphism and granitoid magmatism as well as on post-metamorphic cooling of the exposed crustal cross-sections of southern and northern Calabria. U-Pb dating of monazite from upper crustal paragneisses from southern Calabria yields ages of 295-293 Ma for amphibolite facies metamorphism which are similar to the ages of granulite facies metamorphism in the lower crust and of intrusions of calcalkaline and mesaluminous granitoids (300 ± 10 Ma, Schenk, 1990). Monazite and xenotime of peraluminous granites from the middle to upper crust of the same crustal section provide slightly older intrusion ages of 303-302 Ma. Zircons of a mafic sill in the lower crust yield a lower concordia intercept age of 290 Ma, which can be interpreted as the minimum age for metamorphism or for intrusion.

Dating of monazite from granulite facies migmatites and peraluminous granites of the lower and middle crust from northern Calabria points also to a synchroneity of peak metamorphism and of intrusion at 304-302 Ma. At the end of the granulite facies metamorphism the lower crustal rocks were uplifted into mid-crustal levels (10-15 km). This was followed by nearly isobaric slow cooling (3 °C Ma^{-1}), which seems to be undisturbed by any tectonic event as indicated by biotite and muscovite Rb-Sr and K-Ar ages between 210 and 123 Ma. The thermal history is therefore similar to that of the lower crust of southern Calabria (Schenk, 1990). Rb-Sr and K-Ar dating of an amphibolite facies paragneiss from the upper crust in southern Calabria yield ages considerably younger than those of the middle to lower crust of the same section. This is interpreted as the result of an Alpine overprint which is reported from the upper crust of southern Calabria (30-25 Ma; Bonardi *et al.*, 1987). In combination with previous petrological studies adressing metamorphic textures and *P-T* conditions of rocks of all crustal levels, the new geochronological results suggest that the thermal evolution of the Calabrian crust is mainly controlled by advective heat input through magmatic intrusions into all crustal levels during the late-Hercynian orogeny.

Mineral abbreviations are from Kretz (1983).

3.2 INTRODUCTION

Granulite facies metamorphism and associated granitoid magmatism are important processes during the evolution of a continental crust since they play the dominant role in intra-crustal differentiation. In the exposed crustal cross-section of southern Calabria these processes have been adressed since lower crustal granulite facies metamorphism has been found to be synchronous with calcalkaline to mesaluminous magmatism at 300 ± 10 Ma and all levels of a former continental crust are exposed (Schenk; 1980, 1984, 1990): These include a 7-8 km continuous section through a former lower crust, calcalkaline granitoids (tonalite, Qtz-diorite) in the middle crust and mesaluminous and peraluminous granites which intruded into amphibolite to greenschist facies upper crustal rocks. An indication that internal crustal differentiation processes might have taken place are the occurrences of peraluminous granites in the middle to upper crust, which, however, show slightly younger ages of 293-282 Ma according to Rb-Sr whole rock and mica data (Del Moro *et al.*, 1982). High geothermal gradients in the lower crust of 30-35 °Ckm^{-1} and very high ones in the upper crust of *c.* 60 °Ckm^{-1} (Schenk, 1984; Graeßner & Schenk, 1999) in combination with the observation that mineral growth outlasted the deformation in the upper and the lower crustal rocks as well, suggest a strong influence of the granitoid intrusions on the thermal evolution of this crustal section.

In contrast to the late-Hercynian ages dated in the lower to middle crust, a Rb-Sr biotite age of 330 Ma (Bonardi *et al.*, 1987) from an upper crustal orthogneiss gave evidence of an possible early-Hercynian event. This has been supported by a poorly constrained lower concordia intercept age of 377 ± 55 Ma obtained from discordant zircons of a paragneiss from the same crustal level ('Aspromonte unit'; Schenk, 1990). These data suggested that the crustal evolution of southern Calabria could be more complicated than it was evident from geochronological and petrological data of the lower and middle crust. Since none of the data published so far, constrained the time of peak metamorphism in the middle to upper crust precisely enough in southern Calabria, three paragneisses of different levels of this section have been dated with monazites and zircons. To address the time relationship between magmatism and metamorphism in the upper and lower crust, monazites of two peraluminous granites which intruded at mid- to upper crustal levels have been dated. Intrusive rocks are scarce in the metasedimentary sequence of the lower crust in the Serre. However, zircon data of a mafic body (andesitic composition) seem to indicate synmetamorphic intrusion at 298 ± 5 Ma (Schenk, 1980). In the present study a further mafic to intermediate intrusive body in the lower crust has been dated to check whether the temperatures in the Hercynian lower crust may have been affected by these intrusions.

In the Sila massif of northern Calabria a large unit of granulite facies rocks (*c.* 900 km^2) is exposed, which was metamorphosed during the Hercynian orogeny ('Mt. Gariglione Complex'). This unit represents the lower part of the Alpine 'Sila nappe' which, like the crustal section in southern Calabria, consists in its middle part of a wide range of late-Hercynian granitoids overlain by upper crustal rocks (e.g. Dubois, 1970, 1976). This relatively simple tectonic model has been

modified by e.g. Amodio-Morelli et al. (1976) and Lorenzoni & Zanettin Lorenzoni (1983) who subdivided the high-grade metamorphic rocks into two Alpine units. However, in a recent petrological study a continuous metamorphic gradient through the Mt. Gariglione Complex has been deduced which supports the interpretation that the complex represents a single segment deriving from a former depth range of *c.* 14-21 km in the continental crust (Graeßner & Schenk, in prep.). Dating of peak metamorphism and determination of the post-metamorphic cooling rate at different levels (top - base) of the former lower crustal segment is aimed to check whether different tectonic units may exist in the Mt. Gariglione Complex and whether it resembles the peculiar slow cooling found in the lower crustal section of the Serre (Schenk, 1980). Additionally, the ages of two peraluminous granite intrusions have been evaluated in relation to the time of peak metamorphism in the lower crust.

The ages of peak metamorphism and intrusion have been dated with the U-Pb method to get an overall comparable dataset for the geological events in all crustal levels of the Serre and the Sila during the late-Hercynian orogeny. Since monazite is a very common accessory mineral phase in metasedimentary rocks and peraluminous granites it is very suitable to date high-grade metamorphism and magmatism. Only in the few cases in which monazite has not been found in the studied rocks, zircon has been used for dating. The capability of monazite to retain U-Pb isotopic signatures up to high temperatures and the fact that it yields concordant ages in most cases (e.g. Schenk, 1980; Copeland *et al.*, 1988; Parrish, 1990; Mezger, 1990; Lanzirotti & Hanson, 1995) makes it extreme useful to get high-precision ages of geological events.

3.3 GEOLOGICAL SETTING OF THE CALABRIAN MASSIF

The Calabrian massif of southern Italy is situated between the thrust belts of the Apennines to the north and the Maghrebides to the west. In contrast to the mainly sedimentary rocks of these two mountain belts, the Calabrian massif comprises pre-Alpine continental crust and ophiolitic units which were involved in the Alpine orogeny. The Alpine mountain system became dismembered due to later movements of microplates in the western Mediterranean during subsequent collision between the African and Eurasian plates (e.g. Alvarez, 1976). Many studies (e.g. Amodio-Morelli *et al.*, 1976; Scandone, 1979; Bonardi *et al.*, 1982) regard the Calabrian massif as a piece of Adriatic or African crust that was overthrust first (Alpidic stage) upon Tethyan ophiolitic units in the northwest and after the collision of Europe with Africa thrusted backwards with its underlying base onto the Apenninic carbonate platform in the east (Apenninic stage). In contrast, e.g. Knott (1987), Dietrich (1988), Dewey *et al.* (1989) and Wallis *et al.* (1993) regarded the Calabrian massif as derived from the European continent, thrust only towards the east during subsequent subduction of the Tethys, overriding the ophiolitic units and resting now together with its ophiolitic base upon the Adriatic platform units.

The lithostratigraphic sequence in the exposed crustal cross-section of the Serre and Aspromonte of southern Calabria is very similar to the one in the Sila nappe of northern Calabria

(in the sense of Dubois, 1970, 1976). In both areas granulite facies lower crustal gneisses form continuous sections through a former lower continental crust (Schenk, 1980, 1984, 1990; Graeßner & Schenk, in prep.). These rocks are overlain by two cycles of late-Hercynian granitoids, in which large bodies of mesaluminous to calcalkaline tonalites and granodiorites and subordinate peraluminous granites are distinguished (e.g. D'Amico *et al.*, 1982; Rottura *et al.*, 1990; Fig. 3.1). The granitoids intruded into the overlying amphibolite facies upper crustal gneisses and low-grade Palaeozoic rocks, which, in the Aspromonte, were metamorphosed during Hercynian low-pressure/high-temperature metamorphism (Graeßner & Schenk, 1999). Peak metamorphic conditions in the lower crustal sections range from 740-770 °C at 4-6 kbar (northern Calabria) and 690-800 °C at 5.5-7.5 kbar (southern Calabria; Schenk, 1984; Graeßner & Schenk, in prep.). These *P-T* data reveal a slightly higher former position in the crust for the segment in northern Calabria than for the one in southern Calabria. However, an unusual high geothermal gradient at the time of Hercynian metamorphism in the range of 35-50 °Ckm^{-1} is obvious from both sections and is therefore lower than that deduced from the amphibolite to greenschist facies upper crustal rocks of *c.* 60 °Ckm^{-1} in the Aspromonte of southern Calabria (Graeßner & Schenk, 1999).

Both exposed lower crustal sections, in northern and in southern Calabria, reveal similar *P-T* paths. After prograde metamorphism, characterized by strong heating accompanied by moderate loading, a stage of isothermal uplift of the granulite facies lower crustal rocks into mid-crustal levels was followed by nearly isobaric cooling (Schenk, 1984, 1990; Graeßner & Schenk, in prep.).

3.4 SAMPLE DESCRIPTION

3.4.1 Northern Calabria

Two samples of the granulite facies *metapelitic migmatites* of the lower crustal segment were selected to evaluate the time of peak metamorphism and to constrain the post-peak metamorphic cooling (localities shown in Fig. 3.1). Samples are taken from the stratigraphic upper (sample 50-96) and lower part (sample 35-96) of the lower crustal section along road No. 109 at km 110.4 and 87. The granulitic segment consists mainly of aluminous paragneisses with interlayered quartzofeldspatic leucosomes. These leucosomes form lenses and bands mostly parallel to the foliation and are interpreted as partial melts of the host metapelites. Only the melanosomes of the gneisses consisting of biotite, sillimanite, garnet, quartz, plagioclase were chosen for geochronology. The metapelites were metamorphosed at sillimanite+K-feldspar grade, prograde muscovite+quartz±plagioclase was not stable. Cordierite±K-feldspar may belong to peak-metamorphic assemblages of rocks of all structural levels. Retrograde cordierite coronae surrounding garnet are common in the studied rocks. However, cordierite and K-feldspar were not

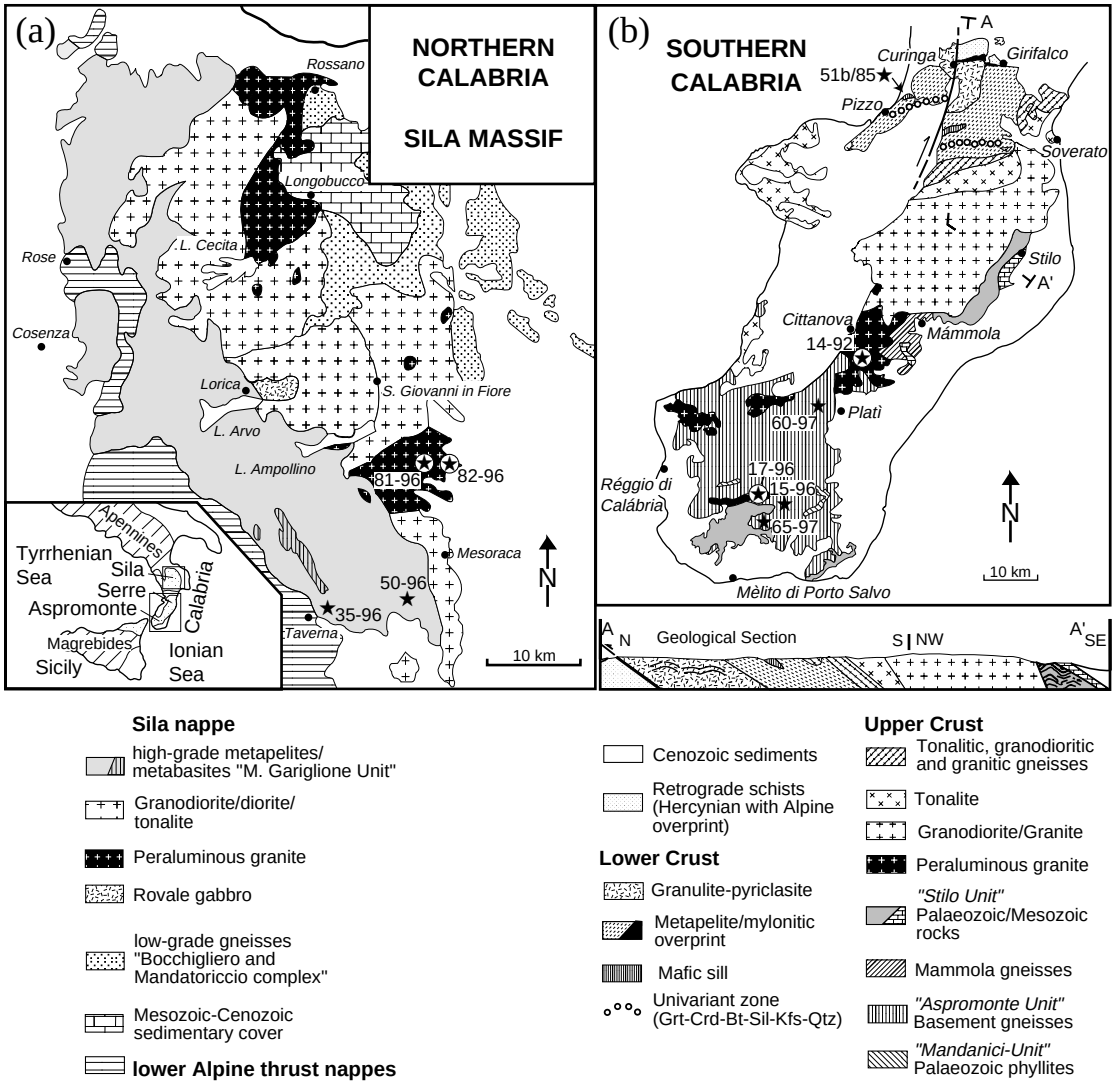

Fig. 3.1 Simplified geological maps of (a) the Sila massif in northern Calabria (modified after Ayuso *et al.*, 1994) and (b) southern Calabria (modified after Schenk, 1980, 1990 and Bonardi *et al.*, 1992). Black stars indicate the locations of samples used for isotopic dating.

present in both samples selected for this study. In sample 50-96 late-stage muscovite+quartz replacing sillimanite+K-feldspar is found, together with retrograde andalusite and mats of fibrolitic sillimanite. These reaction textures and minerals are typical for the structurally higher parts of the lower crustal section in the Sila massif. Monazite is an abundant accessory mineral that occurs as inclusions in biotite, plagioclase and in interstices of the rock fabric.

Two different intrusions of *peraluminous granite* (the so-called 'F. Ampollino' and 'Cotronei' granites) were sampled along road No. 107. The first was taken at the bridge above the river F. Neto near the village of Cotronei (81-96) , the second was collected at the private road of the Enel at the river F. Neto (82-96) (locations see for Fig. 3.1 and in Messina *et al.*, 1994). Both samples show homogeneous, equigranular textures of quartz, plagioclase and K-feldspar in equilibrium with muscovite and biotite. Cordierite and the alumosilicates sillimanite and andalusite are also

described from these intrusions (Messina *et al.*, 1994). Monazite is common as inclusions in plagioclase and biotite and in interstices of the rock fabric.

3.4.2 Southern Calabria

To decipher the age of metamorphism in the middle to upper crust of the crustal section in the Serre and Aspromonte three amphibolite facies *paragneisses* of the 'Aspromonte unit' were collected in the northwest (sample 60-97, middle crust) and in the south (samples 15-96 and 65-97, upper crust) of the Aspromonte. Sample 60-97 was taken at the banks of the river T. Acone at km 64 of the road No. 112 above the village of Platí (Fig. 3.1). The rock consists of prograde biotite, muscovite, quartz and plagioclase and mats of retrograde fibrolitic sillimanite overgrowing micas. Small newly grown kyanite pseudomorphing retrograde fibrolite has been described from this rock type by Platt & Compagnoni (1990). They attribute this late-stage kyanite to an Alpine overprint in this part of the Aspromonte area. These observations correspond also with similar textures observed by Bonardi *et al.* (1984a, 1992) in the central part of the Aspromonte. The deformation of micas and recrystallisation of quartz in the studied rock is evidence of an Alpine overprint. Monazite is abundant in all parts of the rock and forms inclusions in mica and plagioclase.

One *paragneiss* from the upper crust (sample 15-96) was collected at the bridge above the river F. Amendolea below the village of Roccaforte del Greco and just below the contact with the overlying Stilo unit (Fig. 3.1). The paragenetic minerals of this intensively folded gneiss are biotite, garnet, staurolite, andalusite, muscovite, plagioclase and quartz. Reaction textures like staurolite inclusions in andalusite imply to the reaction St +Ms + Qtz = Bt + And ± Grt + V. These textures resemble those observed in the staurolite-andalusite zone of the overlying Stilo unit (Graeßner & Schenk, 1999). However, a difference is the additional occurrence of late-stage fibrolitic sillimanite, overgrowing biotite and muscovite. Monazite occurs as inclusions in biotite, muscovite and plagioclase.

The third *paragneiss* (65-97) forms a *c.* 50 cm thick layer of garnet-biotite-fibrolite rich rock type in biotite-plagioclase gneisses. The sample was taken at the river T. Pisciato, north of the village of Condofuri, just east of the nappe boundary between the Aspromonte and Stilo units (Fig. 3.1). Unfortunately, this rock contained only fractions of small euhedral zircons, but not monazite.

One sample of *peraluminous granite*, the so-called 'Punta d'Atò granite' (Fig. 3.1; Messina & Russo, 1981), was taken to constrain the age of intrusion into the upper crust (17-2-96). The sample was collected at the banks of the river F. di Mèlito, where it cuts the granite in the north of the village of Bagaladi. The rock displays a homogeneous and equigranular texture of quartz, plagioclase and K-feldspar. Additional phases are biotite, muscovite and fibrolitic sillimanite as inclusions in muscovite. Main accessory minerals are monazite and xenotime, included in micas and plagioclase.

A second *peraluminous granite*, the so called 'Cittanova granite' (14-92), was sampled in front of the tunnel Limina at street No. 281 in the west of Gioiosa Ionica (Fig. 3.1). This granite intruded into the middle crust between the large Serre granodiorite to the north and the gneisses of the Aspromonte unit in the south. It shows a slight foliation and consists of quartz, plagioclase, K-feldspar, muscovite, biotite, ±andalusite, ±fibrolite, ±cordierite and ±garnet (Rottura *et al.*, 1986 and references therein). The crystallization age was dated at 291-284 Ma with the Rb-Sr method on biotite and muscovite (Del Moro *et al.*, 1982).

A lense of metamorphosed *gabbroic* to *Qtz-dioritic* composition was sampled (51b/85) from the lower crust. This intrusion into the surrounding granulite facies metapelites crops out at street No. 19 at the railway tunnel north of the river F. Angitola north of Pizzo (Fig. 3.1). This rock type is similar to that described by Schenk (1984) as a 250 m thick sill north of the village of Capistrano, consisting of plagioclase, quartz, biotite, orthopyroxene, clinopyroxene and K-feldspar. U-Pb zircon dating yielded nearly concordant ages of 300-295 Ma (Schenk, 1980).

3.5 ANALYTICAL PROCEDURES

Monazite, xenotime and zircon (<350 μm) were separated from 9-18 kg of fresh rock material using standard techniques (steel jaw-crusher, roller mill, Wilfley table, Frantz magnetic separator, heavy liquids). Prior to dissolution, hand picked grain size fractions were washed in high purity 2 N HNO_3 (monazite, xenotime) or warm 6 N HNO_3 (zircon), in acetone and water to remove any surface contamination. For each monazite and the one xenotime fraction 20 to 60 individual grains were separated, in the analysed zircon fraction the number of individual grains was estimated to be 200-600. Due to the small size of the samples the weight of all grain size fractions were estimated from shape and density of the individual grains, except for three fractions analysed at the beginning of this study (marked with an asterix in Table 3.1), where larger grain size fractions were separated and weighted. Dissolution and chemical extraction (anion exchange columns) of U and Pb were performed following Krogh (1973). Most of the monazite and the xenotime fractions were dissolved in 1 ml 6 N HCl and all zircon fractions in 1 ml 24 N HF in Teflon® bombs within screw-top steel containers at 180 °C for 5 days. Only the monazite fractions of samples 35-96 and 82-96 were dissolved in a mixture of 1 ml 6 N HNO_3 : HCl (5:1) in Savillex® vials on a hotplate after 2 weeks. A mixed ^{205}Pb-^{233}U tracer solution was used for isotope dilution, except for one zircon and two monazite grain size fractions analysed at the beginning of this study (Table 3.1), where a mixed ^{208}Pb-^{235}U spike was used.

Isotope analyses were performed at the 'Zentrallaboratorium für Geochronologie' in Münster using a VG Sector 54 multicollector mass-spectrometer with Daly detector in ion counting mode (for ^{204}Pb) or using simultaneously Faraday detectors (all other isotopes) and a NBS-type Teledyne mass-spectrometer (Rb). U and Pb were loaded on Re filaments with silica gel, H_3PO_4 and 3 N HCl. Measured Pb and U isotopic ratios were corrected for 0.1 % and 0.095 % fractionation per atomic mass unit, based on repeated analyses of standards NBS 982 and NBS U

500 (see Appendix 1). Total procedural blanks during this study range between 0.06-0.02 ng Pb. U blanks were not measured since the very low blanks normally obtained are negligible for the high U amounts analysed. The ages and the error ellipses of Tabel 3.1 and Fig. 3.2 were calculated using the recommended IUGS decay constants (Steiger & Jäger, 1977) and considering the internal 2σ error of the measurements, the uncertainty in the U-Pb ratio of the spike, the error magnification from the spike/sample ratio and the estimated uncertainty in the isotopic composition of the Pb blank. Measured ratios were corrected for initial isotope Pb composition applying the two-stage model of Stacey & Kramers (1975) using the assumed age of the sample.

Muscovite and biotite were separated from small rock pieces (1-2 kg) of the samples collected for the U-Pb studies. Fractions were enriched in micas using standard techniques (steel jaw-crusher, roller mill, Frantz magnetic separator and adherence to a piece of paper). Only the size fraction 160-200 μm has been considered for Rb-Sr and K-Ar dating. After hand picking, possible contaminants between the mica sheets were removed by grinding under ethanol in an agate mortar. Afterwards the mica fractions were washed in ethanol and water in an ultrasonic bath.

Whole rock powder (100 mg) and mica fractions (*c.* 25-40 mg) were mixed with a ^{87}Rb-^{84}Sr tracer solution for isotope dilution prior to dissolution in a mixture of HF : HNO_3 (5:1) in Savilex® vials on a hotplate for 3 days. Chemical extraction of Rb and Sr were performed on cation exchange columns using 2.5 N HCl and loaded on Ta filaments with H_2O or H_3PO_4, respectively. Measured Rb isotopic ratios were corrected for mass fractionation using a factor of 0.9935, determined by repeated measurements of standard NBS 607. Measured Sr ratios were corrected for fractionation based on a $^{86}Sr/^{88}Sr$ ratio of 0.1194. Total blanks for Rb and Sr during the measurements were less than 0.05 and 0.1 ng. The uncertainty in $^{87}Rb/^{86}Sr$ ratios is 1 % (2σ), deduced from repeated measurements. The error in $^{87}Sr/^{86}Sr$ ratios is based on the internal 2σ error of the measurements. The ages were calculated using the least square regression technique of York (1969).

K-Ar dating of micas (*c.* 100 mg) was carried out at the Institut für Geologie und Dynamik der Lithosphäre, Universität Göttingen. K was measured by a flame photometer (Eppendorf) and Ar on a VG 1200-C noble gas mass-spectrometer. A spike with an ^{38}Ar purity of 99.989 % was used. The K-Ar ages were calculated using the recommended IUGS decay constants (Steiger & Jäger, 1977).

Back-scattered electron (BSE) and cathodoluminescence (CL) images of monazite, xenotime and zircon were taken on a JEOL Superprobe JXA 8900 RL at the Geochemisches Institut, Universität Göttingen, operating at an acceleration voltage of 20 kV and a beam current of 25 nA. BSE images reveal internal compositional variations that are due to contrasts in the average atomic number of elements in the mineral and largely reflect differences in the concentrations of light rare earth elements, Th, U and Hf (Hanchar & Miller, 1993; Hawkins & Bowring, 1997, 1999). According to these studies brighter zones of the crystals reflect the higher atomic number with

higher Th/U ratios. The CL emission can be enhanced by REE in particular Dy, Gd, Tb and Y (e.g. Hanchar & Rudnick, 1995).

3.6 RESULTS OF U-Pb GEOCHRONOLOGY

3.6.1 Northern Calabria

From both samples of *metapelitic migmatites* of the lower crustal segment, only clear, subhedral to round monazite crystals and some crystal fragments have been selected for U-Pb geochronology. Both monazite fractions from sample 50-96 plot slightly above the concordia which can be attributed to the presence of excess ^{206}Pb that results from the decay of ^{230}Th (Schärer, 1984). In this case the ^{207}Pb/^{235}U age of 304.1 ± 0.4 Ma is taken as representing the mineral age (Table 3.1, Fig. 3.2a). One grain size fraction of sample 35-96 (80-100 μm) also shows slight reverse discordance yielding a ^{207}Pb/^{235}U age of 302.1 ± 0.5 Ma (Table 3.1, Fig. 3.2a). A second grain size fraction (63-80 μm) of this sample lies slightly discordant below concordia with an ^{207}Pb/^{206}Pb age of 300.1 ± 0.6 Ma. BSE imaging indicates that some grains of both samples are characterized by continuous to discontinuous growth zoning (Fig. 3.3a). Some other grains have irregular, patchy domains that are truncated by marginal growth zones (Fig. 3.3b). According to Hawkins and Bowring (1999), these structures might indicate a sequence of precipitation and dissolution of the monazite from a fluid or a melt due to partial melting of the host metapelite during prograde metamorphism. On the other side different monazite grains from these samples show homogeneous internal compositional structures. The preservation of nearly concordant and similar ages of most of the measured grain size fractions together with the observed internal structures support the interpretation that monazite reveals the age of crystallization during peak metamorphism. The slight discordance of grain fraction 63-80 μm of sample 35-96 (Fig. 3.2a) suggests recent Pb-loss.

From both samples of *peraluminous granites* only clear, euhedral elongated to round monazites as well as some fragments were used. The larger size fraction (80-100 μm) of sample 81-96 yields nearly concordant ages and a ^{207}Pb/^{235}U age of 303.8 ± 0.6 Ma (Table 3.1, Fig. 3.2a). A second fraction of the same sample (63-80 μm) with a ^{207}Pb/^{206}Pb age of 303.8 ± 0.9 Ma plots slightly below concordia suggesting that discordance is due to recent radiogenic Pb-loss (Fig. 3.2a). The only studied grain size fraction of sample 82-96 is slightly reverse discordant, probably caused by excess thorogenic ^{206} Pb, yielding an ^{207}Pb/^{235}U age of 302.1 ± 0.6 Ma (Table 3.1, Fig. 3.2a). BSE images of monazite from all fractions reveal slightly corroded rims and variable internal compositional structures. Some euhedral grains are characterized by

Table 3.1 U-Pb analytical results for monazite, xenotime and zircon from southern and northern Calabria.

				Composition (c)			Measured isotopic ratios (d)			Corrected ratios (e)				Apparent ages (Ma) (f)		
Sample (a)	Size (μm)	Rock type	Estimated weight (mg) (b)	U (ppm)	Pb (ppm)	Common Pb (ng)	$^{206}Pb/^{204}Pb$	$^{208}Pb/^{206}Pb$	$^{207}Pb/^{206}Pb$	$^{206}Pb/^{238}U$	$^{207}Pb/^{235}U$	$^{207}Pb/^{206}Pb$	Correlation coefficient	$^{206}Pb/^{238}U$	$^{207}Pb/^{235}U$	$^{207}Pb/^{206}Pb$
Northern Calabria:																
35-96 M	63-80	paragneiss	0.026	3737	1049	0.08	2048 (0.1)	5.734 (0.004)	0.05899 (0.04)	0.04698 (0.18)	0.3390 (0.20)	0.05233 (0.08)	0.82	295.9	296.4 ± 0.5	300.1 ± 0.6
35-96 M	80-100	paragneiss	0.052	3109	818	0.06	4104 (0.2)	5.217 (0.01)	0.05562 (0.04)	0.04809 (0.18)	0.3466 (0.20)	0.05226 (0.07)	0.87	302.8	302.1 ± 0.5	296.9 ± 0.6
50-96 M	63-80	paragneiss	0.023	6135	1234	0.05	5401 (0.1)	3.705 (0.01)	0.05472 (0.02)	0.04851 (0.25)	0.3494 (0.26)	0.05224 (0.05)	0.97	305.4	304.3 ± 0.6	296.1 ± 0.8
50-96 M	80-100	paragneiss	0.04	6078	1105	0.13	4616 (0.2)	3.256 (0.01)	0.05531 (0.03)	0.04838 (0.18)	0.3492 (0.19)	0.05234 (0.06)	0.88	304.6	304.1 ± 0.4	300.5 ± 0.6
81-96 M	63-80	peral. granite	0.029	17806	1308	0.4	3367 (0.1)	0.7150 (0.01)	0.05665 (0.02)	0.04780 (0.26)	0.3455 (0.27)	0.05242 (0.05)	0.97	301.0	301.3 ± 0.6	303.8 ± 0.9
81-96 M	80-100	peral. granite	0.062	7340	894	0.63	2006 (0.1)	1.830 (0.01)	0.05956 (0.01)	0.04827 (0.25)	0.3487 (0.26)	0.05240 (0.06)	0.97	303.9	303.8 ± 0.6	302.9 ± 0.8
82-96 M	80-100	peral. granite	0.027	1563	328	0.05	1644 (0.2)	3.899 (0.01)	0.06071 (0.04)	0.04807 (0.25)	0.3466 (0.27)	0.05229 (0.09)	0.92	302.7	302.1 ± 0.6	298.0 ± 0.8
Southern Calabria:																
15-96 M	63-80	paragneiss	0.05	4699	791	0.59	1137 (0.04)	2.999 (0.01)	0.06491 (0.01)	0.04695 (0.18)	0.3380 (0.19)	0.05222 (0.07)	0.86	295.7	295.7 ± 0.5	295.1 ± 0.6
15-96 M	<350	paragneiss	*0.119	*4366	*818		2929 (0.3)	3.647 (0.01)	0.05761 (0.02)	0.04580 (0.30)	0.3323 (0.40)	0.05262	0.77	288.7	291.3 ± 0.4	312.4 ± 0.6
60-97 M	40-63	paragneiss	0.014	6795	579	0.07	2493 (0.2)	1.214 (0.004)	0.05770 (0.01)	0.04309 (0.25)	0.3099 (0.26)	0.05217 (0.06)	0.96	272.0	274.1 ± 0.5	292.7 ± 0.8
60-97 M	63-80	paragneiss	0.016	5732	524	0.19	1221 (0.1)	1.253 (0.02)	0.06378 (0.02)	0.04492 (0.25)	0.3231 (0.26)	0.05217 (0.07)	0.94	283.2	284.3 ± 0.6	292.8 ± 0.8
65-97 Zrn	<40	paragneiss	0.08	1483	199	0.99	874 (0.6)	0.1573 (0.10)	0.10421 (0.10)	0.12112 (0.63)	1.4771 (0.65)	0.08844 (0.17)	0.96	737.0	921.0 ± 4.0	1392.2 ± 5.0
65-97 Zrn	40-63	paragneiss	0.57	87	12	0.05	5024 (0.2)	0.1291 (0.04)	0.09418 (0.04)	0.13060 (0.19)	1.6522 (0.20)	0.09175 (0.06)	0.89	791.3	990.4 ± 2.0	1462.2 ± 2.0
14-92 M	40-63	peral. granite	0.018	5718	948	0.09	2606 (0.2)	2.886 (0.01)	0.05763 (0.06)	0.04806 (0.20)	0.3468 (0.23)	0.05233 (0.09)	0.88	302.6	302.3 ± 0.6	299.9 ± 0.7
14-92 M	63-80	peral. granite	0.025	4223	703	0.06	3750 (0.1)	2.909 (0.01)	0.05589 (0.02)	0.04815 (0.21)	0.3472 (0.21)	0.05230 (0.06)	0.94	303.1	302.6 ± 0.5	298.4 ± 0.7
17-96 X	63-100	peral. granite	0.058	23784	1100	0.34	11434 (0.1)	0.06054 (0.02)	0.05357 (0.01)	0.04821 (0.27)	0.3481 (0.27)	0.05236 (0.05)	0.98	303.5	303.3 ± 0.7	301.4 ± 0.9
17-96 M	<350	peral. granite	*0.153	*16123	*896		12740 (1.3)	0.3192 (0.05)	0.05333 (0.38)	0.04701 (0.52)	0.3382 (0.64)	0.05217	0.80	296.1	295.8 ± 0.8	293.2 ± 0.9
51b/85 Zrn	<54	basic intrusion	0.198	836	41	0.09	4151 (0.2)	0.1434 (0.01)	0.05611 (0.02)	0.04756 (0.25)	0.3459 (0.26)	0.05274 (0.05)	0.97	299.5	301.6 ± 0.6	317.7 ± 0.8
51b/85 Zrn	54-85	basic intrusion	*0.933	*466	*22		7039 (0.7)	0.1355 (0.02)	0.05448 (0.06)	0.04674 (0.30)	0.3377 (0.30)	0.05240	0.95	294.5	295.5 ± 0.4	303.0 ± 0.5

(a) Sample name include the type of mineral (*M* monazite, *X* xenotime, *Z* zircon).

(b) Except for samples marked with an asterix (*) weight of all grain size fractions were estimated from spheric shape and a density of 5 g/cm^3 for monazite and 4g/cm^3 for zircon.

(c) Except for samples marked with an asterix (*) compositions were calculated from estimated weight of grain size fraction in (b).

(d) Numbers in parentheses are at the % error reported at the 2 sigma confidence level.

(e) Ratios corrected for fractionation, spike, blank and common Pb, as described in the text. Numbers in parentheses are at the % error reported at the 2 sigma confidence interval.

(f) Uncertainty in the apparent ages in million years at the 2 sigma confidence interval.

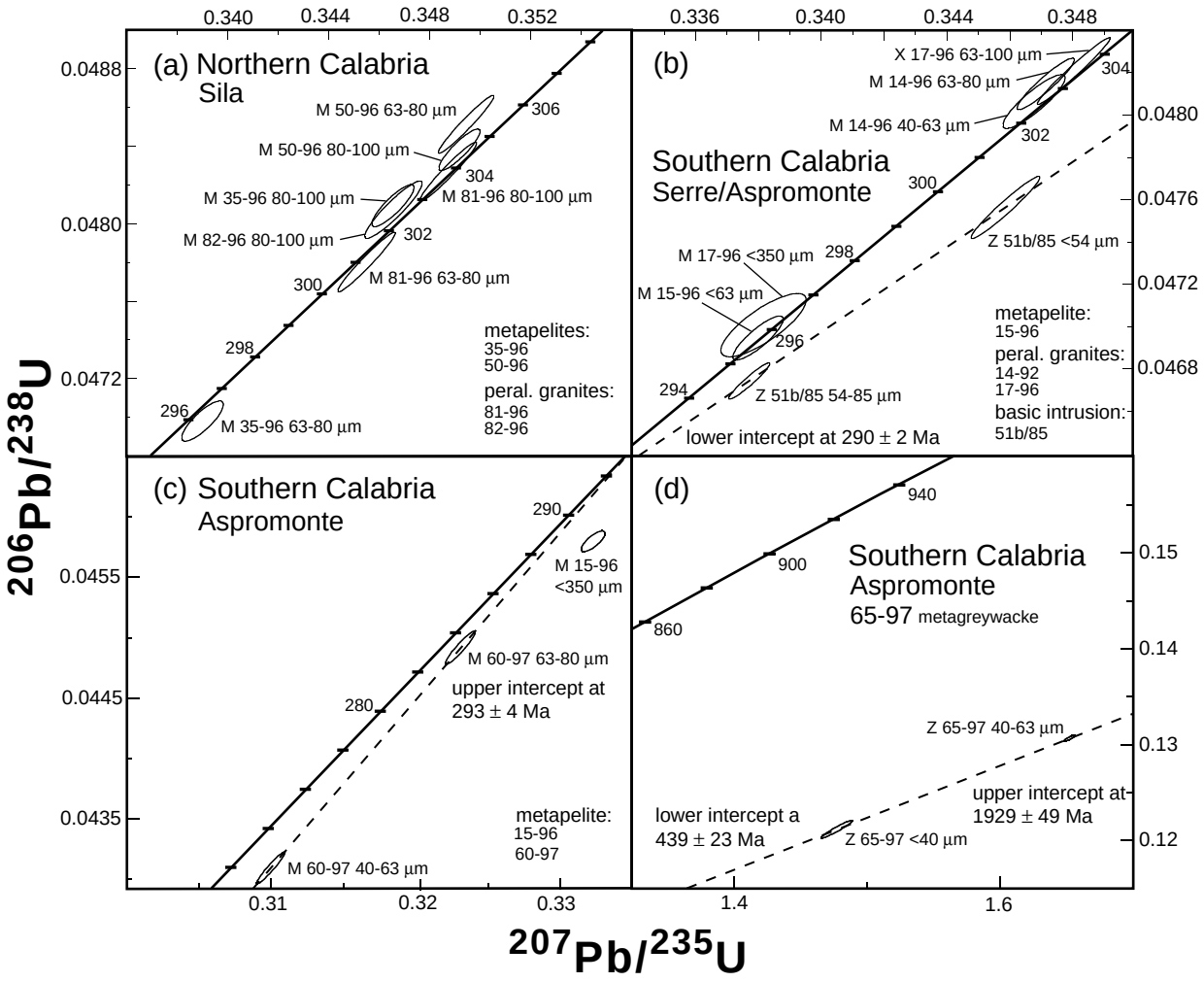

Fig. 3.2 Concordia diagrams for (a) monazite analyses of granulite facies migmatites and peraluminous granites from northern Calabria, (b) and (c) monazite, xenotime and zircon data from paragneisses and peraluminous granites from the upper to middle crust and a metabasic intrusion into the lower crust from southern Calabria, (d) zircon analyses of an amphibolite facies metagreywacke from the upper crust of southern Calabria. Sample name includes the type of mineral dated (*M* monazite, *X* xenotime, *Z* zircon).

concentric growth zoning parallel to crystal faces containing deeply resorbed xenocrystic oscillatory zoned cores (Fig. 3.3c). Other more roundly shaped crystals are irregularly zoned with patchy internal compositional variations (Fig. 3.3d). Since both textures are not only observed in different but also in the same grain fraction and together with their nearly concordant ages we interpret the observed internal compositional variations as a result of episodes of growth and dissolution of monazite during emplacement of the granites (cf. Hawkins and Bowring, 1999).

From these results it is evident that slightly reversly concordant and concordant monazites reveal similar ages of 304-302 Ma for the granulite facies metamorphism and the intrusion of the granites into the middle crust.

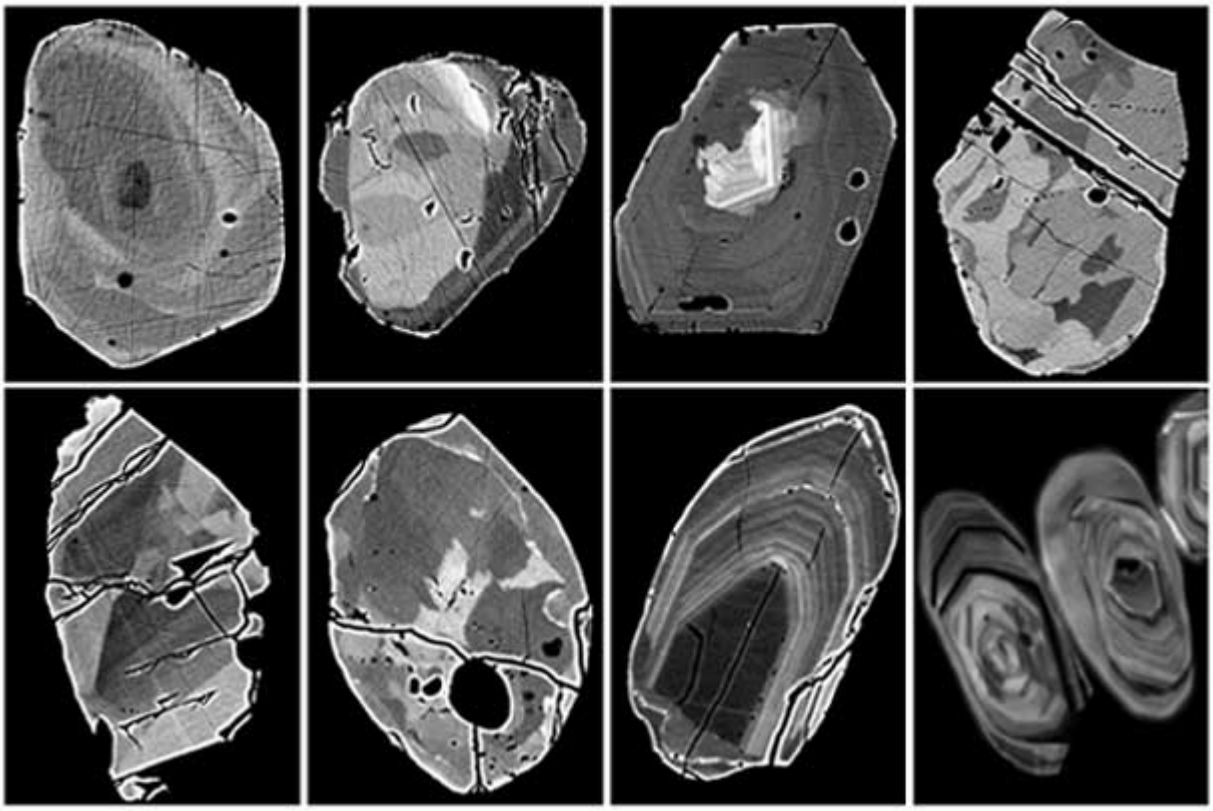

Fig. 3.3 Back-scattered electron images of monazite crystals from paragneisses (a: sample 50-96; b: sample 35-96; e, f: sample 60-97) and peraluminous granite 81-96 (c, d) and a zircon crystal from paragneiss 65-97 (g). Cathodoluminscence image of zircon crystals from a metabasic intrusion 51b/85 (h). Scale bar is 10 μm in every image. For further dicussion see text.

3.6.2 Southern Calabria

From two amphibolite facies *metapelites* of the Aspromonte unit (samples 60-97 and 15-96) clear to slightly clouded subhedral to ellipsoidal shaped partly corroded monazite grains and some additional grain fragments were used for U-Pb dating. BSE imaging indicates that grains of all samples reveal similar internal compositional variations as described above. Monazite from each fraction shows homogeneous compositions to patchy irregular zoning as well as some truncated and partly resorbed regular zones in the cores (Fig. 3.3e,f). Both monazite fractions of sample 60-97 plot strongly discordant below the concordia (Fig. 3.2c, Table 1) probably as a result of Pb-loss induced by an Alpine overprint at 30-25 Ma which has been reported in the Aspromonte area (Bonardi *et al.*, 1987). Individual regression defines an upper intercept age of about 293 ±4 Ma which is similar to the $^{207}Pb/^{206}Pb$ ages of both fractions of 292.7 ± 0.8 Ma (Table 3.1) and is interpreted as the age of amphibolite facies metamorphism. The irregular truncation domains in weakly zoned cores might reflect the growth of secondary monazite due to the Alpine overprint (Fig. 3.3e). Since one monazite fraction of sample 15-96 (63-80 μm) yields concordant ages of 295.7 ± 0.5 Ma (Table 3.1, Fig. 3.2b) a peak metamorphic origin of all compositional variations is

more likely. The second grain fraction (<350 μm) of sample 15-96 with a $^{207}Pb/^{206}Pb$ date of 312.4 ± 0.6 Ma plots strongly discordant below concordia suggesting recent Pb-loss (Fig. 3.2c).

Two analysed grain size fractions of very small (<63 μm), clear, elongated, slightly rounded zircons from the *paragneiss* 65-97 of the amphibolite facies upper crust define a poorly constrained discordia with lower and upper intercept ages of 439 ± 23 and 1929 ± 49 Ma (Fig. 3.2d). The age of the upper intercept is in agreement with those of discordant zircons from metasediments of the upper to lower crust of ~2 Ga (Schenk, 1990). The age of the lower intercept is comparable to the poorly constrained lower concordia intercept ages of zircons from a paragneiss of the upper crust (377 ± 55 Ma; Schenk, 1990). Zircons of both grain size fractions plot at some distance from the upper and lower intercept with the concordia which might result from severe Pb-loss during recrystallization due to late-Hercynian amphibolite facies metamorphism in the upper crust. BSE and Cl images support the interpretation above (Fig. 3.3g). Zircons are characterized by inherited euhedral cores with well preserved primary growth zoning. These cores sometimes include further older anhedral resorbed oscillatory zoned cores bound by inclusion trails parallel to the outline of the inner core. The marginal overgrowth on the cores, cutting the magmatic growth zoning, varies in volume and is mostly homogeneous to weakly zoned and is interpreted as being of late-Hercynian metamorphic origin.

The *peraluminous* Cittanova (14-92) and Punta d'Atò *granites* (17-96) contain clear, greenyellow euhedral well-faceted xenotime (17-97) and yellow elongated euhedral to round monazite grains. Both of the monazite fractions of sample 14-92 plot slightly above concordia yielding $^{207}Pb/^{235}U$ ages ranging from 302.6-302.3 ± 0.6 Ma (Fig. 3.2b; Table 3.1). Most of the monazite BSE images of sample 14-92 reveal nearly homogeneous internal compositional structures whereas in some grains irregular, heterogeneous domains truncating the homogeneous part are also observed. Xenotime of sample 17-96 (63-100 μm) is slightly reverse concordant with a $^{207}Pb/^{235}U$ age of 303.3 ± 0.7 Ma (Fig. 3.2b; Table 3.1). BSE images show growth zoning parallel the crystal shape as well as partially truncated homogeneous cores surrounded by darker euhedral rims. Both structures are interpreted as evidence of crystallization of the grains from a melt. A monazite fraction of this sample (<350 μm) plots nearly concordant on the concordia with a $^{207}Pb/^{235}U$ age of 295.8 ± 0.8 Ma (Fig. 3.2b). This age might be too young compared to the results above reflecting either high-temperature Pb-loss, dynamic recrystallization, secondary overgrowth or recrystallisation (Hawkins & Bowring, 1997). There have been done no BSE images of this grain size fraction due to the scarcity of monazite crystals.

Two fractions of small, clear, elongated euhedral to slightly rounded zircons of a metamorphosed *gabbroic to Qtz-dioritic sill* plot discordant below concordia and define a lower intercept age of 290 ± 2 Ma (Fig. 3.2b). BSE and Cl images reveal that most of the crystals are characterized by fine-scale euhedral magmatic zoning patterns of which some grains show inherited partially resorbed relic cores, also with primary magmatic zoning (Fig. 3.3h). Slightly rounded crystals show a late, nearly homogeneous, overgrowth which cuts and truncates the

magmatic cores described above. Since the zircons have high U concentrations (400-860 ppm) they might have been more susceptible to metamictization than grains with lower U contents and therefore also to recent differential Pb-loss. Recent Pb-loss would have resulted in a rotation of the discordia to a lower meaningless intercept age (cf. Mezger & Krogstad, 1997). The lower intercept at 290 ± 2 Ma would therefore indicate the minimum age of the dated event. The geological interpretation of the lower and upper discordia intercepts are not unequivocal. On the one hand, the upper intercept might be the magmatic crystallization, the lower intercept the metamorphism. However, on the other hand, it may also be that the upper intercept is caused by an inherited component, whereas the lower one reflect the time of magmatic crystallization and metamorphism in the lower crust.

3.7 RESULTS OF Rb-Sr and K-Ar GEOCHRONOLOGY

The results of Rb-Sr and K-Ar dating on muscovite and biotite are used to constrain the cooling history of the granulite facies rocks of the Sila massif. Micas from one metapelite of the upper crust in southern Calabria (sample 15-96) are also used for comparison with previous studies (Schenk, 1980; Del Moro *et al.*, 1982). The geochronological data are compiled in Tables 3.2, 3.3.

Since the closure temperatures for the Rb-Sr system are higher than those of the K-Ar system for biotite and muscovite, the former dating method is expected to give older ages. Additionally, the closure temperature for the Rb-Sr and the K-Ar system in muscovite is significantly higher than in biotite. The one for Rb-Sr in muscovite has been estimated at *c.* 500 ± 50 °C and in biotite at *c.* 350 °C (Hanson & Gast, 1967; Purdy & Jäger, 1976; Dodson, 1979). The closure temperature for K-Ar in muscovite is *c.* 350 ± 40 °C and in biotite *c.* 280 ± 40 °C (Purdy & Jäger, 1976, Harrison *et al.*, 1985). The dated cooling temperatures thus range between *c.* 500 to *c.* 300 °C.

For the granulite facies metapelites from *northern Calabria* Rb-Sr biotite-whole rock isochrones yield ages of 123 ± 1 Ma (sample 35-96) and 189 ± 2 Ma (sample 50-96) (Table 3.2). This is in accordance with the fact that sample 50-96 stems from a more higher structural level than sample 35-96, which is taken from the base of the lower crustal section (Fig. 3.1). During retrograde cooling of the crustal segment the closure temperature of biotite from the top will be crossed earlier than that of biotite from deeper structural levels. This is interpreted as the reason for younger cooling ages in the deeper part of the crust. The K-Ar ages of biotites from the same sample support this interpretation: 128.2 ± 2.6 Ma for sample 35-96 and 175.2 ± 3.6 Ma for sample 50-96 (Table 3.3). The slightly higher K-Ar age of biotite from sample 35-96 might be due to incorporation of excess-Ar.

For sample 50-96 a Rb-Sr muscovite-whole rock isochrone defines an age of 287 ± 8 Ma (Table 3.2). The K-Ar age of 209.9 ± 4.5 Ma (Table 3.3) is lower than the Rb-Sr age but higher than those of biotite in accordance with the higher closure temperature of muscovite. It is similar to

Table 3.2. Rb-Sr isotope analyses used for mineral dating of paragneisses of the upper and lower crust in southern and northern Calabria, respectively.

Sample	Type	Rb (ppm)	Sr (ppm)	$^{87}Rb/^{86}Sr$ (a)	$^{87}Sr/^{86}Sr$ (a)(b)	initial $^{87}Sr/^{86}Sr$	Age (Ma) (c)
15-96	whole rock	193	110.9	5.048	0.73846 (0.003)		
	biotite	453	5.815	237.5	1.26643 (0.010)	0.727	160 ± 2
	muscovite	163	115.7	4.093	0.74092 (0.003)		
35-96	whole rock	57.0	270.4	0.611	0.72433 (0.004)		
	biotite	245	9.898	72.66	0.85009 (0.005)	0.723	123 ± 1
50-96	whole rock	128	214.4	1.727	0.72124 (0.003)		
	biotite	392	2.989	421.5	1.84899 (0.006)	0.717	189 ± 2
	muscovite	162	101.4	4.635	0.73313 (0.007)	0.714	287 ± 8

(a) Ratios corrected for fractionation, spike and blank as described in the text.

(b) Numbers in parentheses are at the % error reported at the 2 sigma confidence interval.

(c) Uncertainty in ages in million years at the 2 sigma confidence interval.

Table 3.3. K-Ar analytical results from biotite and muscovite of paragneisses from the upper and lower crust of southern and northern Calabria, respectively.

Sample	Mineral	Spike (No.)	K2O (wt. %)	40 Ar * (nl/g)	40 Ar * (%)	Age (Ma) (a)
15 - 96	muscovite	2317	8.78	48.01	98.86	162.1 ± 3.5
15 - 96	biotite	2313	8.31	60.29	99.46	212.1 ± 5.9
35 - 96	biotite	2308	8.93	38.24	98.97	128.2 ± 2.6
50 - 96	muscovite	2318	7.72	55.40	98.61	209.9 ± 4.5
50 - 96	biotite	2311	8.77	52.00	99.34	175.2 ± 3.6

(a) Uncertainty in ages in million years at the 2 sigma confidence level.

Dating has been done by H. Arendt, Institut für Geologie und Dynamik der Lithosphäre, Universität Göttingen.

a Rb-Sr age (muscovite-plagioclase) of 203 Ma of a granulite facies aplitic sill in the lower crust of southern Calabria (Schenk, 1980). Therefore it is concluded that the K-Ar age reflects the regular cooling age of the muscovite after Hercynian granulite facies metamorphism, whereas the Rb-Sr age seems to be in error. Disturbance of the Rb-Sr system of the whole rock by infiltration of retrograde Rb-rich fluids stemming from the nearby intruded granites would be an explanation. This would have increased the $^{87}Rb/^{86}Sr$ ratio of the whole rock and therefore also the muscovite-whole rock age. In this case, the effect on the biotite-whole rock age would be minor due to the large spread in $^{87}Rb/^{86}Sr$ ratios.

The metapelite of the upper crust in *southern Calabria* (sample 15-96) yields Rb-Sr and K-Ar biotite ages of 160 ± 2 and 212.1 ± 5.9 Ma (Table 3.2, 3.3). The Rb-Sr biotite age is 25 Ma older than at the top of the lower crustal section (135 Ma; Schenk, 1980) and is younger than expected from its former structural position in the crust. The reason for this might be a mixed mica population that contains Hercynian biotite and grains formed during an Alpine overprint. Alpine

ages of 30-25 Ma have been reported in the Aspromonte area (Bonardi *et al.*, 1987). However, on thin section scale it is not possible to recognize whether all biotite is a peak metamorphic phase or whether some grains were formed during an Alpine overprint. Recrystallized biotite of smaller grain sizes has not been detected. Unexpected is also the obtained K-Ar age, which is higher than the Rb-Sr biotite age. Normally this should not be the case since the closure temperature for Rb-Sr (*c.* 350 °C) is assumed to be higher than that for K-Ar (280 °C). Furthermore, the K-Ar age of the biotite is far too young compared with Rb-Sr results from different upper crustal rocks of Del Moro *et al.* (1982) which are in the range of 293-282 Ma. Also in this case, the reason might be the presence of heterogenous mica populations, but the influence of the younger component on the Rb-Sr age is smaller.

For muscovite of this sample only a K-Ar but no Rb-Sr age has been obtained, which is 162.1 ± 3.5 Ma. This result is too young compared to that of biotite and it appears also to be too young in respect to the structural position of the sample. The reason for this might also be the presence of mixed populations. A Rb-Sr muscovite-whole isochrone age can not be calculated since muscovite contains higher $^{87}Sr/^{86}Sr$ and lower $^{87}Rb/^{86}Sr$ ratios than the whole rock. Fluids which intruded during an Alpine overprint would have changed the whole rock chemistry as discussed previously.

3.8 DISCUSSION

3.8.1 Comparison with previous studies and temperature time history

U-Pb monazite dating of granulite facies paragneisses and of peraluminous granites of the Sila massif in northern Calabria yields similar ages of 304-302 Ma for the time of lower crustal metamorphism and of granite intrusion into the middle crust. Thus, our study provides *c.* 8-15 Ma older ages for the late-Hercynian emplacement of the granites than the study of Ayuso *et al.* (1994) who reported ages of 293-289 Ma ($^{40}Ar/^{39}Ar$ of muscovite and hornblende) from various types of peraluminous and calcalkaline granitoids. We interpret these ages know as cooling ages. A similar situation is given for age data from southern Calabria, where a former study (Del Moro *et al.*, 1982) reported Rb-Sr biotite and muscovite ages for the peraluminous granite of Cittanova (291-284 Ma) which are lower than the monazite U-Pb ages of 303-302 Ma obtained in this study.

For the first time monazite ages of two paragneisses of the upper crust of southern Calabria (Aspromonte unit) are reported here. One concordant monazite and an upper concordia intercept yield ages of 295 and 293 Ma. From this it is evident that peak metamorphism in the upper crust was attained at the same time as in the lower part of this crustal section, where monazite lie concordant between 296 and 290 Ma (Schenk, 1980). The new monazite data are better constraints for the time of metamorphism in the upper crust than the lower concordia intercept ages of 311 ± 95, 377 ± 55 and 439 ± 23 Ma (Schenk, 1990; Schenk and Todt, 1989 and this study). Concordant monazite ages at 296-290 Ma and the lower intercept ages of zircons of granulite facies metapelites, felsic granulites and metabasites of the lower crust at 295-292 and 312 ± 10 Ma

are similar to the intrusion ages of tonalites and dioritic gneisses of the middle crust (295-293 Ma) and of the Serre granodiorite (<314 Ma) of the upper crust (Schenk, 1980, 1990). Dating of discordant zircon from a mafic sill in the lower crust yield a lower intercept age of *c.* 290 Ma which can be interpreted as the time of metamorphism or as the minimum age of intrusion if inherited lead is the reason for discordance. The latter scenario is accounted for a comparable basic intrusion in the lower crust where nearly concordant zircon provided ages of 298 ± 5 Ma (Schenk,1980).

In this study the evaluated U-Pb ages of monazite are interpreted to reflect the time of growth and recrystallization during peak metamorphism. Petrological studies have shown that peak metamorphism in the lower crust has been attained at temperatures of 700-800 °C in southern and 740-770 °C in northern Calabria (Schenk, 1984, 1990; Graeßner & Schenk, in prep.). These temperatures are in the range of or above the temperatures (700 to 750 °C) at which many authors assume, that monazite in a dry system retains its U-Pb isotopic signature (Copeland *et al.*, 1988; Parrish, 1990; Mezger *et al.*, 1990, 1991). If monazite ages would reflect cooling below a closure temperature of *c.* 700-750 °C, rocks with peak metamorphic temperatures of 800 °C, as those at the base of the lower crustal section in southern Calabria, would be expected to have younger monazite ages than rocks from the upper part of this section, where only *c.* 700 °C have been attained (Schenk, 1980, 1990). This holds especially true because of the slow integrated cooling rate of the rocks which is about 2 °CMa^{-1}. This former interpretation of monazite ages as crystallization ages during peak metamorphism is supported by the data of the present study which revealed similar monazite ages in the lower crustal section of the Sila independently of the lithostratigraphic position and the peak metamorphic temperatures of the dated rocks. It is also in agreement with recent findings of DeWolf *et al.* (1993), Spear & Parrish (1996) and Bingen & van Breemen (1998) in high-grade metamorphic terrains. Ages determined for monazite from amphibolite facies paragneisses from the middle to upper crust are also interpreted to reflect growth rather than cooling below a closure temperature. This is in accordance with studies of Smith & Barreiro (1990) and Kingsbury *et al.* (1993) which document monazite growth at temperatures corresponding to the staurolite-in isograd.

In contrast to the results of U-Pb dating, the K-Ar and Rb-Sr ages of biotite and muscovite obtained from migmatitic metapelites of the Sila are much younger than the late-Hercynian metamorphic event and are therefore interpreted as cooling ages. This interpretation is supported by the fact that younger mineral ages were reported from the base than from the top of the lower crustal segment. The regular sequence of mineral ages indicates slow cooling of the lower crustal segment of *c.* 3 °C Ma^{-1} which seems to be undisturbed by any tectonic event between 300 and 130 Ma. However, the cooling path is not well constrained in the time intervall of 300-210 Ma which is between the end of the prograde metamorphism and the closure of muscovite for K-Ar (Fig. 3.4). Borsi & Dubois (1968) reported comparable Rb-Sr biotite and muscovite ages of rocks from the base of the lower crustal section of the Sila nappe. The biotite ages scatter between 205

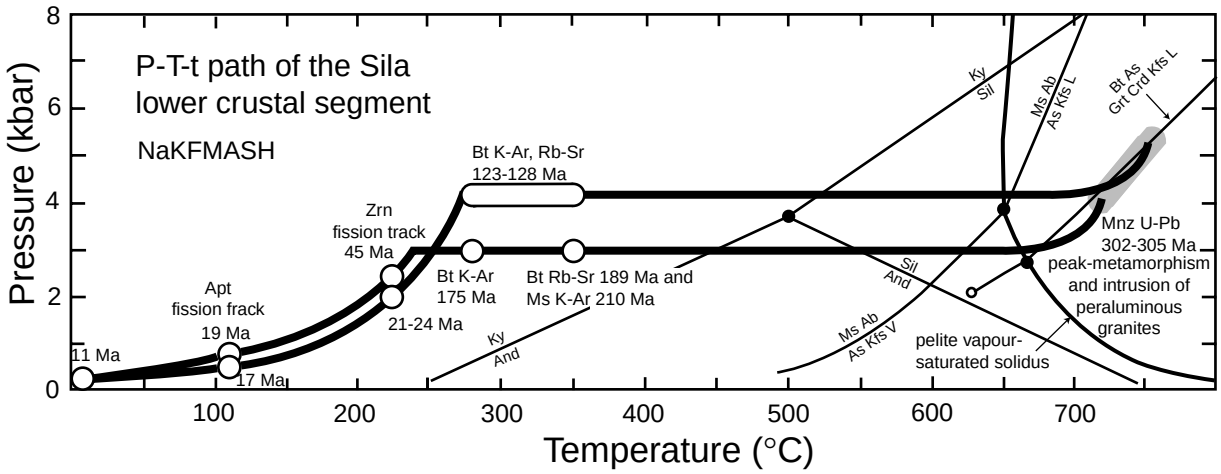

Fig. 3.4 *P-T*-t path of the lower and upper part of the lower crustal segment of the Sila massif in northern Calabria. The grey field shows *P-T* conditions in the granulite facies lower crust during peak metamorphism (Graeßner & Schenk, in prep.). Final uplift of the lower crustal section is deduced from apatite and zircon fission track data of Thomson (1994) and the oldest overlying sediments of Tortonian age (11 Ma). Reaction curves and invariant points in the NaKFMASH system after Spear *et al.* (1999). Closure temperatures of micas are given in the text, those for apatite and zircon fission track ages are 110 ± 10 °C (Green *et al.*, 1989) and 225 ± 25 °C (Hurford, 1991), respectively. See text for further discussion.

and 103 Ma, the muscovite ages between 253 and 210 Ma which is in the range of the mineral ages presented here.

The scenario of post-Hercynian slow cooling of the Sila granulite facies gneisses in mid-crustal levels (10-15 km depth; Fig. 3.4) resembles that deduced for the lower crust in southern Calabria (Schenk, 1980, 1990). Since that crustal section was uplifted into some deeper mid-crustal levels (12-18 km) after late-Hercynian metamorphism the cooling ages of biotites are even somewhat younger (135-110 Ma) than in the Sila. Supplementary cooling ages of feldspar (Rb-Sr), hornblende (K-Ar) and garnet (Sm-Nd) give a good constraint on the regular slow cooling (*c.* 2 °CMa^{-1}) of the lower crustal section in the Serre.

Constraints on the final uplift of the lower crustal section in the Sila massif to surface level are given by apatite and zircon fisson track ages by Thomson (1994). As for Rb-Sr and K-Ar ages of mica, higher apatite and zircon fission track ages are derived from rocks of the structurally upper part (19 and 45 Ma, respectively) than for those from the structurally lower part (17 and 21-24 Ma, respectively) (Fig. 3.4). Thomson (1994, 1998) interprets these ages as reflecting exhumation due to late-orogenic extension and synchronous erosion during the Oligo- to Miocene following continuous NW-directed subduction of the Tethys below the Calabrian massif which gave rise to elevated cooling rates of 5-13 °CMa^{-1} between >45 Ma and *c.* 15 Ma. Cooling of the exposed lower crustal rocks must have ceased at about 11 Ma ago, which accounts for the oldest age of Tortonian sediments resting on top of the Calabrian lower crustal rocks (van Dijk & Okkes, 1991).

The Rb-Sr and K-Ar mineral ages of 160 Ma (biotite) and 212 Ma (muscovite) evaluated from one staurolite-grade metapelite of the upper crust (sample 15-96) seem to be much too young with respect to its structural position and the biotite and muscovite ages of 291-282 Ma for peraluminous granites which intruded into the upper crustal gneisses (Del Moro, et al., 1982). An Alpine metamorphic overprint with Rb-Sr biotite ages of 30-25 Ma has been described in this area (Bonardi *et al.*, 1987, 1992), which might be responsible for the disturbance of the isotopic systems of micas in the analysed samples. Biotite ages older than muscovite ages clearly do not represent cooling ages.

3.8.2 Conclusions

The age of amphibolite and granulite facies metamorphism of upper and lower crustal paragneisses and of intrusion of peraluminous granites into the middle crust of northern and southern Calabria were isotopically dated in this study. In the Sila massif of northern Calabria monazite yield similar U-Pb ages of 304-301 Ma for the granulite facies metamorphism and for the intrusion of the granites into the middle crust. Intrusion ages of comparable granites into the middle to upper crust of southern Calabria (Serre, Aspromonte) reveal similar ages of 303-302 Ma and fall into the age range obtained for the granulite and the amphibolite facies metamorphism in different levels of the crust, and the age of the calcalkaline to mesaluminous granitoids in the whole exposed crustal profile of 310-290 Ma (Schenk, 1980, 1990 and this study).

Previous petrological studies adressing the metamorphic evolution in the upper and in the lower crustal part of southern Calabria have shown that the deformation-crystallization relationship during the prograde metamorphic evolutions in both sections is similar (Schenk, 1984, 1990; Graeßner & Schenk, 1999). The peak metamorphic assemblages grew mainly syntectonically during late-Hercynian metamorphism but mineral growth outlastet the deformation. However, the main difference refers to the prograde evolution of the lower crust which is characterized by a pressure increase not seen in the upper crustal rocks. The new data presented here support the interpretation that this might be caused by magmatic intrusions into the middle crust which proceeded synchronously with metamorphism. These granitoids would have provided the heat for the late static metamorphic stage in all crustal levels and would have led to the observed relatively small temperature difference between the base of the upper crust (620 °C at *c.* 2.5 kbar) and the top of the lower crust (690 °C at 5.5 kbar) (Schenk, 1984; Graeßner & Schenk, 1999). An ancient geotectonic setting of the exposed crustal profile as a continantal arc above a subduction zone would satisfy the petrological and isotopic data (cf. Schenk, 1990).

The same geological scenario can be accounted for the Sila massif of northern Calabria. A petrological study of the lower crustal gneisses has also revealed a late static mineral growth best documented in metabasic rocks (Graeßner & Schenk, in prep.). Together with the dated synchroneity of geological events, the granulite facies metamorphism in the lower crust can be

related to the intrusions of the peraluminous granites into the middle crust. As in southern Calabria fast uplift of the lower granulite facies segment into mid-crustal levels (10-15 km) is followed by slow cooling of 3 °CMa^{-1} (Fig. 3.4). Whether the granite intrusions have affected the thermal conditions in the upper crust of the Sila massif like in southern Calabria, has to be determined in the future.

REFERENCES

Acquafredda, P., Barbieri, M., Lorenzoni, S., Trudu, C. & Zanettin Lorenzoni, E., 1991. The age of volcanism and metamorphism of the Bocchigliero Paleozoic sequence (Sila - Southern Italy). *Rendiconti di Scienze Fisiche e Naturali della Accademia Nazionali dei Lincei,* **9,** 145-156.

Acquafredda, P., Caggianelli, A. & Piccarreta, G., 1992. Late magmatic to subsolidus coronas in gabbroic rocks from the Sila massif (Calabria, Italy). *Mineralogy and Petrology*, **46,** 229-238.

Acquafredda, P., Lorenzoni, S. & Zanettin Lorenzoni, E., 1994. Palaeozoic sequences and evolution of the Calabrian-Peloritan Arc (Southern Italy). *Terra Nova*, **6,** 582-594.

Althaus, E. & Istrate, G., 1990. Granulite facies conditions derived from fluid inclusions: Sila massif, Calabria, Italy. *Neues Jahrbuch für Mineralogie, Monatshefte,* **2,** 65-75.

Alvarez, W., 1976. A former continuation of the Alps. *Bulletin of the geological Society of America*, **87,** 891-896.

Amodio-Morelli, L., Bonardi, G., Colonna, V., Dietrich, D., Giunta, G., Ippolito, F., Liguori, V., Lorenzoni, S., Paglionico, A., Perrone, V., Piccareta, G., Russo, M., Scandone, P., Zanettin-Lorenzoni, L. & Zuppetta, A., 1976. L'arco Calabro-peloritano nell'Orogene Appeninico-Maghrebide. *Memorie della Societá Geologia Italiana*, **17,** 1-60.

Ashworth, J. R., 1972. Myrmekites of exsolution and replacement origins. *Geological Magazine,* **109,** 45-62.

Ayuso, R. A., Messina, A., De Vivo, B., Russo, S., Woodruff, L. G., Sutter, J. F. & Belkin, H. E., 1994. Geochemistry and argon thermochronology of the Variscan Sila batholith, southern Italy: Source rocks and magma evolution. *Contributions to Mineralogy and Petrology*, **117,** 87-109.

Azor, A. & Ballèvre, M., 1997. Low-pressure metamorphism in the Sierra Albarrana area (Variscan belt, Iberian massif). *Journal of Petrology,* **38,** 35-64.

Bégin, N. J. & Pattison, D. R. M., 1994. Metamorphic evolution of granulites in the Minto Block, northern Québec: extraction of peak *P-T* conditions taking account of late Fe-Mg exchange. *Journal of Metamorphic Geology*, **12,** 411-428.

Berman, R. G., 1988. Internally-consistent thermodynamic data for minerals in the system Na_2O-K_2O-CaO-MgO-FeO-Fe_2O_3-Al_2O_3-SiO_2-TiO_2-H_2O-CO_2. *Journal of Petrology,* **29,** 445-522.

Berman, R. G., 1990. Mixing properties of Ca-Mg-Fe-Mn garnets. *American Mineralogist,* **75,** 328-344.

Berman, R. G., 1991. Thermobarometry using multi-equilibrium calculations: a new technique, with petrological applications. *Canadian Mineralogist,* **29,** 833-855.

Berman, R. G. & Aranovich, L. Y., 1996. Optimized standard state and solution properties of minerals I. Model calibration for olivine, orthopyroxene, cordierite, garnet, and ilmenite in the

system FeO-MgO-CaO-Al_2O_3-TiO_2-SiO_2. *Contributions to Mineralogy and Petrology,* **126,** 1-24.

Bhattacharya, A., Mazumdar, A. C. & Sen, S. K., 1988. Fe-Mg mixing in cordierite: constraints from natural data and implications for cordierite-garnet thermometry in granulites. *American Mineralogist,* **3,** 338-344.

Bhattacharya, A., Krishnakumar, K. R., Raith, M. & Sen, S. K., 1991. An improved set of a—X parameters for Fe-Mg-Ca garnets and refinements of the orthopyroxene-garnet thermometer and the orthopyroxene-garnet-plagioclase-quartz barometer. *Journal of Petrology*, **32,** 629-656.

Bingen, B. & van Breemen, O., 1998. U-Pb monazite ages in amphibolite- to granulite-facies orthogneiss reflect hydrous mineral breakdown reactions: Sveconorwegian province of SW Noeway. *Contributions to Mineralogy and Petrology,* **132,** 336-353.

Blümel, P. & Schreyer,W., 1976. Progressive regional low pressure metamorphism in Moldanubian metapelites of the Northern Bavarian Forest, Germany. *Krystalinikum,* **12,** 7-30.

Bohlen, S. R., Wall, V. J. & Boettcher, A. L., 1983. Experimental investigations and geological applications of equilibria in the system FeO-TiO_2-Al_2O_3-SiO_2-H_2O. *American Mineralogist,* **68,** 1049-1058.

Bonardi, G., Gurrieri, S., Messina, A., Perrone, V., Russo, M. & Zuppetta, A., 1979. Osservazioni geologiche e petrografiche sull'Aspromonte. *Bolletino della Società Geologica Italiana*, **98,** 55-73.

Bonardi, G., Messina, A., Perrone, V., Russo, M., Russo, S. & Zuppetta, A., 1980. La finestra tettonica di Cardeto (Reggio Calabria). *Rendiconti della Società Geologica Italiana,* **3,** 3-4.

Bonardi, G., De Vivo, B., Giunta, G., Lima, A., Perrone, V. & Zuppetta, A., 1982. Mineralizzazioni dell'Arco Calabro-Peloritano. Ipotesi genetiche e quadro evolutivo. *Bolletino della Società Geologica Italiana*, **101,** 141-155.

Bonardi, G., Compagnoni, R., Messina, A. & Perrone, V., 1984a. Riequilibrazioni metamorfiche di probabile età alpina nell'Unità dell'Aspromonte - Arco Calabro-Peloritano. *Rendiconti della Società Italiana di Mineralogia e Petrologia*, **39,** 613-628.

Bonardi, G., Messina, A., Perrone, V., Russo, S. & Zuppetta, A., 1984b. L'Unita di Stilo nel settore meridionale dell'Arco Calabro-Peloritano. *Bolletino della Società Geologica Italiana*, **103,** 279-309.

Bonardi, G., Compagnoni, R., Del Moro, A., Messina, A. & Perrone, V., 1987. Riequilibrazioni tettono-metamorfiche alpine nell'Unita dell'Aspromonte, Calabria meridionale. *Rendiconti Società Italiana di Mineralogia e Petrologia*, **42,** 301.

Bonardi, G., Compagnoni, R., Messina, A., Perrone, V., Russo, S., De Francesco, A. M., Del Moro, A. & Platt, J., 1992. Sovrimpronta metamorfica alpina nell'Unità dell'Aspromonte (settore meridionale dell'Arco Calabro-Peloritano). *Bolletino della Società Geologica Italiana*, **111,** 81-108.

Borghi, A., Colonna, V. & Compagnoni, R., 1992. Structural and metamorphic evolution of the Bocchigliero and the Mandatoriccio complexes in the Sila Nappe (Calabrian-Peloritain Arc, Southern Italy). *IGCP No.276* Newsletter,Vol. **5,** 321-334.

Bouillin, J. P., Baudelot, S. & Majeste-Menjoulas, C., 1984. Mise en évidence du Cambro-Ordivizien en Calabre centrale (Italie). Affinités paléogéographiques et consequences structurales. *Compte Rendu de lé Académie des Sciences Paris,* **298,** 89-92.

Borsi, S. & Dubois, R., 1968. Données géochronologiques sur l'histoire hercynienne et alpine de la Calabre centrale. *Comptes Rendus de l'Académie des Sciences de Paris,* **266,** 72-75.

Brodie, K. H. & Rutter, E. H., 1987. Deep crustal extensional faulting in the Ivrea zone of Northern Italy. *Tectonophysics,* **140,** 193-212.

Brown, M., 1998. Unpairing metamorphic belts: P-T paths and a testonic model for the Ryoke Belt, southwest Japan. *Journal of Metamorphic Geology* , **16,** 3-22.

Caggianelli, A., del Moro, A. & Piccarreta, G., 1994. Petrology of basic and intermediate orogenic granitoids from the Sila Massif (Calabria, southern Italy). *Geological Journal,* **29,** 11-28.

Carmichael, D. M., 1969. On the mechanism of prograde metamorphic reactions in quartz-bearing pelitic rocks. *Contributions to Mineralogy and Petrology,* **20,** 244-267.

Chatterjee, N. D. & Froese, E., 1975. A thermodynamic study of the pseudo-binary muscovite-paragonite in the system $KAlSi_3O_8$-$NaAlSi_3O_8$-Al_2O_3-SiO_2-H_2O. *American Mineralogist,* **60,** 985-993.

Chernoff, C. B. & Carlson, W. D., 1997. Disequilibrium for Ca during growth of pelitic garnet. *Journal of Metamorphic Geology,* **15,** 421-438.

Clemens, J. D. & Vielzeuf, D., 1987. Constraints on melting and magma production in the crust. *Earth and Planetary Science Letters,* **86,** 287-306.

Colonna, V., Lorenzoni, S. & Zanettin Lorenzoni, E. 1973. Sull'esistenza di due complessi metamorfici lungo il bordo sud-orientale del massico «granitico» delle Serre (Calabria). *Bolletino della Società Geologica Italiana,* **92,** 861-889.

Copeland, P., Parrish, R. R. & Harrison, T. M., 1988. Identification of inherited radiogenic Pb in monazite and its implications for U-Pb systematics. *Nature,* **333,** 760-763.

Crisci, G. M., Donati, G., Messina, A., Russo, S. & Perrone, V., 1982. L'Unità Superiore dell'Aspromonte. Studio geologico e petrografico. *Rendiconti della Società Italiana di Mineralogia e Petrologia*, **38,** 989-1014.

D'Amico, C., Rottura, A., Maccarone, E. & Puglisi, G., 1982. Peraluminous granitic suite of Calabria-Peloritani Arc (southern Italy). *Rendiconti Società Italiana di Mineralogia e Petrologia,* **38,** 35-52.

Del Moro, A., Pardini, G., Maccarrone, E. & Rottura, A., 1982. Studio radiometrico Rb-Sr di granitoidi peraluminosi dell'Arco Calabro-Peloritano. *Rendiconti Società Italiana di Mineralogia e Petrologia,* **38,** 1015-1026.

Dempster, T. J. & Tanner, P. W. G., 1997. The biotite isograd, Central Pyrenees: a deformation-controlled reaction. *Journal of Metamorphic Geology*, **15,** 531-548.

Dewey, J. F., Helman, M. L., Turco, E., Hutton, D. W. H. & Knott, S. D., 1989. Kinematics of the western Mediterranean. In: *Alpine Tectonics*, (eds Coward, M. P. & Dietrich, D.), pp. 265-283, Geological Society of London, Special Publication, **45**.

DeWolf, C. P., Belshaw, N. & O´Nions, R. K., 1993. A metamorphic history from micron-scale $^{207}Pb/^{206}Pb$ chronometry of Archean monazite. *Earth and Planetary Science Letters*, **114,** 207-220.

Dietrich, D., 1988. Sense of overthrust shear in the Alpine nappes of Calabria (Southern Italy). *Journal of Structural Geology*, **10,** 373-381.

Dodson, M. H., 1979. Theory of cooling ages. In: . *Lectures in isotope geology*, (eds. Jäger, E. & Hunziker, J. C.), pp. 194-202, Springer, New York.

Droop, G. T. R. & Harte, B., 1995. The effect of Mn on the phase relations of medium-grade pelites: constraints from natural assemblages on petrogenetic grid topology. *Journal of Petrology*, **36,** 1549-1578.

Dubois, R., 1970. Phase de serrage, nappes de socle et métamorphisme alpin a la jonction calabre-apennin: la suture calabro-apenninique. *Revue de Géographie Physique et de Géologie Dynamique*, **12,** 221-253.

Dubois, R., 1976. La suture Calabro-Apenninique Cretace-Eocene et L'ouverture Tyrrhenienne Neogene: etude petrographique et structurale de la Calabre centrale. *Thèse de Doctorat, Université Pierre et Marie Curie*, 567 pp.

Dwivedi, S. B., Mohan, A. & Lal, R. K., 1998. Recalibration of the Fe-Mg exchange reaction between garnet and cordierite as a thermometer. *European Journal of Mineralogy*, **10,** 281-289.

Dymoke, P. & Sandiford, M., 1992. Phase relationships in Buchan facies series pelitic assemblages: Calculations with application to andalusite-staurolite parageneses in the Mount Lofty Ranges, South Australia. *Contributions to Mineralogy and Petrology*, **110,** 121-132.

Ebadi, A. & Johannes, W., 1991. Beginning of melting and compositions of first melts in the system Qz-Ab-Or-H_2O-CO_2. *Contributions to Mineralogy and Petrology*, **106,** 286-295.

Eckert, J. O., Newton, R. C. & Kleppa, O. J., 1991. The ΔH of reaction and recalibration of garnet-pyroxene-plagioclase-quartz geobarometer in the CMAS system by solution calorimetry. *American Mineralogist*, **76,** 148-160.

Ferry, J. M., 1976. Metamorphism of calcareous sediments in the Waterville-Vassalboro area, south-central Maine: mineral reactions and graphical analysis. *American Journal of Science*, **276,** 841-882.

Ferry, J. M., 1984. A biotite isograd in south-central Maine, USA: mineral reactions, fluid transfer, and heat transfer. *Journal of Petrology*, **25,** 871-893.

Fitzsimons, I. C. W. & Harley, S. L., 1994. The influence of retrograde cation exchange on granulite P-T estimates and a convergence technique for the recovery of peak metamorphic conditions. *Journal of Petrology*, **35,** 543-576.

Fuhrman, M. L. & Lindsley, D. H., 1988. Ternary-feldspar modeling and thermometry. *American Mineralogist*, **3,** 201-215.

Giaramita, M. J. & Day, H. W., 1991. The four-phase AFM assemblage staurolite-aluminum silicate-biotite-garnet: Extra components and implications for staurolite-out isograds. *Journal of Petrology*, **32,** 1203-1229.

Gibson, R. L., 1992. Sequential, syndeformational porphyroblast growth during Hercynian low-pressure/high-temperature metamorphism in the Canigou massif, Pyrenees. *Journal of Metamorphic Geology*, **10,** 637-650.

Graeßner, T. & Schenk, V., 1999. Low-pressure metamorphism of Palaeozoic pelites in the Aspromonte, southern Calabria: constraints for the thermal evolution in the Calabrian cross-section during the Hercynian orogeny. *Journal of Metamorphic Geology*, **17,** 157-172.

Graham, C. M. & Powell, R. P., 1984. A garnet-hornblende geothermometer: Calibration, testing, and application to the Pelona schist, southern California. *Journal of Metamorphic Geology*, **2,** 13-31.

Green, D. H. & Ringwood, A. E., 1967. An experimental investigation of the gabbro to eclogite transformation and its petrological applications. *Geochimica et Cosmochimica Acta*, **31,** 767-833.

Green, D. H. & Ringwood, A. E., 1972. A comparison of recent experimental data on the gabbro-garnet granulite-eclogite transition. *Journal of Geology*, **80,** 277-288.

Green, P. F., Duddy, I. R., Laslett, G. M., Hegarty, K. A., Gleadow, A. J. W. & Lovering, J. F., 1989. Thermal annealing of fssion tracks in apatite 4. Qualitative modelling techniques and extensions to geological timescales. *Chemical Geology*, **79,** 155-182.

Hames, W. E. & Menard, T., 1993. Fluid-assisted modification of garnet composition along rims, cracks, and mineral inclusion boundaries in samples of amphibolite facies schists. *American Mineralogist*, **78,** 338-344.

Hanchar, J. M. & Miller, C. F., 1993. Zircon zonation patterns as revealed by cathodoluminescence and backscattered electron images: Implications for interpretation of complex crustal histories. *Chemical Geology*, **110,** 1-13.

Hanchar, J. M. & Rudnick, R. L., 1995. Revealing hidden structures: the application of cathodoluminescence and back-scattered electron imaging to dating zircons from lower crustal xenoliths. *Lithos*, **36,** 289-303.

Handy, M. R. & Zingg, A., 1991. The tectonic and rheological evolution of an attenuated cross section of the continental crust - Ivrea crustal section, Southern Alps, Northwestern Italy and Southern Switzerland. *Geological Society of America Bulletin*, **103,** 236-253.

Hanson, G. N. & Gast, P. W., 1967. Kinetic studies in contact metamorphic zones. *Geochimica et Cosmochimica Acta*, **31,** 1119-1153.

Harley, S. L., 1984. An experimental study of the partitioning of Fe and Mg between garnet and orthopyroxene. *Contributions to Mineralogy and Petrology*, **86,** 359-373.

Harley, S. L. & Green, D. H., 1982. Garnet-orthopyroxene barometry for granulites and peridotites. *Nature*, **300,** 697-701.

Harrison, T. M., Duncan, I. & McDougall, I., 1985. Diffusion of ^{40}Ar in biotite: Temperature, pressure and compositional effects. *Geochimica et Cosmochimica Acta*, **49,** 2461-2468.

Harte, B. & Johnson, M. R. W., 1969. Metamorphic history of Dalradian rocks in Glens Clova, Esk and Lethnot, Angus, Scotland. *Scottish Journal of Geology*, **5,** 54-80.

Hawkins, D. P. & Bowring, S. A., 1997. U-Pb systematics of monazite and xenotime: case studies from the Paleoproterozoic of the Grand Canyon, Arizona. *Contributions to Mineralogy and Petrology*, **127,** 87-103.

Hawkins, D. P. & Bowring, S. A., 1999. U-Pb monazite, xenotime and titanite geochronological constraints on the prograde to post-peak metamorphic thermal history of Paleoproterozoic migmatites from the Grand Canyon, Arizona. *Contributions to Mineralogy and Petrology*, **134,** 150-169.

Hodges, K. V. & Spear, F. S., 1982. Geothermometry, geobarometry and the Al_2SiO_5 triple point at Mt. Moosilauke, New Hampshire. *American Mineralogist*, **67,** 1118-1134.

Hodges, K. V. & Crowley, P. D., 1985. Error estimation and empirical geothermobarometry for pelitic systems. *American Mineralogist*, **70,** 702-709.

Holdaway, M. J. 1971. Stability of andalusite and the aluminum silicate phase diagram. *American Journal of Sience*, **271,** 97-131.

Holdaway, M. J. & Lee, S. M., 1977. Fe—Mg cordierite stability in high-grade pelitic rocks based on experimental, theoretical, and natural observations. *Contributions to Mineralogy and Petrology*, **63,** 175-198.

Hollocher, K., 1991. Prograde amphibolite dehydration reactions during high-grade regional metamorphism, cntral Massachusetts, USA. *American Mineralogist*, **76,** 956-970.

Holtz, F. & Johannes, W., 1994. Maximum and minimum water contents of granitic melts: implications for chemical and physical properties of ascending magmas. *Lithos*, **32,** 149-159.

Hudson, N. F. C., 1980. Regional metamorphism of some Dalradian pelites in the Buchan Area, N. E. Scotland. *Contributions to Mineralogy and Petrology*, **73,** 39-51.

Hurford, A. J., 1991. Uplift and cooling pathways derived from fission track analysis and mica dating: A review. *Geologische Rundschau*, **80,** 349-368.

Käse, H.-R. & Metz, P., 1980. Experimental investigation of the metamorphism of siliceous dolomites. IV. Equilibrium data for the reaction: 1 Diopside + 3 Dolomite = 2 Forsterite + 4 Calcite + 2 CO_2. *Contributions to Mineralogy and Petrology*, **73,** 151-159.

Kern, H. & Schenk, V., 1985. Elastic wave velocities in rocks from a lower crustal section in Southern Calabria (Italy). *Physics of the Earth and Planetary Interiors*, **40,** 147-160.

Kern, H. & Schenk, V., 1988. A model of velocity structure beneath Calabria, southern Italy, based on laboratory data. *Earth and Planetary Science Letters*, **87,** 325-337.

Kingsbury, J. A., Miller, C. A., Wooden, J. L. & Harrison, T. M., 1993. Monazite paragenesis and U-Pb systematics in rocks of the eastern Mojave Desert, California, U.S.A.: Implications for thermochronometry. *Chemical Geology*, **110,** 147-167.

Kleemann, U. & Reinhardt, J., 1994. Garnet-biotite thermometry revisited: The effect of Al^{VI} and Ti in biotite. *European Journal of Mineralogy*, **6,** 925-941.

Klein, U., Schumacher, J. C. & Czank, M., 1996. Mutual exsolution in hornblende and cummingtonite: compositions, lamellar orientations, and exsolution temperatures. *American Mineralogist*, **81,** 928-939.

Knott, S. D., 1987. The Liguride Complex of southern Italy - a Cretaceous to Paleogene accretionary wedge. *Tectonophysics*, **142,** 217-226.

Koziol, A. M. & Newton, R. C., 1988. Redetermination of the anorthite breakdown reaction and improvement of the plagioclase-garnet-Al_2SiO_5-quartz geobarometer. *American Mineralogist*, **73,** 216-233.

Kretz, R., 1983. Symbols for rock-forming minerals. *American Mineralogist*, **68,** 277-279.

Krogh, T. E., 1973. A low-contamination method for hydrothermal decomposition of zircon and extraction of U and Pb for isotopic age determinations. *Geochimica et Cosmochimica Acta*, **37,** 485-494.

Laird, J., 1988. Chlorites: metamorphic petrology. In: *Hydrous phyllosilicates* (ed Bailey, S. W.), Reviews in Mineralogy, **19,** 405-453, Mineralogical Society of America.

Lamb, W. M. & Valley, J. W., 1988. Granulite facies amphibole and biotite equilibria, and calculated peak-metamorphic water activities. *Contributions to Mineralogy and Petrology*, **100,** 349-360.

Lanzirotti, A. & Hanson, G. N., 1995. U-Pb dating of major and accessory minerals formed during metamorphism and deformation of metapelites. *Geochimica et Cosmochimica Acta*, **59,** 2513-2526.

Le Breton, N., 1983. Reflexions a propos de quelques geothermometres et geobarometres des roches metapelitiques. Application aux gneiss pelitiques de Grande Sila (Calabre Centrale, Italie). *Thèse de Doctorat, Université d'Orleans*, 223 pp.

Le Breton, N. & Thompson, A. B., 1988. Fluid-absent (dehydration) melting of biotite in metapelites in the early stages of crustal anatexis. *Contributions to Mineralogy and Petrology*, **99,** 226-237.

Leake, B. E., Woolley, A. R., Arps, C. E. S., Birch, W. D., Gilbert, M. C., Grice, J. D., Hawthorne, F. C., Kato, A., J., K. H., Krivovichev, V. G., Lintjout, K., Laird, J., Mandarino, J., Maresch, W. V., Nickel, E. H., Rock, N. M. S., Schumacher, J. C., Smith, D. C.,

Stephenson, N. C. N., Ungaretti, L., Whittaker, E. J. W. & Youzhi, G., 1997. Nomenclature of amphiboles. Report of the Subcommittee on Amphiboles of the International Mineralogical Association Commission on New Minerals and Mineral Names. *European Journal of Mineralogy*, **9,** 623-651.

Lee, H. Y. & Ganguly, J., 1988. Equilibrium compositions of coexisting garnet and orthopyroxene: experimental determinations in the system FeO-MgO-Al_2O3-SiO_2, and applications. *Journal of Petrology*, **29,** 93-113.

Lorenzoni, S. & Zanettin Lorenzoni, E., 1983. Note illustrative della carta geologica della Sila alla scala 1 : 200.000. *Memorie della Societá Geologia Italiana*, **36,** 317-342.

Mäder, U. K., Percival, J. A. & Berman, R. G., 1994. Thermobarometry of garnet-clinopyroxene-hornblende granulites from the Kapuskasing structural zone. *Canadian Journal of Earth Sciences*, **31,** 1134-1145.

Mahar, E. M., Baker, J. M., Powell, R., Holland, T. J. B. & Howell, N., 1997. The effect of Mn on mineral stability in metapelites. *Journal of Metamorphic Geology*, **15,** 223-238.

Martignole, J. & Sisi, J.-C., 1981. Cordierite-garnet-H2O equilibrium: a geologocal thermometer, barometer and water fugacity indicator. *Contributions to Mineralogy and Petrology*, **77,** 38-46.

Massonne, H.-J. & Schreyer, W., 1987. Phengite geobarometry based on the limiting assemblage with K-feldspar, phlogopite, and quartz. *Contributions to Mineralogy and Petrology*, **96,** 212-224.

Mather, J. D., 1970. The biotite isograd and the lower greenschist facies in the Dalradian rocks of Scotland. *Journal of Petrology*, **11,** 253-275.

McMullin, D. W. A., Berman, R. G. & Greenwood, H. J., 1991. Calibration of the SGAM thermobarometer for pelitic rocks using data from phase-equilibria experiments and natural assemblages. *The Canadian Mineralogist*, **29,** 889-908.

Messina, A. & Russo, S., 1981. I graniti peraluminosi del versante meridionale dell' Aspromonte (Calabria). *Bolletino della Società Geologia Italiana*, **100,** 3-14.

Messina, A., Compagnoni, R., De Vivo, B., Perrone, V., Russo, S., Barbieri, M. & Scott, B. A., 1991a. Geological and petrochemical study of the Sila massif plutonic rocks (Northern Calabria, Italy). *Bolletino della Società Geologia Italiana*, **110,** 165-206.

Messina, A., Russo, S., Perrone, V. & Giacobbe, A., 1991b. Calc-alkaline late-variscan two mica-cordierite-Al-silicate-bearing intrusions of the Sila batholith (northern sector of the Calabrian-Peloritan Arc-Italy). *Bolletino della Società Geologia Italiana*, **110,** 365-389.

Messina, A., Russo, S., Borghi, A., Colonna, V., Compagnoni, R., Caggianelli, A., Fornelli, A. & Piccareta, G., 1994. Il massico della Sila settore settentrionale dell'arco Calabro-Peloritano. Guida all'escursione del gruppo "I basamenti cristallini e i granitoidi circum-mediterranei: evoluzione petrogenetica e implicazioni geodinamiche". *Bolletino della Società Geologia Italiana*, **113,** 539-586.

Mezger, K., 1990. Geochronology in granulites. In: *Granulites and crustal evolution,* (eds. Vielzeuf, D., Vidal, P.H.), pp. 451-470, Kluwer Academic Publishers, Dordrecht.

Mezger, K., Krogstad, E. J., 1997. Interpretation of discordant U-Pb zircon ages: An evaluation. *Journal of Metamorphic Geology*, **15,** 127-140.

Mezger, K., Rawnsley, C. M., Bohlen, S. R. & Hanson, G. N., 1991. U-Pb garnet, sphene, monazite, and rutile ages: Implications for the duration of high-grade metamorphism and cooling histories, Adirondack Mts., New York. *Journal of Geology*, **99,** 415-428.

Mezger, K., Essene, E. J., van der Pluijm, B. A. & Halliday, A. N., 1993. U-Pb geochronology of the Grenville orogen of Ontario and New York: Constraints on ancient crustal tectonics. *Contributions to Mineralogy and Petrology*, **114,** 13-26.

Mirwald, P. W., 1986. Ist Cordierit ein Geothermometer? *Fortschritte der Mineralogie, Beiheft 1*, **64,** 119.

Miyashiro, A., 1973. Metamorphism and Metamorphic Belts. George Allen & Unwin Ltd, London, 492 pp.

Miyashiro, A. & Shido, F., 1985. Tschermak substitution in low- and middle-grade pelitic schists. *Journal of Petrology*, **26,** 449-487.

Parrish, R. R., 1990. U-Pb dating of monazite and its application to geological problems. *Canadian Journal of Earth Sciences*, **27,** 1431-1450.

Pattison, D. R. M., 1989. *P-T* conditions and the influence of graphite on pelitic phase relations in the Ballachulish aureole, Scotland. *Journal of Petrology*, **30,** 1219-1244.

Pattison, D. R. M., 1992. Stability of andalusite and sillimanite and the Al_2SiO_5 triple point: Constraints from the Ballachulish Aureole, Scotland. *Journal of Geology*, **100,** 423-446.

Perkins, D. & Chipera, S. J., 1985. Garnet-orthopyroxene-plagioclase-quartz barometry: Refinement and application to the English River subprovince and the Minnesota River valley. *Contributions to Mineralogy and Petrology*, **89,** 69-80.

Phillips, E. R. & Ransom, D. M., 1970. Myrmekite and non-myrmekite plagioclase compositions in gneisses from Broken Hill, New South Wales. *Mineralogical Magazine*, **37,** 729-732.

Platt, J. P. & Compagnoni, R., 1990. Alpine ductile deformation and metamorphism in a Calabrian basement nappe (Aspromonte, south Italy). *Eclogae geologico Helvetica*, **83,** 41-58.

Pouchou, J. L. & Pichoir, F., 1984. A new model for quantitative X-ray microanalyses, Part I. Application to the analyses of homogenous samples. *La Recherche Aérospatiale*, **3,** 13-38.

Purdy, J. W. & Jäger, E., 1976. K-Ar ages on rock-forming minerals from the Central Alps. *Memoirs of the Institute of Geology and Mineralogy, University of Padova*, **30,** 1-31.

Quitzow, H. W., 1935. Der Deckenbau des kalabrischen Massivs und seiner Randgebiete. *Abhandlungen der Gesellschaft für Wissenschaften Göttingen, III Folge,* **13,** 63-179.

Raase, P., Raith, M., Ackermand, D. & Lal, R. K., 1986. Progressive metamorphism of mafic rocks from greenschist to granulite facies in the Dharwar Craton of south India. *Journal of Geology*, **94,** 261-282.

Robinson, P. R., Hollocher, K. T., Tracy, R. J. & Dietsch, C. W., 1982. High grade Acadian regional metamorphism in south-central Massachusetts. In: *NEIGC 74th Annual Meeting of the State Geological and Natural History Survey of Connecticut , guidebook for fieldtrips in Connecticut and South-Central Massachusetts* (eds Joesten, R.A. & Quarrier, S.S.), 289-340, The University of Connecticut, Storrs.

Rottura, A., Atzori, P., Bargossi, G. M., Del Moro, A., Grassi, G., Laurenzi, M. A., Maccarrone, E., Macera, P., Paglionico, A., Petrini, R., Pezzino, A., Piccarreta, G. & Poli, P., 1986. The late Hercynian granitoids from southern sectors of Calabrian Arc (southern Italy). Excursion guide to the annual field meeting of 'Granitologues', pp. 62, Bologna.

Rottura, A., Bargossi, G. M., Caironi, V., Del Moro, A., Maccarrone, E., Macera, P., Paglionico, A., Petrini, R., Piccareta, G. & Poli, G., 1990. Petrogenesis of contrasting Hercynian granitoids from the Calabrian Arc, southern Italy. *Lithos*, **24,** 97-119.

Scandone, P., 1979. Origin of the Tyrrhenian Sea and Calabrian Arc. *Bolletino della Società Geologia Italiana*, **98,** 27-34.

Schärer, U., 1984. The effect of initial ^{230}Th disequilibrium on young U-Pb ages: The Makalu case, Himalaya. *Earth and Planetary Science Letters*, **67,** 191-204.

Schenk, V., 1980. U-Pb and Rb-Sr radiometric dates and their correlation with metamorphic events in the granulite-facies basement of the Serre, southern Calabria (Italy). *Contributions to Mineralogy and Petrology*, **73,** 23-38.

Schenk, V., 1984. Petrology of felsic granulites, metapelites, metabasics, ultramafics, and metacarbonates from southern Calabria (Italy): prograde metamorphism, uplift and cooling of a former lower crust. *Journal of Petrology*, **25,** 255-298.

Schenk, V., 1989. P-T-t path of the lower crust in the Hercynian fold belt of southern Calabria. In: *Evolution of metamorphic belts* (eds Daly, J. S., Cliff, R. A. & Yardley, B. W. D.), Geological Society Special Publication, **43,** 337-342.

Schenk, V., 1990. The exposed crustal cross section of southern Calabria, Italy: Structure and evolution of a segment of Hercynian crust. In: *Exposed cross-sections of the continental crust,* (eds Salisbury, M. H. & Fountain, D. M.), 21-42, Klüwer, Dordrecht, Netherlands.

Schenk, V. & Todt, W., 1989. The age of the Adriatic crust in Calabria (Southern Italy): constraints from U-Pb zircon data. *Terra Abstracts*, **1,** 350.

Schumacher, R., Schenk, V., Raase, P. & Vitanage, P. W., 1990. Granulite facies metamorphism of metabasic and intermediate rocks in the Highland Series of Sri Lanka. In: *High-grade metamorphism and anatexis* (eds Brown, M. & Ashworth, J. R.), 235-271, Allen & Unwin, London.

Smith, H. & Barreiro, B., 1990. Monazite U-Pb dating of staurolite grade metanorphism in pelitic schists. *Contributions to Mineralogy and Petrology*, **105,** 602-615.

Spear, F. S., 1988. Thermodynamic projection and extrapolation of high-variance mineral assemblages. *Contributions to Mineralogy and Petrology*, **98,** 346-351.

Spear, F. S. & Cheney, J. T., 1989. A petrogenetic grid for pelitic schists in the system SiO_2-Al_2O_3-FeO-MgO-K_2O-H_2O. *Contributions to Mineralogy and Petrology*, **101,** 149-164.

Spear, F. S. & Menard, T., 1989. Program GIBBS: A generalized Gibbs method algorithm. *American Mineralogist*, **74,** 942-943.

Spear, F. S. & Florence, F. P., 1992. Thermobarometry in granulites: Pitfalls and new approaches. *Precambrian Research*, **55,** 209-241.

Spear, F. S. & Parrish, R. R., 1996. Petrology and cooling rates of the Valhalla complex, British Columbia, Canada. *Journal of Petrology*, **37,** 733-765.

Spear, F. S., Kohn, M. J. & Cheney, J. T., 1999. *P-T* paths from anatectic pelites. *Contributions to Mineralogy and Petrology*, **134,** 17-32.

Stacey, J. S. & Kramers, J. D., 1975. Approximation of terrestrial lead isotope evolution by a two-stage model. *Earth and Planetary Science Letters*, **26,** 207-221.

Steiger, R. H. & Jäger, E., 1977. Subcommision on geochronology: Convention on the use of decay constants in geo- and cosmochronology. *Earth and Planetary Science Letters*, **36,** 359-362.

Stevens, G. & Clemens, J. D., 1993. Fluid-absent melting and the roles of fluids in the lithosphere: a slanted summary? *Chemical Geology*, **108,** 1-17.

Symmes, G. H. & Ferry, J. M., 1992. The effect of whole-rock MnO content on the stability of garnet in pelitic schists during metamorphism. *Journal of Metamorphic Geology*, **10,** 221-237.

Thompson, A. B., 1976. Mineral reactions in pelitic rocks: II. Calculation of some P-T-X(Fe-Mg) phase relations. *American Journal of Science*, **276,** 425-454.

Thompson Jr., J. B., 1957. The graphical analyses of mineral assemblages in pelitic schists. *American Mineralogist*, **42,** 842-858.

Thomson, S. N., 1994. Fission track analysis of the crystalline basement rocks of the Calabrian Arc, southern Italy: Evidence of Oligo-Miocene late-orogenic extension and erosion. *Tectonophysics*, **238,** 331-352.

Thomson, S. N., 1998. Assessing the nature of tectonic contacts using fission-track thermochronology: an example from the Calabrian Arc, southern Italy. *Terra Nova*, **10,** 32-36.

van Dijk, J. P. & Okkes, F. W. M., 1991. Neogene tectonostratigraphy and kinematics of Calabrian basins: Implications for the geodynamics of the Central Mediterranean. *Tectonophysics*, **196,** 23-60.

Vielzeuf, D. & Montel, J. M., 1994. Partial melting of metagreywackes. part I. Fluid-absent experiments and phase relationships. *Contributions to Mineralogy and Petrology*, **117,** 375-393.

Vry, J. K., Brown, P. E. & Valley, J. W., 1990. Cordierite volatile content and the role of CO_2 in high-grade metamorphism. *American Mineralogist*, **75,** 71-88.

Wagener-Lohse C. & Blümel, P., 1984. Prograde Metamorphose vom Niederdruck-Typ in der Grenzzone Saxothuringikum/Moldanubikum E'Tirschenreuth/NE-Bayern. *Fortschritte der Mineralogie*, **62,** Beiheft 1, 254-255.

Wallis, S. R., Platt, J. P. & Knott, S. D., 1993. Recognition of syn-convergence extension in accretionary wedges with examples from the Calabrian Arc and the Eastern Alps. *American Journal of Science*, **293,** 463-494.

Wang, G.-F., Banno, S. & Takeuchi, K., 1986. Reactions to define the biotite isograd in the Ryoke metamorphic belt, Kii Peninsula, Japan. *Contributions to Mineralogy and Petrology*, **93,** 9-17.

Whittington, A., Harris, N. & Baker, J., 1998. Low-pressure anatexis: the significance of spinel and cordierite from metapelitic assemblages at Nanga Parbat, northern Pakistan. In: *What drives metamorphism and metamorphic reactions?* (eds Treloat, P. J. & O'Brien, P. J.), 183-198, Geological Society of London Special Publications, **138**.

Yardley, B. W. D., 1989. An introduction to metamorphic petrology. Longman Scientific & Technical, 248 pp.

York, D., 1969. Least squares fitting of a straight line with correlated errors. *Earth and Planetary Science Letters*, **5,** 320-324.

Zanettin Lorenzoni, E., 1980. The high grade metamorphic rocks of the Monte Gariglione Unit (Calabria, Italy). Metamorphic evolution and geoogical environment. *Memorie della Societá Geologia Italiana*, **34,** 85-100.

APPENDIX

APPENDIX A.
Analytical procedure

APPENDIX B.

Mineral assemblages

Appendix A. Analytical Procedure

Appendix A. Analytical Procedure

Table A.1. Results of measurements of the NBS 982 standard during the course of this study.

No.	$^{206}Pb/^{204}Pb$	$^{208}Pb/^{206}Pb$	$^{207}Pb/^{206}Pb$
1	36.64099 (0.018)	0.99846 (0.008)	0.46658 (0.004)
2	36.66111 (0.020)	0.99883 (0.004)	0.46665 (0.003)
3	36.65360 (0.027)	0.99903 (0.007)	0.46656 (0.004)
4	36.65673 (0.021)	0.99878 (0.005)	0.46670 (0.003)
5	36.62692 (0.036)	0.99828 (0.003)	0.46665 (0.003)
average	36.64767 (0.024)	0.99868 (0.005)	0.46663 (0.003)

mass fractionation factor 0.1 % amu

Table A.2. Results of measurements of the NBS 500 standard during the course of this study.

No.	$^{235}U/^{238}U$
1	1.00197 (0.006)
2	1.00239 (0.006)
3	1.00270 (0.004)
4	1.00267 (0.003)
5	1.00272 (0.003)
6	1.00280 (0.005)
average	1.00254 (0.0045)

mass fractionation factor 0.095 % amu

Numbers in parentheses are at the % error reported at the 2 sigma confidence level

Appendix B. Mineral assemblages

Table B.1. Metapelites, metagreywackes, calcareous rocks, Aspromonte, Stilo unit, S-Calabria.

Sample	rock type	Qtz	Ms	Chl	Bt	Pl	Kfs	Grt	St	Sil	And	Crd	Ilm	Cal	Ank
Chlorite zone:															
28-93	metapelite	#	#	#		#							#		
25-87	metapelite	#	#	#									#		
29-1-93	metapelite	#	#	#		#							#		
30-1-93	metapelite	#	#	#		#							#		
31-1-93	metapelite	#	#	#		#							#		
32-1-93	metapelite	#	#	#									#		
66-1-93	metapelite	#	#	#		#							#		
67-1-93	metapelite	#	#	#		#							#		
68-1-93	metapelite	#	#	#		#							#		
69-1-93	metapelite	#	#	#									#		
203-94	metapelite	#	#	#									#		
204-94	metapelite	#	#	#									#		
205-94	metapelite	#	#	#									#		
207-94	metapelite	#	#	#		#							#		
Biotite zone:															
29-87	metagreywacke	#	#		#	#							#		
33-1-93	metagreywacke	#	#	#	#	#	#						#		
34-1-93	metagreywacke	#	#		#	#							#		
37-1-93	metagreywacke	#	#	#	#	#							#		
71-1-93	metagreywacke	#	#		#	#							#		
159-2-94	metagreywacke	#	#		#	#							#		
Ca 10	calcareous rock	#	#	#	#	#							#	#	#
36-1-93	calcareous rock	#	#	#	#								#	#	
70-1-93	calcareous rock	#	#	#		#							#	#	
125-2-94	calcareous rock	#	#	#	#	#							#	#	
65-1-94	metapelite	#	#	#	#								#		
Garnet zone:															
39-1-93	metagreywacke	#	#	#	#	#							#		
65-1-93	metagreywacke	#	#		#	#							#		
226-1-94	metagreywacke	#	#	#	#	#							#		
83-1-94	metagreywacke	#	#		#	#							#		
Ca 11-2	metagreywacke	#	#		#	#							#		
5-2-96	metapelite	#	#	#				#					#		
8-96	metapelite	#	#	#									#		
10-96	metapelite	#	#	#	#	#		#					#		
31/87	metapelite	#			#	#							#		
38-1-93	metapelite	#	#	#		#		#					#		
38-3-93	metapelite	#	#	#		#		#					#		
39-2-93	metapelite	#	#	#		#		#					#		
43-2-93	metapelite	#	#	#	#								#		
44-1-93	metapelite	#	#	#	#	#		#					#		
44-2-93	metapelite	#	#	#				#					#		
41a/85	metapelite	#	#		#	#		#			#		#		
43-1-93	metapelite	#	#	#	#	#					#		#		
61-1-93	metapelite	#	#	#	#								#		
62-1/2-93	metapelite	#	#	#	#	#		#					#		
62-3-93	metapelite	#	#	#				#					#		
63-2-93	metapelite	#	#	#		#							#		
64-1-93	metapelite	#	#	#		#							#		
78-2-94	metapelite	#	#	#	#	#							#		
79-2-94	metapelite	#	#	#	#	#		#					#		
80-2-94	metapelite	#	#	#		#		#					#		
84-1-94	metapelite	#	#		#								#		
88-1-94	metapelite	#	#	#	#	#		#					#		
114-1-94	metapelite	#	#	#	#	#							#		
116-1-94	metapelite	#	#	#	#			#					#		
132-1-94	metapelite	#	#		#			#			#		#		
134-1-94	metapelite	#	#		#	#		#			#		#		
140-1-94	metapelite	#	#	#	#	#		#					#		
141-1-94	metapelite	#	#	#		#		#					#		
142-1-94	metapelite	#	#	#		#		#					#		
143-1-94	metapelite	#	#	#				#					#		
144-3-94	metapelite	#	#	#	#	#		#					#		
146-1-94	metapelite	#	#	#	#			#					#		

Table B.1. continued. Metapelites, metagreywackes, calcareous rocks, Aspromonte, Stilo unit, S-Calabria.

Sample	rock type	Qtz	Ms	Chl	Bt	Pl	Kfs	Grt	St	Sil	And	Crd	Ilm
Garnet zone:													
147-1-94	metapelite	#	#	#	#	#		#					#
149-1-94	metapelite	#	#	#	#	#		#					#
178-1-94	metapelite	#	#		#			#			#		#
179-1-94	metapelite	#	#		#	#		#					#
180-1-94	metapelite	#	#	#	#								#
182-1-94	metapelite	#	#	#	#	#					#		#
183-1-94	metapelite	#	#	#									#
185-1-94	metapelite	#	#	#	#	#		#					#
213-1-94	metapelite	#	#	#	#	#		#					#
214-1-94	metapelite	#	#	#	#	#		#					#
215-1-94	metapelite	#	#	#	#	#		#					#
216-1-94	metapelite	#	#		#	#		#			#		#
217-2-94	metapelite	#	#	#	#	#		#					#
218-1-94	metapelite	#	#	#	#	#							#
219-1-94	metapelite	#	#	#	#	#		#					#
220-1-94	metapelite	#	#	#		#		#					#
221-1-94	metapelite	#	#	#		#							#
Staurolite-andalusite zone:													
40-1-93	metagreywacke	#	#	#	#	#							#
45-1-94	metagreywacke	#	#	#				#					#
46-2-93	metagreywacke	#	#		#								#
90-1-94	metagreywacke	#	#		#	#							#
92-1-94	metagreywacke	#	#		#	#							#
1-2-94	metapelite	#	#		#	#		#			#		#
2-2-94	metapelite	#	#		#			#			#		#
5-2-94	metapelite	#	#		#	#		#			#	#	#
6-1-94	metapelite	#	#		#			#			#		#
6-96	metapelite	#	#		#	#			#		#		#
7-1-94	metapelite	#	#		#	#		#	#		#		#
7-96	metapelite	#	#		#	#		#	#		#		#
9-1-94	metapelite	#	#		#			#			#		#
10-1-94	metapelite	#	#		#			#	#		#		#
11-1-94	metapelite	#	#		#			#	#		#		#
11-2-94	metapelite	#	#		#	#		#	#		#		#
Ca 12-1	metapelite	#	#		#	#		#					#
Ca 12-2	metapelite	#	#		#	#		#			#	#	#
12-96	metapelite	#	#		#	#					#		#
13a	metapelite	#	#		#	#		#	#		#		#
13-1-94	metapelite	#	#		#				#				#
13-2-96	metapelite	#	#	#	#	#							#
14-1-94	metapelite	#	#		#			#	#		#		#
19-1-94	metapelite	#	#		#								#
24-1-94	metapelite	#	#		#	#							#
31/87	metapelite	#	#		#	#					#		#
34/87	metapelite	#	#		#	#		#			#		#
45-1-93	metapelite	#	#		#	#		#	#		#		#
46-1-93	metapelite	#	#		#	#							#
47-93	metapelite	#	#		#	#		#	#		#		#
48-1-93	metapelite	#	#	#	#	#							#
50-1-93	metapelite	#	#		#	#		#	#		#		#
51-1-93	metapelite	#	#		#			#	#				#
54-2-93	metapelite	#	#		#	#					#		#
55-1-93	metapelite	#	#	#	#	#							#
55-3-93	metapelite	#	#		#	#							#
55-1-94	metapelite	#	#		#								#
56-4-93	metapelite	#	#		#	#							#
57-1-94	metapelite	#	#		#	#							#
58-1-94	metapelite	#	#		#	#							#
62-1-97	metapelite	#	#		#	#		#	#		#	#	#
62-2-97	metapelite	#	#		#	#			#		#		#
84-4-94	metapelite	#	#		#			#	#		#		#
85-1-94	metapelite	#	#		#	#		#			#		#
98-1-94	metapelite	#	#		#	#							#
123-1-96	metapelite	#	#		#	#		#	#		#		#
124-1-96	metapelite	#	#		#	#		#	#				#
136-2-94	metapelite	#	#		#			#					#
165-1-94	metapelite	#	#		#			#	#		#		#

Table B.1. continued. Metapelites, metagreywackes, calcareous rocks, Aspromonte, Stilo unit, S-Calabria.

Sample	rock type	Qtz	Ms	Chl	Bt	Pl	Kfs	Grt	St	Sil	And	Crd	Ilm
Staurolite-andalusite zone:													
168-1-94	metapelite	#	#		#	#		#	#		#		#
169-94	metapelite	#	#		#				#		#		#
171-2-94	metapelite	#	#		#	#		#	#		#		#
173-1-94	metapelite	#	#		#	#		#			#		#
174-1-94	metapelite	#	#		#	#		#			#		#
176-1-94	metapelite	#	#		#			#	#		#		#
8061/92	metapelite	#	#		#	#		#					#
8063/92	metapelite	#	#		#	#		#			#		#
Sillimanite-muscovite zone:													
2-96	metapelite	#	#			#				#			#
3-96	metapelite	#	#		#	#						#	#
5-1-96	metapelite	#	#	#		#		#					#
29-1-94	metapelite	#	#		#	#							#
33-1-94	metapelite	#	#		#	#							#
35/87	metapelite	#	#		#	#							#
38-1-94	metapelite	#	#		#	#							#
57-2-93	metapelite	#	#		#	#							#
90-1-96	metapelite	#	#		#						#		#
93-3-96	metapelite	#	#	#		#							#
95-2-96	metapelite	#	#		#	#				#	#		#
96-2-96	metapelite	#	#		#	#				#			#
98-1-96	metapelite	#	#		#	#							#
99-2-96	metapelite	#	#		#	#							#
100-2-96	metapelite	#	#		#					#			#
101-1-96	metapelite	#	#		#	#				#			#
102-1-96	metapelite	#	#		#	#							#
103-3-96	metapelite	#	#		#	#				#			#
104-4-96	metapelite	#	#		#	#				#			#
106-1-96	metapelite	#	#		#	#				#			#
107-1-96	metapelite	#	#		#	#				#			#
113-2-94	metapelite	#	#		#	#							#
113-2-96	metapelite	#	#		#	#							#
113-3-96	metapelite	#	#		#	#					#		#
166-1-94	metapelite	#	#		#	#							#
167-2-94	metapelite	#	#		#	#							#

Table B.2. Metapelites, Aspromonte, Aspromonte unit, southern Calabria.

Sample	rock type	Qtz	Ms	Chl	Bt	Pl	Kfs	Grt	St	Sil	And	Crd	Ilm
14-96	metapelite	#	#		#	#		#		#			#
15-96	metapelite	#	#		#	#		#	#	#	#		#
16-96	metapelite	#	#		#	#		#		#			#
108-1-96	metapelite	#	#		#	#				#			#
109-96	metapelite	#	#		#	#							#
110-1-96	metapelite	#	#		#	#				#			#
111-1-96	metapelite	#	#		#	#							#
112-2-96	metapelite	#	#		#	#					#		#
114-1-96	metapelite	#	#		#	#				#			#
116-1-96	metapelite	#	#		#	#							#
117-1-96	metapelite	#	#		#	#		#		#			#
117-2-96	metapelite	#	#		#	#		#					#
119-1-96	metapelite	#	#		#	#							#
121-2-96	metapelite	#	#		#	#		#					#
122-1-96	metapelite	#	#		#	#							#
125-1-96	metapelite	#	#		#	#							#

Table B.3. Metapelites, Mt. Gariglione Complex, Sila massif, northern Calabria.

Sample	Bt	Grt	Sil	Pl	[Myr]	Qtz	Crd	[Crd]	Kfs	[And]	[Ms]	Spl	[St]	Ilm	Rt
25-96*	#	#		#		#								#	
27-96	#	#	#				#	#						#	
30-1/2-96	#	#	#	#	#	#								#	
30-3-96	#	#	#	#	#	#			#					#	
31-96*	#	#		#		#								#	
32-96*	#	#		#		#			#						
35-96G	#	#		#		#								#	
35-1-96	#	#	#			#								#	
35-1a-96	#	#	#			#									
35-2-96	#	#		#		#			#					#	
36-96	#	#	#			#	#	#					#	#	
39-2-96	#	#		#		#									
40-96	#	#	#	#		#								#	
41-1-96	#	#		#		#	#	#						#	
41-2-96	#	#		#		#								#	
41-3-96	#	#	#	#		#			#					#	
41-4-96	#	#	#	#		#	#	#						#	
42-96	#	#	#	#		#	#	#						#	
43-96	#	#	#	#	#	#			#					#	
46-96	#	#	#	#	#	#	#	#				#		#	
47-96	#	#		#		#								#	
50-1-96	#	#	#	#	#	#				#	#			#	
50-4-96	#	#	#	#	#	#	#	#		#	#	#	#		
51-96	#	#	#	#		#								#	
53-96	#	#	#	#		#								#	
55-96	#	#	#	#	#	#	#	#						#	
56-1-96	#	#		#	#	#								#	
56-2-96*	#	#	#	#		#	#	#	#					#	#
57-1-96	#	#	#	#		#	#	#						#	#
57-4-96	#	#	#	#		#		#						#	#
71-1-96	#	#		#		#					#			#	
71-2-96	#	#		#		#								#	
73-96	#	#	#	#	#	#	#	#		#	#	#	#	#	
74-1-96	#			#		#			#		#			#	
74-2-96	#	#		#		#					#			#	
75-1-96	#		#	#	#	#					#			#	
75-2-96	#			#		#				#	#			#	
76-96	#	#	#	#	#	#				#	#			#	
77-96	#	#	#	#		#								#	
78-2-96	#	#		#		#								#	
80-96	#	#	#	#		#								#	
83-96	#	#	#	#	#	#	#	#	#					#	
85-96	#	#	#	#		#								#	
86-96	#	#	#	#		#	#	#						#	
89-96	#			#	#	#					#			#	
55/85	#	#	#	#		#								#	
57a/85	#	#	#	#	#	#			#					#	
57b/85	#	#	#	#		#	#	#	#			#		#	
58a/85	#	#	#	#	#	#			#					#	
58b/85	#	#	#	#		#	#	#	#			#	#	#	
60a/85	#	#	#	#		#								#	
65/85	#		#	#	#	#	#				#			#	
66/85	#	#	#			#								#	
69b,c,d/85	#	#	#	#	#	#								#	
70a,b/85	#	#	#	#		#	#	#						#	
72a/85	#	#	#	#		#								#	
72b,c/85	#	#	#	#	#	#			#					#	
72e/85	#	#		#		#								#	

[#] retrograde minerals
* mylonite

Table B.3. continued. Metapelites, Mt. Gariglione Complex, Sila massif, northern Calabria.

Sample	Bt	Grt	Sil	Pl	[Myr]	Qtz	Crd	[Crd]	Kfs	[And]	[Ms]	Spl	[St]	Ilm	Rt	[Ky]
3-1/2-96	#	#	#	#		#								#	#	
5-2-97	#	#	#	#		#								#	#	
8-3-97	#	#		#		#								#		
10-97	#	#		#		#								#		
12-97	#	#	#	#		#				#	#	#		#		
13-97	#	#			#	#	#	#	#					#		
14-97	#	#	#		#	#	#	#	#			#		#		
15-97	#		#	#		#								#		
17-97	#	#	#	#	#	#	#	#	#					#		
18-97	#	#	#	#		#	#							#		
20-97	#	#	#	#		#	#	#						#		
21-97	#	#	#	#	#	#	#	#	#					#		
22-97	#	#	#	#	#	#	#	#			#			#		
23-97	#	#	#	#	#	#					#			#		
24-97	#	#	#			#					#			#		
25-97	#	#	#			#								#		
26-97	#	#	#	#	#	#	#	#	#					#		
28-97	#	#	#	#			#	#				#		#	#	
29-97	#	#		#		#								#		
30-97	#	#		#		#					#			#		
31-97	#	#	#	#	#	#	#	#		#	#			#		
32-97	#	#	#	#		#	#	#		#	#			#		
33-97	#	#	#	#	#	#	#	#			#	#		#		
34-97	#	#	#	#		#	#	#	#	#	#			#		
36-1-97	#	#	#	#	#	#	#	#		#	#	#	#	#		
36-2-97	#	#	#	#	#	#				#	#			#		
39-1-97	#		#	#		#	#							#		
39-2-97	#		#	#	#	#	#			#		#		#		
40-97	#	#	#	#		#				#				#	#	
42-2-97	#	#	#	#	#	#	#	#			#	#		#		
43-97	#	#	#	#	#	#	#		#	#	#			#		
44-97	#		#	#		#					#			#		
46-97	#		#			#				#	#			#		
47-97	#		#			#					#			#		
48-97	#		#	#	#	#	#				#			#		
49-97	#	#	#	#	#	#	#	#			#			#		
50-97	#		#	#	#	#			#		#			#		
66-97	#	#	#	#		#								#		
67-97	#	#	#			#	#	#						#	#	
C1-22/II	#	#	#	#		#	#	#					#	#		#
C7A	#		#		#	#	#			#	#			#		
C7D	#	#	#	#		#	#	#						#		
C8A	#	#	#	#		#	#	#			#			#		
C8F	#	#	#		#	#	#	#	#		#			#		
C9A	#	#	#	#	#	#	#	#			#			#		
C10-1	#	#	#	#	#	#	#				#			#		
C10-2	#	#	#	#	#	#			#		#			#		
C11B	#	#	#	#	#	#			#		#			#		
C12A	#	#	#	#		#	#			#	#			#		
C15A	#	#	#	#		#					#			#		
C16A	#	#	#			#					#			#		
C16B	#	#	#			#								#		
C17	#	#	#	#	#	#			#		#			#		
C18B	#	#	#	#		#								#		
C24B	#	#	#	#	#	#								#		
C26C	#	#	#	#	#	#	#	#	#			#		#		
C46A	#		#	#		#					#			#		
C47B	#	#	#	#	#	#	#	#			#	#		#		
C47D	#	#	#	#	#	#	#	#		#	#	#		#		

[#] retrograde minerals

Table B.4. Metabasites, Mt. Gariglione Complex, Sila massif, northern Calabria.

Sample	Plag	Opx	Cpx	Grt	Hbl	Cum	Qtz	Bt	Ilm	[Hbl]	[Cum]	[Grt]
26-96	#			#			#	#	#	#	#	#
28-96	#		#				#					
29-96	#	#					#			#	#	#
30-96	#						#	#	#	#	#	
38-96	#				#		#					
44-96	#		#				#			#		
45-96	#						#		#	#	#	
50-3-96	#			#			#	#	#		#	#
52-96	#			#			#			#	#	#
54-96				#			#		#		#	
57-2-96	#	#					#	#				
57-3-96				#			#			#	#	
63-96	#		#				#		#	#	#	
78-1-96			#				#		#	#		
79-1-96	#			#				#			#	#
79-2-96	#	#		#			#	#	#	#	#	
84-1-96	#	#					#	#	#	#		
84-2-96	#	#		#			#	#	#			#
60b/85	#							#			#	
67c/85	#						#		#	#		
67d/85	#						#		#	#	#	
68b/85	#						#	#		#	#	
68c/85	#	#					#	#		#	#	
69a/85	#							#	#	#	#	
73b/85				#			#				#	
1-1-97	#			#	#			#	#		#	
1-3-97	#			#	#			#	#		#	
1-4-97							#		#	#	#	
2-1-97	#			#			#	#	#	#	#	
2-2-97	#	#					#	#	#	#	#	
2-3-97	#	#					#		#		#	
4-97	#			#			#		#		#	
7-2-97	#						#	#	#		#	
9-97	#			#			#	#	#		#	#
11-1-97	#	#		#			#	#	#	#	#	#
16-2-97	#						#		#		#	
18-2-97	#						#	#	#		#	
27-1-97	#	#		#			#	#	#		#	
29-97 G	#			#			#	#	#		#	
29-97 GII	#			#			#	#	#		#	
35-1-97	#			#	#		#	#	#	#	#	#
35-2-97	#			#	#		#	#	#	#	#	#
37-97				#			#	#	#		#	
41-97	#						#	#	#	#	#	
68-97	#			#			#	#	#		#	

[#] retrograde minerals

Table B.5. Olivine-metagabbros, Mt. Gariglione Complex, Sila massif.

Sample	Plag	Opx	Cpx	Ol	Spl	[Prg]	[Spl]	[Opx]	[Cpx]
7-1-97	#	#	#	#	#	#	#		#
1-8-97	#	#	#	#	#	#	#	#	#

[#] retrograde minerals